Inverse engineering in quantum and classical systems via shortcut to adiabaticity

A thesis submitted by

Koushik Paul

to

Indian Institute of Technology Guwahati
in partial fulfillment of the requirements
for the award of the degree of
Doctor of Philosophy in Physics

Supervisor

Dr. Amarendra Kumar Sarma

Department of Physics
Indian Institute of Technology Guwahati
Guwahati - 781039, Assam, India

Declaration

The work contained in the thesis entitled "*Inverse engineering in quantum and classical systems via shortcut to adiabaticity*" has been carried out at the Department of Physics, Indian Institute of Technology Guwahati, India by me under the supervision of Dr. Amarendra Kumar Sarma. The material of this thesis has not been submitted elsewhere for any other degree. Works presented in the thesis are all my own unless referenced to the contrary in the text.

(Koushik Paul)
Department of Physics
Indian Institute of Technology Guwahati
Guwahati - 781039, India

March 15, 2018

Certificate

It is certified that the work contained in the thesis entitled "*Inverse engineering in quantum and classical systems via shortcut to adiabaticity*" by Mr. Koushik Paul, a Ph.D. student of the Department of Physics, Indian Institute of Technology Guwahati is carried out under my supervision and has not been submitted elsewhere for the award of any other degree.

(Dr. Amarendra Kumar Sarma)
Department of Physics
Indian Institute of Technology Guwahati
Guwahati - 781039, India

March 15, 2018

To my beloved Grandparents

" dadu & dida "

Acknowledgment

First and foremost, I would like to express my gratitude to my Ph.D. supervisor, Dr. Amarendra Kumar Sarma, for allowing me to do my research under his guidance. His door was always open whenever I needed his advice for my research. His enthusiasm, patience, intellect, ideas, and passion for research have always motivated me a lot. He always inspired me and gave me the freedom to express my ideas. Apart from academics, he earned my respect as a wonderful human being. I will always cherish all these years working and interacting with him.

I would like to thank the chairman of my doctoral committee Dr. Ashwini Kumar Sharma, doctoral committee members Dr. Padma Kumar Padmanavan and Dr. Manabendra Sarma for reviewing my progress every year and for their frank comments and valuable suggestions. I am thankful to all other members of the Physics department for their help and support.

I am grateful to Indian Institute of Technology Guwahati, and Government of India, Ministry of Human Resource Development for the financial support. I wish to thank Department of Physics, IIT Guwahati for providing me the necessary computational facilities. I thank all the technical assistants of the department of physics, specially Mr. Basab Bijoy Purkayastha, for their assistance in various ways during my research period.

I would like to thank my group members Bijita, Subhadeep, Monika, Jyoti and Dipti for all the interaction and discussions we had. A special thanks to Subhadeep for his constant support and encouragement towards me. I am also thankful to my senior Dr. Samit Kumar Gupta for all his advices.

A heartfelt thanks to Anabilda. You are like my elder brother. There are no words to express how much support and affection you showed towards me. Rumi, a special thanks to you for being so friendly and cheerful. Sudinda, Bishuda and BhargavJi, a lot of thanks for making me feel at home from the very first day. I miss all those discussion and arguments, we used to have. Sayandeep, thanks to you for all the love and respect for me. My boyhood friends Hari and Abir, a lot of thanks

to you for making me feel loved and special.

My friends Kallol, Ramiz, Ashis, Sourav, Abhijit, Rahul, Shibananda, Noor, Nawaj a special thanks to all of you for all those wonderful moments. My fellow batchmates, Ramji and Prahlad, thank you for all the help, specially during the course work. I would also like to thank my football mates, Subhankar, Srikrishna, Gourab, Dr. Arindam, Sourav (Bharatiya), Uday, Anirban, Soumenda(Boss), Sumit, Karuna, Dr. Debasish (DK) and Sayan (RC).

At last but not the least, I would like to express my love and respect to my parents Subodh Paul and Aparna Paul. Without their unconditional support and continuous encouragement, this journey would not have been possible. My wonderful brothers Chanchal and Rintu, many many thanks to you for your love and support. Satabdi, my dearest friend and companion of my life, I owe you a world of thanks for the belief and faith you have shown for me and supporting me through all the ups and downs of my life.

Abstract

Shortcut to adiabatic passage methods, developed to circumvent the shortcomings of the usual adiabatic passage methods in quantum optics, now finds immense applications in diverse areas of physics. It finds its applications in quantum information science, Bose-Einstein condensates, Ultra-cold atoms, non-Hermitian systems and even in waveguide optics and biological systems. In this thesis, we have applied the so-called transitionless quantum driving (TQD) and Lewis-Reisenfeld Invariant (LRI) shortcut methods to a variety of classical and quantum systems to enhance the efficiency and fastness of certain processes related to the system. We have proposed a variety of schemes and protocols in this regard. For example, we show how it is possible to prepare an entangled state in extremely short time without losing robustness and efficiency; how to achieve high fidelity power switching in a waveguide coupler at an arbitrarily short length, attainment of fast soliton compression in a nonlinear waveguide, wireless power transfer between two coils and so on.

Publications

Publications in journals:

1. *Shortcut to adiabatic passage in a waveguide coupler with a complex-hyperbolic-secant scheme*,

   Koushik Paul and Amarendra K. Sarma, **Physical Review A**, **91**, 053406 (2015)

2. *High-Fidelity Entangled Bell States via Shortcuts to Adiabaticity*,

   Koushik Paul and Amarendra K. Sarma, **Physical Review A**, **94**, 052303 (2016).

3. *Fast and efficient wireless power transfer via transitionless quantum driving*,

   Koushik Paul and Amarendra K. Sarma, **Scientific Reports**, **8**, 4134 (2018).

4. *Nonlinear compression of temporal solitons in an optical waveguide via inverse engineering*,

   Koushik Paul and Amarendra K. Sarma, **Europhysics Letters**, **121**, 64001 (2018)

Publications in conference proceedings:

1. *Efficient shortcut techniques in evanescently coupled waveguides*,

   Koushik Paul and Amarendra K. Sarma, Journal of Physics: Conference Series **759**, 012056 (2016).

2. *Creation of entangled states via Transitionless Quantum Driving*,

   Koushik Paul and Amarendra K. Sarma, 13th International Conference on Fiber Optics and Photonics, OSA Technical Digest (online), **paper W3A.30** (Optical Society of America, 2016)

Conference attended

Poster presentation

1. *Transitionless quantum driving based studies in evanescently coupled waveguides*, **Koushik Paul** and Amarendra K. Sarma, TEQIP symposium to celebrate the international year of light, 31 October, 2015, IIT Guwahati, Guwahati, India.

2. *Efficient shortcut techniques in evanescently coupled waveguides*, **Koushik Paul** and Amarendra K. Sarma, 58^{th} XXVII IUPAP Conference on Computational Physics: CCP2015 2 - 5 December 2015, IIT Guwahati, Guwahati, India.

3. *Creation of entangled states via Transitionless Quantum Driving*, **Koushik Paul** and Amarendra K. Sarma, PHOTONICS-2016, 4 - 8 December, 2016, IIT Kanpur, Kanpur, India.

Participation

4. ICTS School and Discussion Meeting on Frontiers in Light-Matter Interactions, 8 - 12 December, 2014, IACS, Kolkata, India.

5. ICTS school on Open Quantum Systems, 24 - 28 July, 2017, ICTS, Bangalore, India.

6. SERB school on frontiers in quantum optics, 1 - 19 December, 2017, IIT Guwahati, Guwahati, India.

Contents

1 Introduction **1**

2 Shortcut to adiabaticity: A brief review **11**

2.1 The adiabatic theorem 11

2.2 Adiabatic passage: A demonstration of adiabatic theorem 14

2.3 Shortcut to adiabaticity 16

2.3.1 Transitionless quantum driving 17

2.3.2 Lewis-Riesenfeld invariant based approach 19

2.4 Chapter summary 20

3 Preparation of entangled states using shortcut to adiabaticity **21**

3.1 The system 22

3.2 Adiabatic method 22

3.3 Transitionless quantum driving 26

3.4 Lewis-Riesenfeld Invariant based approach 29

3.5 Chapter summary 33

4 Efficient and fast optical power transfer in waveguide couplers using shortcut methods **35**

4.1 Two waveguide coupler 36

4.1.1 Coupled mode theory 36

4.1.2 Adiabaticity in two waveguide coupler 38

4.1.3 TQD in two waveguide coupler 39

4.1.4 Invariant based STA in two waveguide coupler 40

4.1.5 Results and discussion 42

4.2 Three waveguide coupler 48

4.3 Chapter summary 52

5 Nonlinear compression of temporal solitons in an optical waveguide via inverse engineering **53**
5.1 The model and theory 54
5.1.1 Variational analysis 55
5.2 Compression via adiabatic process 56
5.3 Compression via inverse engineering 59
5.4 Chapter summary 62

6 Fast and efficient wireless power transfer via transitionless quantum driving **63**
6.1 Coupled mode theory 64
6.2 Energy transfer protocols 66
6.2.1 Adiabatic following 66
6.2.2 Shortcut to adiabaticity 68
6.3 Results and discussion 70
6.4 Chapter summary 77

7 Conclusion **79**

Bibliography **82**

List of Figures

3.1 Energy diagram of triplet system involving all three states $|\psi_{\uparrow\uparrow}\rangle$, $|\psi^{+}_{\downarrow\uparrow}\rangle$ and $|\psi_{\downarrow\downarrow}\rangle$. Adiabatic energies are shown in solid lines and the diabatic energies are shown in dashed lines. Clearly $|\psi_{\downarrow\downarrow}\rangle$ does not interact with the other two diabatic states for our choice of $\Omega(t)$. 24

3.2 (a) Final population of the entangled state $|\psi^{+}_{\downarrow\uparrow}\rangle$ against Ω_0 and α with the parameters chosen as $\omega = \xi$, $T = 20\xi^{-1}$, (b) Evolution of population when adiabatic condition is satisfied with $\omega = \xi$, $\alpha = 0.45\xi$, $T = 10\xi^{-1}$ and $Q = 0.1$ (c) Evolution of poplulation when adiabatic condition is not satisfied with $\omega = \xi$, $\alpha = 0.45\xi$, $T = 10\xi^{-1}$ and 25

3.3 (a) Final population of the entangled state $|\psi^{+}_{\downarrow\uparrow}\rangle$ against Ω_0 and α using Transitionless driving algorithm with the parameters chosen as $\omega = \xi$, $T = 20\xi^{-1}$, (b) Evolution of population when adiabatic condition is not satisfied with $Q = 50$ which requires less time to transfer the population to the entangled state. 28

3.4 (a) Polynomials $\beta(t)$ (dashed red) and $\gamma(t)$ (solid blue) derived from the boundary conditions by using polynomial approach with $\gamma(t) = \sum_{j=0}^{4} g_j t^j$ and $\beta(t) = \sum_{j=0}^{5} b_j t^j$, (b) Forms of the designed external field $\Omega_{LR}(t)$ (solid blue) and $\Delta_{LR}(t)$ (dashed red). 30

3.5 Evolution of population for $H(t)$ and $I(t)$ using the functions $\beta(t)$, $\gamma(t)$, $\Omega_{LR}(t)$ and $\Delta_{LR}(t)$. $H(t)$ follows an adiabatic-like path (dashed red and solid blue) while $I(t)$ does not (dotted purple and dot-dashed green). 32

3.6 Fidelity $\mathscr{F}$ in terms of total transition time for three different approaches, adiabatic (dash-dotted blue), TQD approach (solid purple) and LRI based approach (dashed red). 33

4.1 Schematic for adiabatic directional coupler with allen-Eberly coupling scheme. β_1 and β_2 are propagation constants for waveguide one and two respectively. Coupler length is L. Maximum of the coupling occurs at $L/2$. 36

4.2 Spatial evolution of fractional beam power with respect to z for (a) adiabatic case with $L = 100mm$, (b) STA using TQD where $L = 1mm$, 41

4.3 Spatial profile of coupling and mismatch. (a) $\Delta_{eff}(z)$ (dashed) and $\kappa_e ff(z)$ (z) (solid) determined from transitionless driving method. Contour plots for output power with varying κ_0 and device length L. (b) for adiabatic coupler and (c) for STA coupler. STA coupler shows high fidelity over adiabatic coupler. 43

4.4 Fractional power output ρ_{22} vs propagation distance for $\Delta_0 = \kappa_0 = 1$ (a) for $L = 4mm$, (b) for $L = 10mm$. 44

4.5 Coupling efficiency for adiabatic and STA coupler with varying device length. parameters are same as in Fig. (4.4) 45

4.6 (a) Profile of $\beta(z)$ (dashed) and $\gamma(z)$ (solid), determined through polynomial ansatz with the coefficients determined using the boundary conditions, (b) Spatial profile of coupling and mismatch, $\Delta(z)$ (dashed) and $\kappa(z)$ (solid) determined through L-R Invariant based method. 46

4.7 Spatial evolution of fractional beam power with respect to z for L-R invariant based approach, (a) using the designed Hamiltonian and (b) using the invariant. 47

4.8 Schematic for three waveguide directional coupler with counter intuitive coupling scheme. 49

4.9 (a) Contour plots for output power with varying κ_0 and device length $L = 100mm$ for adiabatic coupler, (b) fractional beam power output vs. propagation distance for $\Delta_0 = \kappa_0 = 1$, adiabatic coupler takes long propagation distance to complete power switch. 50

4.10 (a) fractional beam power output vs. propagation distance for $\Delta_0 = \kappa_0 = 1$, three waveguide STA coupler shows complete power switching regardless of the propagation distance. (b) Coupling efficiency for adiabatic and STA coupler with varying device length. 51

5.1 Comparison of the compression of Soliton width $\alpha(\xi)$ as a function of ξ with $\gamma_0 = 2$. Adiabatic compression (solid blue) is achieved for $\lambda = 1$, $\delta = 1$, $\xi_f = 50$. Non adiabatic compression (dash-dotted brown) is shown for $\lambda = 1$, $\delta = 10$, $\xi_f = 5$. $\alpha_m(\xi)$ using Eq. (5.11) (dotted black) follows adiabatic path exactly. 57

5.2 Controlling Soliton width using reverse engineering, (a) $\alpha(\xi)$ analytical (dash-dotted blue) and reverse engineered (solid brown) and (b) Non-linearity parameter $\gamma(\xi)$ as chosen in Eq. (5.12) (dash-dotted blue) and reverse engineered (solid brown) with the parameters $\lambda = 1$, $\delta = 10$, $\xi_f = 5$ and $\gamma_0 = 2$. 58

5.3 Comparison of reverse engineered nonlinear profile $\gamma(\xi)$ with different ξ_f with $\lambda = 1$ and $\xi_f \times \delta = 50$. 60

5.4 (a) Soliton intensity at the input (dotted blue) and the output (solid red) end. (b) Contour plot for spatio-temporal evolution of soliton intensity. 61

6.1 (a) Typical wireless power transfer system consists of two coils separated by a distance d, (b) Schematic of the coils. Two lossy LC circuits, *Source* and *Drain* with losses Γ_s and Γ_d respectively, coupled to each other by inductive coupling. The resonant frequencies are ω_s and ω_d and also $\omega_s \neq \omega_d$. 65

6.2 Evolution of energy from the *Source* coil (solid red) to the *Drain* coil (dash-dotted blue) with $\Gamma_s = \Gamma_d = 4 \times 10^3 s^{-1}$, $\delta = 2 \times 10^5 s^{-1}$. (a) Adiabatic evolution for the time window $2t_0$ where $\kappa_0 = 4 \times 10^4 s^{-1}$, $\beta = 3 \times 10^9 s^{-2}$ and $t_0 = 10^{-4} s$, followed by energy evolution using TQD with weaker coupling strenght $\kappa_0 = 4 \times 10^2 s^{-1}$ and decreasing time windows (b) $\beta = 3 \times 10^9 s^{-2}$ and $t_0 = 10^{-4} s$, (c) $\beta = 3 \times 10^{10} s^{-2}$ and $t_0 = 10^{-5} s$, (d) $\beta = 3 \times 10^{11} s^{-2}$ and $t_0 = 10^{-6} s$, ... 69

6.3 Schematic representation of Frequency sweep of $\omega_s(t)$ (or $\Delta(t)$ when ω_d = constant). The sweep is linear with slope β according to L-Z model. For adiabatic evolution $|\beta| = \beta_{adiabatic}$ is small (solid red) and $|\beta| = \beta_{TQD}$ is high for the TQD method. Time period required for adiabatic case is large accordingly i.e. $T_{TQD} < T_{Adiabatic}$. 71

6.4 Comparison of efficiency (η) as a function of δ between adiabatic (dashed-dotted) and tqd based methods (solid) for different $\kappa_0/\Gamma_{s,d}$ values: $\kappa_0/\Gamma_{s,d} = 10$ (red), $\kappa_0/\Gamma_{s,d} = 50$ (purple), $\kappa_0/\Gamma_{s,d}$=100 (green) where $\Gamma_w = 10^4 s^{-1}$. Time windows (T) for the evolution are as follows: (a) $T = 200\mu s$, (b)$T = 20\mu s$ (c) $T = 2\mu s$. 72

6.5 Dependence on the distance d of the (a) coupling $\kappa(d)$ between the *source* and the *drain* coil (dash-dotted blue), additional coupling $\kappa_a(d)$ (dotted brown) and effective coupling $\kappa_{eff}(d)$ for TQD (solid red), (b) efficiency $\eta(d)$ for adiabatic method (dash-dotted blue) and for TQD (solid brown) 73

6.6 Contour plots for efficiency with respect to the variations in κ ($\times 10^4 s^{-1}$) and intrinsic losses $\Gamma_s = \Gamma_d$ ($\times 10^3 s^{-1}$) and $\Gamma_w = 10^4 s^{-1}$. (a), (b), (c) for adiabatic case and (d), (e), (f) for TQD method with $t_0 = 10^{-4} s$ in (a) and (d), $t_0 = 10^{-5} s$ in (b) and (e) and $t_0 = 10^{-6} s$ in (c) and (f). 75

6.7 Ratio of energy cost for TQD and adiabatic power transfer with respect to decreasing time window, $\kappa_0 = 4 \times 10^2 s^{-1}$ (solid red) and $\kappa_0 = 4 \times 10^4 s^{-1}$ (dash-dotted blue). 76

Chapter 1

Introduction

From the early days of quantum mechanics, the mechanism of transferring population from one state to another remains at the heart of the theory. In the early twentieth century, studies were mainly confined to the excitation owing to incoherent radiation. Einstein was the first who described incoherent excitation[1] of a two-state atom via the *rate equations*[2] (differential equation for excitation probabilities with A and B coefficients). The probability of population of a two-state system to be found in the excited state is given by

$$P = \frac{1}{2}\big[1 - exp\big(- B \int_{-\infty}^{t} I(t')dt'\big)\big]$$

Here $I(t)$ is the intensity of the incident radiation. From this we can very easily see that at most 50% of the total population can be transferred from the ground state to the excited state. This engineering is used in several applications, such as the *optical pumping*, the *stimulated emission pumping* (SEP) etc, but due to the low selectivity of the process, transfer efficiency so obtained was only about 10%.

With the introduction of LASER, scientific community was able to produce an intense, nearly-monochromatic coherent electromagnetic field which proved to be very useful for probing and controlling quantum systems. A surge of theoretical rectification of many previously known quantum effects in the field of quantum methodology took place subsequently. The application of coherent radiation to a quantum system showed significantly different results compared to those predicted by Einstein's rate equations. Various new methods based on the interaction of coherent radiation with different types of quantum systems emerged. One famous method for transferring population between quantum states using resonant excitation is the so-called Rabi oscillation. To describe this method, one generally starts

with time dependent Schrödinger equation with an appropriate exact Hamiltonian. By finding the coefficients of the corresponding states of the total wave function we can measure the probability of finding the system in a particular state. In case of two state atomic systems, when the coherent radiation is resonant, the population oscillates between the excited and the ground state. The probability for being in the excited state is given by $P_e = \sin^2(\frac{\Omega t}{2})$, where Ω is known as the Rabi frequency. Ωt is known as the pulse area. If the radiation varies in amplitude with time, then the pulse area becomes $A = \int_{-\infty}^{t} \Omega(t')dt'$. Clearly, when the pulse area has the value of $(2n+1)\pi$ *i.e*, odd multiple of π (the so-called π pulse) we shall have complete population transfer. However in real situations, atoms roam around randomly with high velocity and thus experience Doppler shift. So maintaining resonant condition in real environment is tough. Moreover for an ensemble of atoms, the velocity dependent interactions and fluctuations of the radiation intensity should be taken into account. On averaging, the excitation probability gives $\frac{1}{2}$. Also, in practical cases maintaining a precise value of the pulse area is challenging.

To overcome such difficulties and to achieve near perfect fidelity in manipulating state populations, which can be facilitated by robust experimental parameters, the idea of exploiting adiabatic evolution came into picture. Quantum adiabatic processes emerged as one of the most robust and effective methods for driving a system in a controlled way. In an adiabatic process, the external perturbation of the system varies so slowly that the system has time to adapt to the changes in the perturbation. As a result the system remains in it's initial eigenstate for a given time dependent Hamiltonian, and the transition probability becomes zero between the instantaneous eigenstates. In the field of light-matter interaction, this method is known as the adiabatic passage. In two-level and three-level atomic systems, various adiabatic passage methods like *rapid adiabatic passage* (RAP), *Stark shift chirped rapid adiabatic process* (SCRAP), *stimulated Raman passage* (STIRAP) [3–6] etc. have been studied extensively. In other fields of contemporary physics such as solid state physics [7] and waveguide optics [8], these methods also has been successfully implemented. The adiabatic passage method requires strong interaction (large Rabi frequency) and smooth pulse shape in general. Most importantly, as the system follows adiabatic evolution, it requires large interaction time. Thus, the system undergoing adiabatic passage is vulnerable against decoherences as it has more time to interact with the environment, which results into decrease in the efficiency of the process. Therefore the disadvantage of this method is that, even being very robust, it is constrained to be very slow. For the techniques like NMR, Cavity QED etc,

where robustness is of primary concern, adiabatic passage is quite successful. But when it involves issues like designing quantum gates, quantum computations etc, where speed is a matter of importance, this method is not that useful.

In search for a robust as well as a fast method, the scientific community came up with few new ideas. *Shortcut to adiabaticity* (STA) is one of them. A whole bunch of different techniques for STA have been proposed in the last ten years. One such STA technique is the so-called *counter diabatic algorithm* (CDA) proposed by Demirplak *et al.* in 2003[9,10]. A similar technique named *transitionless quantum driving* (TQD) presented in a different way by M. V. Berry in 2009[11]. Both the techniques proposes similar procedure of adding additional interaction to the initial Hamiltonian to nullify the effect of non-adiabatic terms to drive the system exactly along the adiabatic path. These ideas were first exploited by Chen *et al.* in 2010 in two and three level atomic systems and they termed it as the *shortcut to adiabatic passage* (SHAPE) method[12]. They showed that, it is possible to drive an atomic system beyond the adiabatic limit and which is also fast compared to the resonant excitation using an additional interaction. Huge surge of studies in this regard followed afterward. STA in Quantum state transfer[13–15], in Bose-Einstein condensates[16], ultra-cold gases[17], non-hermitian systems[18–20], fast ion trapping[21,22] and experimentally realizable STA in many body systems using counter diabatic driving[23], quantum Ising model[24] etc. are few examples. Significant developments of STA are made by J. G. Muga and co-workers with different new ideas. One such idea is the so-called multiple Schrödinger pictures[25] where they have shown that using multiple unitary transformation it is possible to represent interaction picture dynamical equations by different physical processes which is useful to produce better realizable STA. In a subsequent study, they came up with the idea of superadiabatic iteration using a nonconvergent sequence of nested interaction pictures to produce shortcut to adiabaticity[26]. L. Giannelli *et al.*, studied superadiabatic iteration to analyze population transfers in three level quantum systems[27].

Another widely used and robust method for STA is the *Lewis-Riesenfeld invariant* (LRI) based shortcut method[28,29]. In this method one uses a Hamiltonian that possesses symmetry (*SU2* to be specific). A dynamical invariant can be found for such Hamiltonians (The Lewis-Riesenfeld invariant) which generally does not commute with the Hamiltonian itself. One can inverse engineer the parameters of the Hamiltonian by imposing the necessary conditions to make the invariant commute with the Hamiltonian at the boundaries so that the desired initial and final states are preserved. In principle, that can deliver an infinitely fast evolution as it neither

has to follow the adiabatic path nor to obey the adiabatic condition. In several studies this method has been exploited rigorously. To cite a few: preparing various entangled states[30–32], manipulating two and three level quantum systems[33,34], power transfer in optical waveguides[35,36] and so on. Many groups have contributed to inverse engineering based STA techniques significantly. In particular, the works done by the group of A. del Campo is noteworthy. To cite a few examples: They, for the first time showed the existence of classical shortcuts for scale-invariant dynamical process[37]. A. del Campo and M. G. Boshier introduced L-R invariants to engineer STA in nonharmonic traps[38]. Again, A. del Campo introduced the concept of fast frictionless dynamics in BEC[39] and ultracold gases[40] which is proved to be useful in the context of quantum thermodynamics[41].

As far as experimental realization is concerned, various experiments have been carried out in the recent past. For example, J. Zhang *et al.*[42] implemented CDA method, for fast passage, on the electron spin of a single nitrogen vacancy center in diamond. In another experiment based on TQD, a Bose-Einstein condensate of Rubidium atoms loaded into an optical lattice shows high fidelity of 0.98, using time-dependent frequency differences between the two counter propagating beams that generates the optical lattice[43,44]. Superadiabatic transitionless driving is implemented to speed up STIRAP in a solid state lambda system by B. B. Zhou *et al.*[45]. Different STA techniques are experimentally realized in a trapped ion system where S. An. *et al.* achieved precise and flexible control of quantum evolution over a single $^{171}Yb^{+}$ ion using a pair of Raman beams[46]. S. Deng *et al.* realized the inverse engineering based STA in strongly coupled systems composed of three dimensional unitary Fermi gas to prepare a stationary final state for the non-adiabatic compression and expansion[47]. Also in a similar system, using local counterdiabatic driving, quantum friction is suppressed in the finite time thermodynamics, of a strongly coupled quantum fluid[48].

Another STA technique, worth mentioning is the so-called *fast-forward approach*, pioneered by Masuda and Nakamura, for fast time evolution of a wave function using a driving potential[49]. Later it was exploited to speed up the adiabatic dynamics[50]. In subsequent studies, fast forward approach has been applied to achieve STA in different physical systems such as charged particle in electromagnetic field[51], STIRAP[52], entangled states[53] etc. Although various variants of STA methods are available, in this thesis by STA methods we will refer to the TQD and the LRI based techniques only.

The topics and aim of research

In this thesis, we report our studies with regard to application of the STA methods in various diverse systems, briefly discussed below.

(a) *Entangled state Preparation:* Entanglement is one of the fundamental concepts in the field of quantum information and quantum computation in modern physics. The search for tools to prepare different entangled states such as Bell states, Greenberger-Horne-Zeilinger (GHZ) states[54], W states[55], bosonic NOON states[56], squeezed spin states[57] etc. using different arrangements and processes like spontaneous parametric down conversion[58], using fiber couplers and quantum dots or using different cavity arrangements[59–61] has gathered momentum in last few decades. Numerous attempts have been made in this regard. M. Barbieri *et al.* produced two-photon polarization mixed states using a high brilliance source[62]. A. Ling *et al.* prepared Bell states with controlled white noise[63]. Generation of entangled states has also been attempted theoretically, using quantum Markov processes and Hilbert space engineering[64,65]. Various other studies as well are performed to prepare different entangled states[66,67]. Despite all these proposed methods, adiabatic following proved to be one of the most robust methods for entangled state generation. R. G. Unnayan *et al.* in 2001 proposed a method to prepare entangled states in a pair of two-state systems based upon adiabatic passage using time dependent external magnetic field[68]. L-B Chen *et al.* produced n-cavity mode W state in a coupled cavity system using adiabatic passage[69]. Similarly J. Song *et al.* created N atom W states between two distant cavities[70] and Y. Liang *et al.* studied it using quantum Zeno dynamics along with the adiabatic passage[71]. C. Marr *et al.* proposed a method to prepare entangled state using dissipation assisted adiabatic passage[72]. Not only the adiabatic methods but STA methods are also studied in order to prepare various types of entangled states such as GHZ states[30,73], photonic NOON states[74], atoms inside cavities[75–78] and various others. Motivated by these works, in this thesis, we propose a method to prepare entangled state in a coupled pair of spin 1/2 particles using both STA techniques. We show that it is possible to prepare an entangled state in extremely short time without losing robustness and efficiency.

(b) *Waveguide couplers:* Recently, based on the analogies between quantum mechanics and wave optics, many techniques have been proposed to manipulate light in various waveguide structures. Two and three level atomic systems has one to one correspondence in parameters with the waveguide coupler systems. It is possible to

visualize typical quantum phenomena like Rabi oscillations[79,80], adiabatic passage in the waveguide coupler systems. Moreover, the ability to replicate laser-matter interactions (Rabi frequency, detuning etc.) by simple geometric bending or twisting of the guiding photonic structures makes it easier for implementation. Several works regarding application of quantum phenomena in waveguide structures has been carried out in past. Few examples are as follows: S. Longhi *et al.*, A Salandrino *et al.* and G. Della Valle *et al.* demonstrated adiabatic light transfer in coupled waveguide arrays[81–84], S. Kazazis *et al.* studied effects of nonlinearity in directional couplers[85]. A. M. Kenis *et al.*, T. A. Ramadan *et al.* and X. Sun *et al.* proposed robust designs to realize adiabatic passage in coupler systems[86–88]. F. Dreisow *et al.* proposed transfer of light via continuum in coupled waveguide systems[89]. Not only the adiabatic methods but also the STA methods has been studied in coupler structures. S-Y Tseng and co-workers studied different STA techniques in various waveguide settings such as counterdiabatic mode-evolution based coupled-waveguide devices[90], asymmetric direction couplers[91], short-length and robust polarization rotators in periodically poled Lithium niobate[92], Robust coupled-waveguide devices using shortcuts to adiabaticity[93]. G. Della Valle *et al.* extended the optical STA to full-wave problems for the Helmholtz equation in a infinite dimensional system[94]. In a similar context, we study waveguide directional couplers by exploiting the framework of STA methods with a configuration-dependent complex-hyperbolic-secant scheme. Our approach shows much superiority in terms of robustness and fidelity in power switching compared to the adiabatic approach.

(c)*Soliton compression:* Solitons are self-reinforcing non-linear localized waves that propagate without spreading and have particle-like properties[95] and observed in various systems[96–98]. In optics, temporal bright solitons are of particular interest owing to its various possible applications in optical communication. Recently, temporal soliton pulse compression studies are getting tremendous boost after a couple of experimental studies. For example, Gerome *et al.* and D. G. Ouzounov *et al.* reported soliton compression in a tapered hollow-core photonic band gap fiber[99,100]. Colman *et al.* demonstrated pulse compression based on high-order solitons in photonic crystal waveguides[101]. Blanco-Redondo *et al.*, experimentally demonstrated soliton-effect pulse compression of picosecond pulses in silicon[102]. Countless theoretical and numerical studies regarding soliton compression such as ultrashort soliton generation[103], soliton compression of femtosecond pulses in quadratic media[104], higher order soliton pulse compression[105], high energy few-cycle pulses by soliton compression[106] and many others are also performed. One of the soliton compression

methods that has been widely used is the so-called adiabatic soliton compression. For example, M. L. Quiroga-Texieiro *et al.* demonstrated soliton compression via adiabatic amplification[107]. Not only theories but experiments are also performed in various platforms. Chernikov *et al.* studied the adiabatic compression of picosecond and subpicosecond soliton pulses in optical fiber[108], Abdullaev *et al.* showed adiabatic soliton matter wave compression in BEC in the presence of a parabolic confining potential[109]. Inverse engineering based STA techniques can also be applied in such systems[110]. In this context, we propose a novel technique, based on inverse engineering method, to achieve fast compression of temporal solitons in a nonlinear waveguide. We demonstrate that soliton compression could be achieved, in principle, at an arbitrarily small distance by inverse engineering the pulse width and the nonlinearity of the medium.

(d) *Wireless power transfer:* Not only in quantum and optical systems, the method of adiabatic methods can be extensively studied in various other branches of science. Wireless power transfer (WPT) is one possible application[111]. Modern day WPT techniques mainly use mutual induction between coils and rely on two fundamental principles which are the so-called near-field non-radiative magneto-inductive effects and the resonant coupling between both the emitter and the receiver coils[112]. After the pioneering work of A. Kurs *et al.* on WPT via strongly coupled magnetic resonances[113], there has been a surge of studies in WPT. B. C. Cannon and coworkers' study to realize WPT for multiple small receivers[114], T. Samurai *et al.*'s work on WPT for electric vehicles[115], A. P. Sample *et al.*'s analysis of magnetically coupled resonators[116] and several others[117,118] are few examples and are of extreme importance. However in all these studies, it is extremely important to maintain the resonance between the emitter and the receiver[119]. Otherwise it may result in decrease in the efficiency. To solve this A. A. Rangelov *et al.* came up with a new idea to implement adiabatic passage in two and three coupled off-resonant coils to achieve WPT[120–122]. Here we present a robust and efficient method for WPT using TQD, in two LC circuits, coupled inductively and off-resonant to each other.

Outline of the thesis

In the following, we present a more elaborate plan of the thesis by including a description of the various problems that have been addressed in the form of different chapters of the thesis. There are a total of seven chapters. **Chapter 1** has already

provided adequate introduction to our thesis and contains the recent developments of different STA techniques.

Chapter 2: This chapter gives a theoretical framework of two major STA methods in great detail. Starting from the adiabatic theorem, we discussed adiabatic conditions for two-level quantum system. TQD and LRI based shortcut methods are discussed in the context of two level quantum systems also.

Chapter 3: In this chapter, motivated by the fact that a great deal of study is performed to prepare entangled states in different systems using adiabatic methods, we study the preparation of an entangled state using *STA* methods. A system composed of a pair of spin 1/2 particles, coupled by their intrinsic exchange interaction, is considered. We have applied both the *STA* methods to prepare a Bell state from an unentangled state with the application of a time dependent external magnetic field. It is shown that the Bell state can be prepared almost instantaneously using TQD and LR invariant based method, whereas the adiabatic evolution requires larger time width which is subjected to decay or decoherences. For invariant based approach we designed the control fields using polynomial ansatz. A fidelity almost equal to unity can be achieved and maintained using those methods.

Chapter 4: Waveguide directional couplers provide significant similarities with two or three level quantum systems. In this chapter we have studied directional couplers made of two and three evanescently coupled adjacent waveguides. We assume that the propagation constants are different for each waveguide and varies along the propagation distance. Spatial separation between two adjacent waveguides also varies with increasing distance. When the coupler length is large, they generally show complete power transfer from one waveguide to another (adiabatic coupler). Although, it is difficult to achieve complete power transfer in short distances. However it is possible to inverse engineer the power transfer for desirable distances using the above stated STA methods. For waveguide coupler we used an Allen-Eberly like mismatch in propagation constants and coupling profile. It can be seen that power can be transferred in arbitrarily short coupler length either using the additional coupling designed from TQD or by reverse engineering the mismatch in propagation constants and the coupling using the LR invariant method. In both cases, the efficiency of the coupler can be enhanced significantly.

Chapter 5: This chapter focuses on a passive nonlinear Schrödinger system with constant GVD parameter and distributed nonlinear parameter. We consider a passive waveguide with varying nonlinearity and study the compression of temporal solitary waves with an engineered nonlinearity. We propose a novel method based on the STA techniques to achieve fast compression of solitary waves. Starting with a bright solitary wave solution for the nonlinear Schrödinger equation (NLSE), we performed variational analysis to find the variational equations for the parameters related to the solitary wave such as width, chirp, velocity, center position etc. It is shown that for a particular switching strength of the chosen nonlinear function, the width of the soliton can be compressed upto a minimum point. In general, that takes place adiabatically with respect to the propagation distance. To achieve such compression in shorter distances, we inverse engineered the nonlinearity function with a predefined initial and final width of the soliton. We numerically solved the NLSE with the inverse engineered nonlinerity. We find that soliton compression can be achieved in shorter distances, with smooth inverse engineered nonlinear profile, which could possibly be exploited for various short distance communication related applications of temporal solitons.

Chapter 6: In this chapter we provide an efficient method to obtain wireless power transfer (WPT) using the TQD method. We chose a typical WPT system which consists of two lossy coils, namely the *source* and the *drain* with different resonant frequencies, and are coupled inductively. Our study shows that using periodic adiabatic frequency sweep it is possible to achieve power transfer between the two coils. However, this requires slow sweeping rate to achieve the power transfer, resulting in loss of power from the source coil itself. Using TQD method one can determine the rate of frequency sweeping required to deliver the power from the source coil to the drain coil as soon as possible. The effect of intrinsic decay can be reduced significantly with the application of the TQD protocol. The coupling efficiency is shown to be increasing with the decreasing time window and increasing coupling to decay ratio. We have also performed distance dependent studies which demonstrates that distance insensitive WPT could be achieved.

Chapter 7: Here we provide the *conclusions* of the thesis. In this chapter we conclude with a highlight of the results obtained in the thesis. We also provide a future plan based on the work that we present in the thesis.

Chapter 2

Shortcut to adiabaticity: A brief review

Shortcut to adiabaticity (STA) methods are a set of techniques that reproduce the same final population or the same final state as done via the adiabatic processes but in a much shorter and finite time[123]. Despite the advantages of controlling a system to follow an adiabatic evolution, there are several drawbacks that we have already discussed in the previous chapter. Contrary to the adiabatic processes, these STA methods, in principle, with the help of additional interaction or sometimes by designing a new Hamiltonian using proper boundary conditions, can drive the system infinitely fast. The robustness and near perfect fidelity nature of the adiabatic processes are preserved in these STA techniques. As these methods provides arbitrarily fast dynamics, they are less vulnerable to the decoherences, decays and effects of interaction with the environment. In this chapter we elaborate on two STA methods that are exploited in this thesis. Starting with a brief description of the adiabatic theorem in the next section and its application in two level quantum system, we gradually develop the TQD and the L-R invariant based shortcut methods in the subsequent sections.

2.1 The adiabatic theorem

The term *adiabatic* has been widely used in two different branches of physics. In thermodynamics, an adiabatic process is the one which occurs without transfer of heat between the system and the environment. But we will discuss the *adiabatic* processes in the context of quantum mechanics. In quantum mechanics the adiabatic processes are governed by the adiabatic theorem which is first stated by Born and

Fock[124] and later by various others[125,126]. It states that if the Hamiltonian of a particular quantum system changes gradually from some initial form H_i to some final form H_f and if the system is initially in the n^{th} eigenstate of H_i, then after the evolution it will be carried into the n^{th} eigenstate of H_f provided the eigenspectrum remains non-degenerate throughout the transition from H_i to H_f.

Let us consider a time dependent Hamiltonian $H(t)$ with it's instantaneous eigenstates $|\phi_n(t)\rangle$, forming a complete orthonormal set. Thus,

$$H(t)\,|\phi_n(t)\rangle = E_n(t)\,|\phi_n(t)\rangle \tag{2.1}$$

$E_n(t)$ is the energy of the n^{th} eigenstate. The total wave function can be written as

$$|\Phi(t)\rangle = \sum_n c_n(t)\mathrm{e}^{i\theta_n(t)}\,|\phi_n(t)\rangle\,, \tag{2.2}$$

where $\theta_n(t)$ is the dynamical phase factor when the eigen energies are time dependent and is given by,

$$\theta_n(t) = -\frac{1}{\hbar}\int_0^t E_n(t')\mathrm{d}t' \tag{2.3}$$

The time dependent Schrödinger equation for such quantum systems reads as:

$$i\hbar\frac{\partial\,|\Phi(t)\rangle}{\partial t} = H(t)\,|\Phi(t)\rangle \tag{2.4}$$

Upon substituting Eq. (2.2) into Eq. (2.4) and taking inner product with $\langle\phi_m(t)|$, one finds a set of coupled differential equation for the coefficients, given by

$$\dot{c}_m(t) = -\sum_n c_n(t)\langle\phi_m(t)|\dot{\phi}_n(t)\rangle\mathrm{e}^{i(\theta_n(t)-\theta_m(t))} \tag{2.5}$$

In obtaining Eq. (2.5), the orthonormality condition, i.e. $\langle\phi_m(t)|\phi_n(t)\rangle = \delta_{mn}$, is taken into account. Again differentiating Eq. (2.4) and taking inner product with $\phi_m(t)$ one gets,

$$\langle\phi_m(t)|\dot{\phi}_n(t)\rangle = \frac{\langle\phi_m(t)|\,\dot{H}(t)\,|\phi_n(t)\rangle}{E_n(t)-E_m(t)}. \tag{2.6}$$

Thus, from Eq. (2.5) and Eq. (2.6) we obtain

$$\dot{c}_m(t) = -c_m(t)\langle\phi_m(t)|\dot{\phi}_m(t)\rangle - \sum_n c_n(t)\frac{\langle\phi_m(t)|\,\dot{H}(t)\,|\phi_n(t)\rangle}{E_n(t)-E_m(t)}\mathrm{e}^{-\frac{i}{\hbar}\int_0^t[E_n(t')-E_m(t')]\mathrm{d}t'} \tag{2.7}$$

Up to this point the results are exact. Clearly the second term characterizes the interaction between individual eigenstates which arises due to the external field present in the Hamiltonian. Therefore, here we invoke the adiabatic approximation by choosing the external field to be slowly varying which, can be expressed mathematically as

$$\frac{\partial H(t)}{\partial t} \to 0 \tag{2.8}$$

Hence we neglect the second term in Eq. (2.7) which makes the equation decoupled and the solution looks like:

$$c_m(t) = c_m(0)\mathrm{e}^{i\gamma_m(t)}, \tag{2.9}$$

where $\gamma_m(t)$ is known as the so-called geometric phase and of the form,

$$\gamma_m(t) = i\int_0^t \langle\phi_m(t')|\dot{\phi}_m(t')\rangle \mathrm{d}t' \tag{2.10}$$

Thus if a system was in the state ϕ_m at $t = 0$, then $c_m(0) = 1$ and $c_n(0) = 0$ for all $m \neq n$, then from Eq. (2.2) we can write

$$|\Phi_m^{ad}(t)\rangle = \mathrm{e}^{i\theta_m(t)}\mathrm{e}^{i\gamma_m(t)}\,|\phi_m(t)\rangle \tag{2.11}$$

Hence, apart from the couple of phase factors which does not affect the instantaneous probability at all, the system remains in the initial eigenstate. However, adiabatic approximation [Eq. (2.8)] has to be valid, which indeed refers to the slow variation of the external parameters.

The adiabatic condition: To understand the adiabatic approximation properly let us go back to Eq. (2.5). Consider that the system is undergoing adiabatic evolution in a state $n = k \neq m$, i.e., $|c_k(t)|^2 \approx 1$ and $|c_m(t)|^2 \ll 1$. under such assumption Eq. (2.5) reads as

$$\dot{c}_m(t) = -\langle\phi_m(t)|\dot{\phi}_k(t)\rangle \mathrm{e}^{i(\theta_k(t)-\theta_m(t))} \tag{2.12}$$

As $\dot{H}$ is very small, $c_m(t)$, $E(t)$ and $\phi(t)$ also vary slowly. Hence the solution for $c_m(t)$ becomes,

$$\begin{aligned} c_m(t) &= -\int_0^t \mathrm{d}\tau \langle\phi_m(\tau)|\dot{\phi}_k(\tau)\rangle \mathrm{e}^{-\frac{i}{\hbar}(E_k(\tau)-E_m(\tau)\tau)} \\ &\approx -i\hbar\frac{\langle\phi_m(t)|\dot{\phi}_k(t)\rangle}{(E_k(t)-E_m(t))}\left[\mathrm{e}^{-\frac{i}{\hbar}(E_k(t)-E_m(t))t}-1\right] \end{aligned} \tag{2.13}$$

Now if,

$$\left|\langle\phi_m(t)|\dot{\phi}_k(t)\rangle\right| \ll \frac{(E_k(t)-E_m(t))}{\hbar}, \tag{2.14}$$

then $c_m(t) \approx 0$. Eq. (2.14) is called the adiabatic condition. It can also be written as

$$\left|\,\langle\phi_m(t)|\,\dot{H}(t)\,|\phi_n(t)\rangle\,\right| \ll \frac{(E_k(t)-E_m(t))^2}{\hbar} \tag{2.15}$$

Eq. (2.14) and Eq. (2.15) are known as adiabatic conditions in general. The application of adiabatic approximation is discussed in the following section.

2.2 Adiabatic passage: A demonstration of adiabatic theorem

There exists many physical processes where the adiabatic theorem can be applied fruitfully. We are going to elaborate it in the context of a two level quantum system. A discrete two level quantum system is one of the fundamental and exactly solvable systems in quantum physics. Consider a two state system with the bare states $|1\rangle$ and $|2\rangle$ having energies E_1 and E_2 with energy difference $\hbar\omega_0$. A general state can be written as $\psi(t) = \sum_{j=1,2} c_j(t)\mathrm{e}^{-iE_jt/\hbar}\,|j\rangle$, where $c_j(t)$ is the probability coefficient of the j^{th} state and, constrained by the relation $\sum_{j=1,2}|c_j(t)|^2 = 1$. The Schrödinger equation for such a system is given by:

$$i\hbar\frac{d}{dt}\mathbf{C}(t) = H(t)\mathbf{C}(t); \qquad \mathbf{C}(t) = \begin{pmatrix} c_1(t) \\ c_2(t) \end{pmatrix}, \tag{2.16}$$

where $c_1(t)$ and $c_2(t)$ satisfies the initial condition

$$c_1(t=-\infty) = 1, \qquad c_2(t=\infty) = 0 \tag{2.17}$$

The Hamiltonian, under *rotating wave approximation* and in the interaction picture (or equivalently in the rotating frame of reference) is given by

$$H(t) = \frac{\hbar}{2}\begin{pmatrix} 0 & \Omega(t) \\ \Omega(t) & 2\Delta(t) \end{pmatrix} \tag{2.18}$$

$\Delta = (E_2 - E_1)/\hbar$ is the detuning parameter. Diagonal elements of the Hamiltonian represents energies of the diabatic states. Basically, by application of the field the lower level E_1 gets shifted by the energy of the field $\hbar\omega(t)$ and the system is shifted to the interaction region[127]. New energy levels 0 and Δ represents the bare levels E_1 and E_2 respectively. $\Omega(t)$ represents the coupling between the two states due to the external field. $\Omega(t)$ can be different for different systems (e.g. Rabi frequency for atomic systems). $\Omega(t)$ can be taken to be real without loss of generality. Eigenvalues (energies) of the Hamiltonian in Eq.(2.27) are given by:

$$\varepsilon_{\pm}(t) = \frac{\hbar\Delta(t)}{2} \pm \frac{\hbar}{2}\sqrt{\Omega(t)^2 + \Delta(t)^2} \tag{2.19}$$

The instantaneous eigenstates of Eq.(2.18) are

$$|\Phi_+(t)\rangle = \sin\Theta(t)\,|1\rangle - \cos\Theta(t)\,|2\rangle \tag{2.20a}$$

$$|\Phi_-(t)\rangle = \cos\Theta(t)\,|1\rangle + \sin\Theta(t)\,|2\rangle \tag{2.20b}$$

These states are also known as the adiabatic states or dressed states. $\Theta(t)$ is the angle of mixing which satisfies,

$$\tan 2\Theta(t) = \frac{\Omega(t)}{\Delta(t)} \tag{2.21}$$

To achieve population transfer in this system, different approaches can be taken. One can apply a resonant field ($\Delta = 0$) with a fixed pulse area so that population can oscillate between those two states (Rabi oscillation). Also, one can follow the frequency sweep (Δ has to be time dependent) approach, where one initially starts with a off-resonant field and sweep the detuning $\Delta(t)$ from a large negative value to some large positive value. The key point is to vary the frequency or the detuning very slowly, so that the Hamiltonian becomes slowly varying function of time. Suppose at $t \to -\infty$ our system was in the dressed state $|\Phi_+\rangle$, then using Eq. (2.20a) and Eq. (2.21), we find that

$$|\Phi_+(t \to -\infty)\rangle = |1\rangle\,, \qquad |\Phi_+(t \to \infty)\rangle = |2\rangle$$

At the starting of the frequency sweep, $\Delta(t) < 0$ and the adiabatic state $|\Phi_+(t)\rangle$ corresponds to the diabatic state $|1\rangle$. After sweep, $\Delta(t) > 0$ and it corresponds to the state $|2\rangle$. At $t = 0$ the adiabatic states shows an avoided crossing. Moreover the sweep is sufficiently slow such that the system remains in the adiabatic state it

started. This eventually leads to complete population transfer from the state $|1\rangle$ to the state $|2\rangle$. However one might think how slow is the slow enough to have such an adiabatic population transfer. To answer that, we once again invoke the adiabatic condition in Eq. (2.14) which reads in this case as:

$$\left|\langle\Phi_-(t)|\dot{\Phi}_+(t)\rangle\right| \ll \frac{(\varepsilon_+(t)-\varepsilon_-(t))}{\hbar} \tag{2.22}$$

which gives,

$$\left|\dot{\Delta}\Omega - \dot{\Omega}\Delta\right| \ll \left[\Delta^2+\Omega^2\right]^{\frac{3}{2}} \tag{2.23}$$

If we consider the external interaction to be near resonant so that Δ is minimum, the second term in the L.H.S. of Eq. (2.23) can be neglected. Hence the criterion for adiabatic evolution reduces to:

$$\left|\dot{\Delta}\right| \ll \Omega^2 \tag{2.24}$$

Thus it is evident that the rate of change of frequency should be very small compared to the strength of the external field. If we choose $\Delta(t)$ and $\Omega(t)$ according to the Landau-Zener model[128–130] :

$$\Delta(t) = \beta^2 t \tag{2.25a}$$

$$\text{and} \quad \Omega(t) = \Omega_0 \tag{2.25b}$$

then the Landau-Zener formula provides the transition probability between the adiabatic states. It is given by:

$$p = exp\left(-\frac{\pi\Omega_0^2}{2|\dot{\Delta}|}\right). \tag{2.26}$$

As the frequency sweep becomes slow i.e., $\dot{\Delta} \to 0$, the transition probability p becomes almost equals to zero. Hence the system remains in its initial adiabatic state, which is $|\Phi_+(t)\rangle$ in this case and the population gets transferred from $|1\rangle$ to $|2\rangle$ in the process.

2.3 Shortcut to adiabaticity

The concept of shortcut methods for adiabatic processes have been originated from the drawbacks of adiabatic theorem itself. In general, if a time dependent pertur-

bation is added to a system, there exists a certain transition probability so that the system gets transferred from the initial adiabatic state to some other adiabatic state. One can apply the relevant adiabatic conditions to make the system follow the initial adiabatic state through the course of the entire time evolution which takes place infinitely slowly (adiabatically). In this section we discuss the possibility of fast evolution of the system where one does not need to follow the adiabatic theorem. However there exists a number of methods to drive the system beyond adiabatic limit. These methods are known as shortcut to adiabaticity methods. In this section we will be discussing the possibility of fast evolution of the system using two such STA methods namely, the transitionless quantum driving (TQD) and the Lewis-Riesenfeld invariant (LRI) based engineering.

2.3.1 Transitionless quantum driving

Transitionless Quantum Driving or TQD is proposed by M. V. Berry [11] and alternatively by Demirplak *et al.* [9,10], first indicated that it is possible to inverse engineer the system Hamiltonian from a set of predefined eigenstates, to drive it exactly. As Berry puts it: " *Nevertheless, in what can be regarded as a 'reverse engineering' perspective, it is easy to find Hamiltonians $H(t)$, associated with any chosen $H_0(t)$, that drive the instantaneous eigenstates of $H_0(t)$ exactly* " [11]. According to this method, the transition probability between the instantaneous eigestates can be made zero, to make the time evolution exact. To appreciate it, let us consider the Hamiltonian

$$H(t) = \sum_n |\phi_n(t)\rangle E_n(t) \langle\phi_n(t)| \tag{2.27}$$

The instantaneous eigenstates of this Hamiltonian are the adiabatic states, which are given by:

$$|\Phi_n(t)\rangle = e^{i\xi_n(t)} |\phi_n(t)\rangle , \tag{2.28}$$

This is same as Eq. (2.11), where $\xi_n(t) = \theta_n(t) + \gamma_n(t)$ is the adiabatic phase. To inverse engineer the system , the adiabatic states needs to satisfy the Schrödinger equation:

$$i\hbar \frac{\partial |\Phi_n(t)\rangle}{\partial t} = H'(t) |\Phi_n(t)\rangle \tag{2.29}$$

Here $H'(t)$ is the inverse engineered Hamiltonian. To find $H'(t)$, first a time-dependent unitary operator of the following form must be defined,

$$U(t) = \sum_n e^{i\xi_n(t)} \left|\phi_n(t)\right\rangle \left\langle\phi_n(0)\right| \tag{2.30}$$

It must be noted that, any time-dependent unitary operator is a solution of the Schrödinger equation

$$i\hbar \frac{\partial U(t)}{\partial t} = H'(t)U(t) \tag{2.31}$$

which leads to

$$H'(t) = i\hbar \frac{\partial U(t)}{\partial t} U^\dagger(t) \tag{2.32}$$

Now using Eq. (2.30) and Eq. (2.32) one can find the required inverse engineered Hamiltonian as follows:

$$\begin{aligned} H'(t) &= \sum_n \left|\phi_n(t)\right\rangle E_n(t) \left\langle\phi_n(t)\right| \\ &\quad + i\hbar \sum_n \left[\left|\partial_t \phi_n(t)\right\rangle \left\langle\phi_n(t)\right| - \left\langle\phi_n(t)\right| \partial_t \phi_n(t)\right\rangle \left|\phi_n(t)\right\rangle \left\langle\phi_n(t)\right| \right] \\ &= H(t) + H_1(t) \end{aligned} \tag{2.33}$$

$H_1(t)$ is the additional interaction required to nullify the effect of the non-adiabatic contributions. This can be alternatively written as:

$$H_1(t) = i\hbar \sum_{m \neq n} \frac{\left|\phi_m(t)\right\rangle \left\langle\phi_m(t)\right| \partial_t H(t) \left|\phi_n(t)\right\rangle \left\langle\phi_n(t)\right|}{E_n(t) - E_m(t)} \tag{2.34}$$

The new engineered Hamiltonian $H'(t)$ drives the adiabatic states along the adiabatic path but without generating any transition probability between them. Therefore, the adiabatic states behave like dynamical stationary eigenstates or moving eigenstates of $H'(t)$. To implement such a Hamiltonian we first need to specify a set of well specified eigenstates with known energies. In fact, as in this case, we have freedom to choose $E_n(t)$. We could have a infinite set of Hamiltonians that serve our cause. One simple choice is $E_n(t) = 0$ which left us with, from Eq. (2.33),

$$H_1(t) = i\hbar \sum_n \left|\partial_t \phi_n(t)\right\rangle \left\langle\phi_n(t)\right| \tag{2.35}$$

This is completely off-diagonal in nature in the adiabatic basis and therefore represents a coupling among the adiabatic states. For instance, if we calculate $H_1(t)$ for

eigenstates in Eq. (2.20a) and Eq. (2.20b), we obtain[9]:

$$H_1(t) = i \begin{pmatrix} 0 & \dot{\Theta}(t) \\ -\dot{\Theta}(t) & 0 \end{pmatrix} \tag{2.36}$$

Moreover, at the start and at the end of the evolution, $H_1(t)$ should remain zero in order to keep $|\phi_n(t)\rangle$ an eigenstate of $H'(t)$ for all time.

2.3.2 Lewis-Riesenfeld invariant based approach

Another well established and famous method for achieving shortcut for adiabatic processes is the Lewis-Riesenfeld invariant based inverse engineering[28]. For a system, that is governed by a symmetric, Hermitian, time dependent Hamiltonian $H(t)$, it is always possible to find a Hermitian dynamical invariant $I(t)$ satisfying

$$i\hbar \frac{\partial I(t)}{\partial t} - [I(t), H(t)] = 0 \tag{2.37}$$

This invariant is generally known as the Lewis-Riesenfeld invariant. It's expectation values with respect to the instantaneous eigenstates $\{|\phi_n(t)\rangle\}$ do not depend on time. $|\phi_n(t)\rangle$ or any other arbitray solution of the Schrödinger equation can be expressed in terms of the orthonormal eigenstates of $I(t)$, are given by:

$$|\psi_n(t)\rangle = e^{-i\alpha_n(t)} |\phi_n(t)\rangle \tag{2.38}$$

$\alpha_n(t)$ is known as the Lewis-Riesenfeld phase, which is given by:

$$\alpha_n(t) = \frac{1}{\hbar} \int_0^t \mathrm{d}t' \, \langle \psi_n(t')| \, i\hbar \frac{\partial}{\partial t'} - H(t') \, |\psi_n(t')\rangle \, . \tag{2.39}$$

The eigenvalue equation for $I(t)$ can be written as,

$$I(t) \, |\psi_n(t)\rangle = \lambda_n \, |\psi_n(t)\rangle \tag{2.40}$$

Since $I(t)$ is the Hermitian dynamical invariant, the eigenvalues λ_n are real constants and in general $I(t)$ can be written as

$$I(t) = \sum_n |\psi_n(t)\rangle \, \lambda_n \, \langle \psi_n(t)| \tag{2.41}$$

Now to inverse engineer the time-dependent Hamiltonian, similar to the TQD method, we construct a time-dependent unitary operator, but this time using the eigenstates of $I(t)$ and the Lewis-Riesenfeld phase, as follows:

$$U(t) = \sum_n |\psi_n(t)\rangle \, e^{i\alpha_n(t)} \, \langle\psi_n(0)| \tag{2.42}$$

Now putting it into the Schrödinger equation, the inversed engineered Hamiltonian can be easily constructed, using Eq. (2.31) as given below:

$$H_I(t) = -\hbar \sum_n |\psi_n(t)\rangle \, \dot{\alpha}_n(t) \, \langle\psi_n(t)| + i\hbar \sum_n \big[\, |\partial_t \psi_n(t)\rangle \, \langle\psi_n(t)| \tag{2.43}$$

In general, for a particular invariant, there can be many possible Hamiltonians based on the choices of $\alpha_n(t)$. In fact, as a consequence of the existence of $\alpha_n(t)$, the eigenstates of $H(t)$ and $I(t)$ do not coincide. So to drive the system from an initial Hamiltonian $H(0)$ to a final $H(t_f)$, in such a way that the populations in the initial and the final instantaneous bases are the same, we need to impose $[H(0), I(0)] = 0 = [H(t_f), I(t_f)]$, so that both $H(t)$ and $I(t)$ share the same eigenstates at least at the boundaries. In physical applications, the Hamiltonians $H(0)$ and $H(t_f)$ are given, and we set the initial and the final configurations of the external parameters. Then we define $I(t)$ and its eigenvectors accordingly, so that the commutation relations are obeyed at the boundary and, finally, $H_I(t)$ is designed via Eq. (2.43). As far as the exact evolution of the adiabatic states is concerned, it does not matter as one gets the desired final state at the end of the evolution.

2.4 Chapter summary

To summarize, in this chapter we discussed the adiabatic theorem and the relevance of the adiabatic condition. The realization of the adiabatic theorem in the context of a two level system, which manifests that if the time evolution is sufficiently slow, one can have complete population transfer between two bare states. STA methods enable us speeding the process infinitely, in principle. In the TQD method, we construct an additional interaction term to make the transition probability zero between the adiabatic states in order to drive the system along a particular adiabatic state. On the other hand, in the invariant based approach, we construct the L-R invariant and a new set of Hamiltonians, using the eigenstates of the L-R invariant. Discussion for realization of inverse engineering using the invariant method is also provided.

Chapter 3

Preparation of entangled states using shortcut to adiabaticity

Entanglement is a key concept in modern quantum physics. In recent past, few works showed that adiabatic following can be implemented successfully for the preparation of entangled states. In this context, the work by R. G. Unnayan et al.[68] is of tremendous significance, in which they described the adiabatic evolution from an un-entangled state to an entangled state. They considered a combination of a pair of two-state systems, consists of two spin $\frac{1}{2}$ particles coupled by their intrinsic exchange interaction and an external time dependent magnetic field. Such a system, when the magnetic field is switched off, can be represented in terms of conventional singlet and triplet states, among which two are basically the entangled Bell states for a bipartite system. With the magnetic field being switched on, these four states get coupled to each other. Choosing these four states as basis, one can readily study the adiabatic evolution of this system. However the issue of long preparation time, inherent with the adiabatic passage method, still remains. In this chapter [1], our goal is to overcome this issue. It is worthwhile to mention that A. del Campo *et al.* first studied the TQD based STA for N interacting spins[24] which led to the preparation of various entangled states in various subsequent studies. Here we study the possibilities for the preparation of entangled states in a coupled spin pair system by using the shortcut techniques.

[1]The results presented in this chapter have been published in a paper, K. Paul and A. K. Sarma, " *High-fidelity entangled Bell states via shortcuts to adiabaticity* " , Phys. Rev. A **94**, 052303 (2016).

3.1 The system

Let us consider two spin $\frac{1}{2}$ particles, say A and B, are coupled via exchange interaction along z direction. A time dependent magnetic field $\mathbf{B}(t) = \{B_x(t), B_y(t), B_z(t)\}$ is applied externally. The Hamiltonian for such a system is given by[68,131]:

$$\begin{aligned} H(t) &= 4\xi \hat{S}_A^z \otimes \hat{S}_B^z + \mu \mathbf{B}(t).(\hat{\mathbf{S}}_A + \hat{\mathbf{S}}_B) \\ &= H_0 + H'(t) \end{aligned} \tag{3.1}$$

Here ξ denotes the exchange interaction parameter and μ is the gyromagnetic ratio. $\hat{\mathbf{S}}_A$ and $\hat{\mathbf{S}}_B$ are the respective spin operators. H_0 is time independent and represents exchange interaction between these spins. Orthonormal eigenstates of H_0 are as follows:

$$|\psi_{\uparrow\uparrow}\rangle = |\uparrow\rangle_A|\uparrow\rangle_B \tag{3.2a}$$

$$|\psi^+_{\downarrow\uparrow}\rangle = \frac{1}{\sqrt{2}}(|\uparrow\rangle_A|\downarrow\rangle_B + |\downarrow\rangle_A|\uparrow\rangle_B) \tag{3.2b}$$

$$|\psi_{\downarrow\downarrow}\rangle = |\downarrow\rangle_A|\downarrow\rangle_B \tag{3.2c}$$

$$|\psi^-_{\downarrow\uparrow}\rangle = \frac{1}{\sqrt{2}}(|\uparrow\rangle_A|\downarrow\rangle_B - |\downarrow\rangle_A|\uparrow\rangle_B), \tag{3.2d}$$

where $|\uparrow\rangle$ and $|\downarrow\rangle$ stands for spin-up and spin-down states respectively. $|\uparrow\rangle_A|\uparrow\rangle_B$ denotes the tensor (or direct) product, $|\uparrow\rangle_A \otimes |\uparrow\rangle_B$, between these two states. One can readily recognize these as the triplet and the singlet states, in which, $|\psi^+_{\downarrow\uparrow}\rangle$ and $|\psi^-_{\downarrow\uparrow}\rangle$ are also famously known as the Bell states.

3.2 Adiabatic method

Upon choosing those states as the basis and with the magnetic field being taken into account, the interaction Hamiltonian could be written as ($\hbar = 1$),

$$H(t) = \begin{pmatrix} \xi - \overline{B}_z(t) & \frac{1}{\sqrt{2}}(\overline{B}_x(t) + i\overline{B}_y(t)) & 0 & 0 \\ \frac{1}{\sqrt{2}}(\overline{B}_x(t) - i\overline{B}_y(t)) & -\xi & \frac{1}{\sqrt{2}}(\overline{B}_x(t) + i\overline{B}_y(t)) & 0 \\ 0 & \frac{1}{\sqrt{2}}(\overline{B}_x(t) - i\overline{B}_y(t)) & \xi + \overline{B}_z(t) & 0 \\ 0 & 0 & 0 & -\xi \end{pmatrix} \tag{3.3}$$

Here we have taken $\overline{\mathbf{B}}(t) = \mu \mathbf{B}(t)$. From Eq. (3.3), it is evident that the $|\psi^-_{\downarrow\uparrow}\rangle$ state remains uncoupled even after the application of the magnetic field. The other three

states are coupled to each other by the transverse components of the magnetic field. Hence one can neglect $|\psi^{-}_{\downarrow\uparrow}\rangle$ while studying the system dynamics and the effective Hamiltonian can be written as,

$$H(t) = \begin{pmatrix} \xi - \overline{B}_z(t) & \frac{1}{\sqrt{2}}(\overline{B}_x(t) + i\overline{B}_y(t)) & 0 \\ \frac{1}{\sqrt{2}}(\overline{B}_x(t) - i\overline{B}_y(t)) & -\xi & \frac{1}{\sqrt{2}}(\overline{B}_x(t) + i\overline{B}_y(t)) \\ 0 & \frac{1}{\sqrt{2}}(\overline{B}_x(t) - i\overline{B}_y(t)) & \xi + \overline{B}_z(t) \end{pmatrix} \tag{3.4}$$

Since the magnetic field is time dependent and it contributes to both the diagonal and the off-diagonal terms of the interaction Hamiltonian, its choice is crucial. For our calculations we have chosen the magnetic field components as follows:

$$\overline{B}_x(t) = \Omega(t)\cos(\omega t) \tag{3.5a}$$
$$\overline{B}_y(t) = \Omega(t)\sin(\omega t) \tag{3.5b}$$
$$\overline{B}_z(t) = \alpha^2 t \tag{3.5c}$$

Here α is a parameter having the dimension of frequency. Also let us apply a basis transformation in order to find the interaction Hamiltonian using the following transformation:

$$\begin{pmatrix} c_{\uparrow\uparrow} \\ c^{+}_{\downarrow\uparrow} \\ c_{\downarrow\downarrow} \end{pmatrix} = \begin{pmatrix} e^{i(\omega-\xi)t} & 0 & 0 \\ 0 & e^{-i\xi t} & 0 \\ 0 & 0 & e^{-i(\omega+\xi)t} \end{pmatrix} \begin{pmatrix} a_{\uparrow\uparrow} \\ a^{+}_{\downarrow\uparrow} \\ a_{\downarrow\downarrow} \end{pmatrix} \tag{3.6}$$

Here $c_{\uparrow\uparrow}$, $c^{+}_{\downarrow\uparrow}$ and $c_{\downarrow\downarrow}$ are the probability amplitudes of old basis (Eq. (3.1)) while $a_{\uparrow\uparrow}$, $a^{+}_{\downarrow\uparrow}$ and $a_{\downarrow\downarrow}$ represents the new basis. One notable thing is that probability in both the basis remains same. In this new basis the Hamiltonian can be written as:

$$H_I(t) = \begin{pmatrix} \omega - \overline{B}_z(t) & \frac{1}{\sqrt{2}}\Omega(t) & 0 \\ \frac{1}{\sqrt{2}}\Omega(t) & -2\xi & \frac{1}{\sqrt{2}}\Omega(t)) \\ 0 & \frac{1}{\sqrt{2}}\Omega(t)) & -\omega + \overline{B}_z(t) \end{pmatrix} \tag{3.7}$$

The diagonal elements in Eq. (3.7) are generally known as the diabatic energies. They represent the original base states (Eq. (3.1)) in the interaction picture (therefore can be called diabatic states). They cross each other to produce the so-called

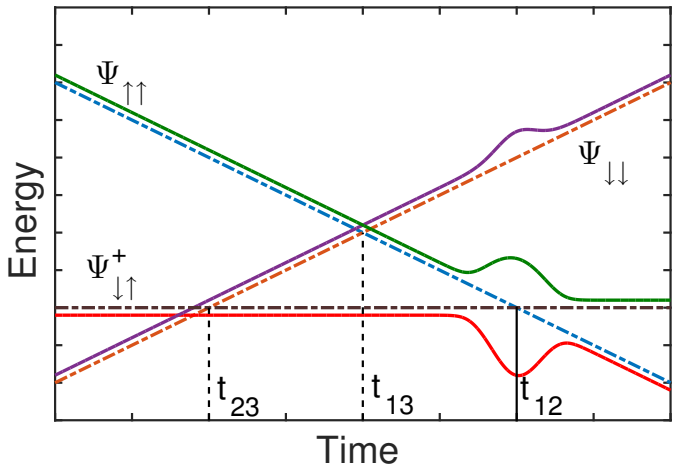

Figure 3.1: Energy diagram of triplet system involving all three states $|\psi_{\uparrow\uparrow}\rangle$, $|\psi^{+}_{\downarrow\uparrow}\rangle$ and $|\psi_{\downarrow\downarrow}\rangle$. Adiabatic energies are shown in solid lines and the diabatic energies are shown in dashed lines. Clearly $|\psi_{\downarrow\downarrow}\rangle$ does not interact with the other two diabatic states for our choice of $\Omega(t)$.

level crossings at different times,

$$t_{12} = (\omega + 2\xi)/\alpha^2 \tag{3.8a}$$

$$t_{13} = \omega/\alpha^2 \tag{3.8b}$$

$$t_{23} = (\omega - 2\xi)/\alpha^2 \tag{3.8c}$$

However, in the context of adiabatic dynamics, the level crossing is avoided by choosing the external field ($\Omega(t)$) centered around the time where the crossing occurs. We choose $\Omega(t)$ to be centered at t_{12} where the first two energies cross each other. To achieve the transition between the first two states it can be taken as,

$$\Omega(t) = \Omega_0 \exp[-(t - t_{12})^2/T^2] \tag{3.9}$$

Since $\Omega(t)$ is centered at t_{12}, it effectively remains zero at other crossings. However, one needs to choose the width, T, of the pulse $\Omega(t)$ appropriately, since for a large T, $\Omega(t)$ might interfere with the other two crossings. As a result the interaction is restricted only between the first two diabatic states[68]. Fig. (3.1) shows that at times t_{23} and t_{13}, the adiabatic energies follow the diabatic one and crosses each other[2]. But at t_{12} we have avoided crossing while adiabatic states interchanges the

[2]Actually the dashed lines and the corresponding solid lines coinside with each other except at t_{12}. They are given a little off-set for better understanding.

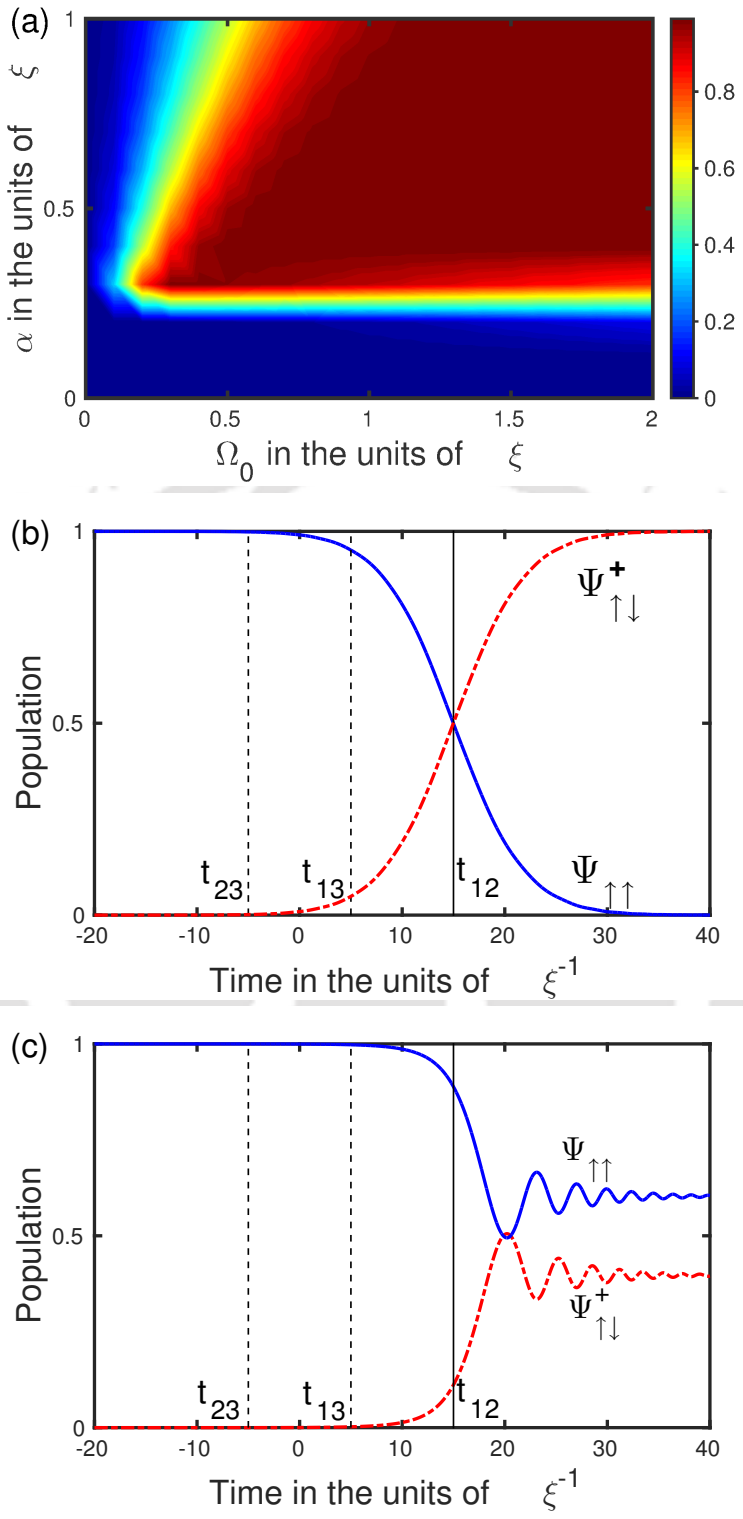

Figure 3.2: (a) Final population of the entangled state $|\psi^{+}_{\downarrow\uparrow}\rangle$ against Ω_0 and α with the parameters chosen as $\omega = \xi$, $T = 20\xi^{-1}$, (b) Evolution of population when adiabatic condition is satisfied with $\omega = \xi$, $\alpha = 0.45\xi$, $T = 10\xi^{-1}$ and $Q = 0.1$ (c) Evolution of poplulation when adiabatic condition is not satisfied with $\omega = \xi$, $\alpha = 0.45\xi$, $T = 10\xi^{-1}$ and
$Q = 2.0$

initial diabatic states. Therefore we can further simplify our system by eliminating the contribution of $|\psi_{\downarrow\downarrow}\rangle$ from $H_I(t)$. Hence Eq. (3.7) can be rewritten as,

$$H_I(t) = \begin{pmatrix} \frac{\Delta(t)}{2} & \frac{1}{\sqrt{2}}\Omega(t) \\ \frac{1}{\sqrt{2}}\Omega(t) & -\frac{\Delta(t)}{2} \end{pmatrix} \tag{3.10}$$

Here

$$\Delta(t) = \omega + 2\xi - \alpha^2 t \tag{3.11}$$

The adiabatic condition near t_{12} is given by: $Q \ll 1$, where $Q(t_{12}) = \alpha^2/2\Omega_0^2$. In Fig. (3.2a), we numerically plotted the population of the entangled state $|\psi_{\downarrow\uparrow}^+\rangle$ while varying α and Ω_0. It clearly shows that for small Ω_0 and larger α, population of $|\psi_{\downarrow\uparrow}^+\rangle$ does not reach to maximum. Also a critical value of $\alpha = \alpha_c \sim 0.25\xi$ is required for population transfer as, for α being less than α_c does not allow $\Delta(t)$ to reach the crossing. For $Q = 0.1$, the evolution of population from $|\psi_{\uparrow\uparrow}\rangle$ to $|\psi_{\downarrow\uparrow}^+\rangle$ is shown in Fig. (3.2b), where population increases adiabatically from 0 to 1 in the entangled state. However, when the adiabatic condition is not satisfied, for $Q = 2$ interchange of population does not occur at all. It should be noted that, in Fig. (3.2b) and 3.2c) we have chosen $T = 10\xi^{-1}$ which is in accordance with the previous study made by Unanyan *et al.*, which shows that for such a choice, the level crossings at t_{13} and t_{23} remains unaffected[68].

3.3 Transitionless quantum driving

To apply TQD for this system we must specify the instantaneous eigenstates of the Hamiltonian in Eq. (3.10). The instantaneous (or adiabatic) eigenvectors of $H_I(t)$ are given by

$$[|\phi_+(t)\rangle, |\phi_-(t)\rangle]^T = U(\theta(t))^\dagger [|\psi_{\uparrow\uparrow}\rangle, |\psi_{\downarrow\uparrow}^+\rangle]^T \tag{3.12}$$

$U(\theta(t))$ represents a 2D axis rotation where $\theta(t)$ is the angle of mixing and can be expressed as

$$\theta(t) = \tan^{-1}[-\sqrt{2}\Omega(t)/\Delta(t)] \tag{3.13}$$

These states also satisfy the Schrödinger equation and the interaction Hamiltonian can be expressed in the $|\phi_\pm(t)\rangle$ basis (adiabatic basis) by using a time dependent unitary transformation,

$$H_a(t) = U^\dagger H_I(t) U - iU^\dagger \dot{U} \tag{3.14}$$

$H_a(t)$ is generally known as the adiabatic Hamiltonian. According to Berry's algorithm of transitionless quantum driving, it is always possible to construct a driving Hamiltonian, which cancels out the non-adiabatic part from the adiabatic Hamiltonian. Addition of a driving term in $H_a(t)$ drives the system exactly along the adiabatic path even when adiabatic limit is crossed. The driving Hamiltonian, $H_1(t)$ is constructed from the instantaneous eigenstates which is Hermitian and purely off-diagonal in nature, can be written in adiabatic basis as[11],

$$H_1(t) = i\sum_m [|\partial_t\phi_m(t)\rangle\langle\phi_m(t)| - \langle\phi_m(t)|\partial_t\phi_m(t)\rangle|\phi_m(t)\rangle\langle\phi_m(t)|] \tag{3.15}$$

$H_1(t)$ can be realized by introducing another extra field to the system which can be of different form in different systems. With the application of $H_1(t)$, the adiabatic evolution will be followed in infinitely short time even with smaller field amplitude Ω_0 and rapid $\Delta(t)$ variation. Using Eq. (3.12) and Eq. (3.15), we calculate the driving Hamiltonian in the diabatic basis as follows[9]:

$$H_1(t) = \begin{pmatrix} 0 & i\Omega_a(t) \\ -i\Omega_a(t) & 0 \end{pmatrix} \tag{3.16}$$

Here $\Omega_a = \dot{\theta}/2$ represents the additional driving interaction. This can solely be evaluated from the mixing angle itself, which indeed makes the peak value of $\Omega_a(t)$ comparable with Ω_0. The total Hamiltonian, in $[|\psi_{\uparrow\uparrow}\rangle, |\psi^+_{\downarrow\uparrow}\rangle]^T$ basis, to perform TQD will be $H_f(t) = H_I(t) + H_1(t)$. Addition of $H_1(t)$ includes an additional phase, $\zeta(t) = 2\tan^{-1}(-\dot{\theta}(t)/\sqrt{2}\Omega(t))$. To simplify things further, another unitary transformation can be introduced. This leads to:

$$H_f(t) = \begin{pmatrix} \Delta_f(t) & \Omega_f(t) \\ \Omega_f(t) & -\Delta_f(t) \end{pmatrix}, \tag{3.17}$$

where,

$$\Delta_f(t) = [\Delta(t) - \dot{\zeta}(t)/2]/2 \qquad \text{and} \qquad \Omega_f = \sqrt{\Omega^2 + \Omega_a^2} \tag{3.18}$$

This final transformation can be realized through a simple axis rotation to the diabatic states:

$$|\overline{\psi}_{\uparrow\uparrow}\rangle = e^{+i\zeta(t)/2}|\psi_{\uparrow\uparrow}\rangle, \qquad |\overline{\psi}^+_{\downarrow\uparrow}\rangle = e^{-i\zeta(t)/2}|\psi^+_{\downarrow\uparrow}\rangle \tag{3.19}$$

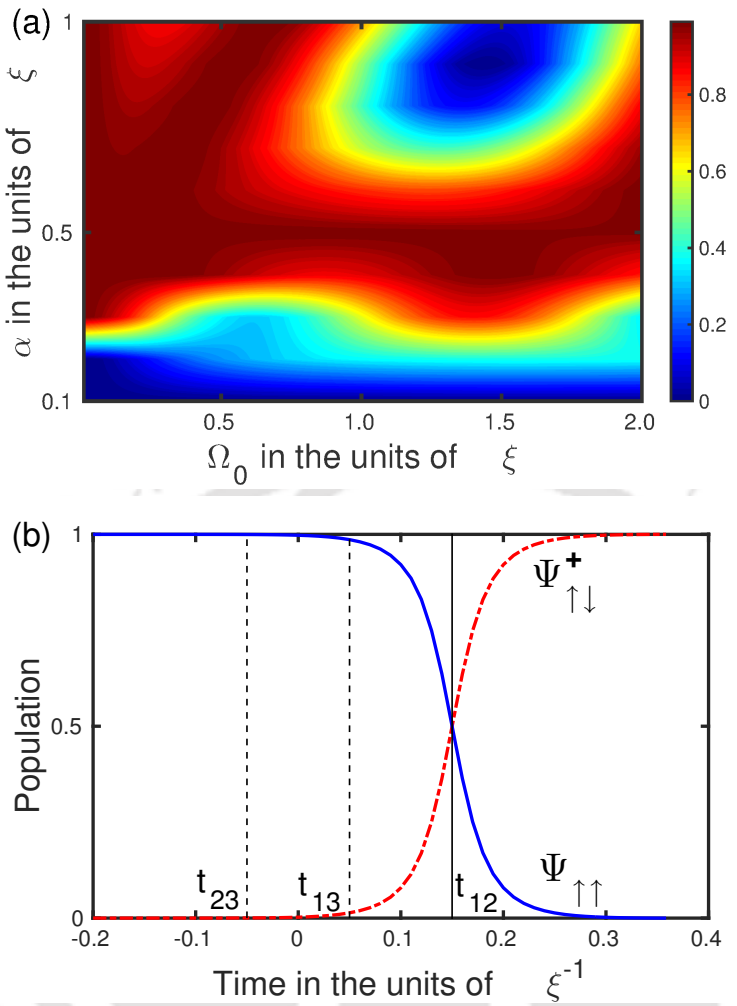

Figure 3.3: (a) Final population of the entangled state $|\psi^{+}_{\downarrow\uparrow}\rangle$ against Ω_0 and α using Transitionless driving algorithm with the parameters chosen as $\omega = \xi$, $T = 20\xi^{-1}$, (b) Evolution of population when adiabatic condition is not satisfied with $Q = 50$ which requires less time to transfer the population to the entangled state.

However, that does not affect the intrinsic properties of the system. In Fig. (3.3a) we show the final population of the entangled state when the dynamics is governed by $H_f(t)$, which demonstrates that even for very small values of Ω_0, the final population of $|\psi^{+}_{\downarrow\uparrow}\rangle$ tends to unity. The interaction time has been scaled down to 1% compared to that required in the adiabatic case. This causes violation of the adiabatic condition as Q value goes up to as high as 50. However, the population still gets transferred along the adiabatic path as shown in Fig. (3.3b).

3.4 Lewis-Riesenfeld Invariant based approach

The basic formalism for the TQD method is to remove the non-adiabatic contribution from the adiabatic Hamiltonian. But in case of LRI based approach, to speed up the population transfer, a dynamical Invariant is being used which satisfies the general invariant equation, $dI(t)/dt = 0$. The interaction Hamiltonian can be expressed as a linear combination of the Pauli matrices:

$$H_I(t) = \frac{\Omega(t)}{\sqrt{2}}\sigma_x + \frac{\Delta(t)}{2}\sigma_z \tag{3.20}$$

Therefore $H_I(t)$ possesses $SU(2)$ symmetry (as Pauli matrices satisfy the Lie algebra) and hence a Hermitian dynamical invariant can be constructed. We write this invariant in the following way[13,28,29]:

$$I(t) = \frac{\kappa_0}{2}(\sin\gamma\cos\beta\sigma_x - \sin\gamma\sin\beta\sigma_y + \cos\gamma\sigma_z) \tag{3.21}$$

Here κ_0 is an arbitrary constant, which has the dimension of frequency. The eigenstates of $I(t)$ with eigenvalues $\lambda = \pm 1$, are as follows:

$$|n_+(t)\rangle = \cos(\frac{\gamma(t)}{2})e^{i\beta}\,|\psi_{\uparrow\uparrow}\rangle + \sin(\frac{\gamma(t)}{2})\,|\psi^+_{\downarrow\uparrow}\rangle \tag{3.22a}$$

$$|n_-(t)\rangle = \sin(\frac{\gamma(t)}{2})\,|\psi_{\uparrow\uparrow}\rangle + \cos(\frac{\gamma(t)}{2})e^{-i\beta}\,|\psi^+_{\downarrow\uparrow}\rangle \tag{3.22b}$$

The parameters γ and β are both time dependent and they characterize $I(t)$. Upon substituting $I(t)$ in the invariant equation, we derive the following conditions that are required for $I(t)$ to be dynamical invariant:

$$\dot{\gamma}(t) = \sqrt{2}\Omega_{LR}\sin\beta(t) \tag{3.23a}$$

$$(\Delta_{LR}(t) + \dot{\beta}(t))\sin\gamma(t) = \sqrt{2}\Omega_{LR}(t)\cos\gamma(t)\cos\beta(t) \tag{3.23b}$$

In invariant based approach we generally construct the fields $\Omega_{LR}(t)$ and $\Delta_{LR}(t)$ from $\gamma(t)$ and $\beta(t)$. Eq. (3.23) predicts the nature of dependence of $\Omega_{LR}(t)$ and $\Delta_{LR}(t)$ on $\gamma(t)$ and $\beta(t)$. Another notable thing is that adiabatic states in Eq. (3.12) are related to $|n_\pm(t)\rangle$ (Eq. (3.22)) via the Lewis-Riesenfeld phase $\eta_\pm(t)$ by the relation,

$$|\phi_\pm(t)\rangle = e^{i\eta_\pm(t)}\,|n_\pm(t)\rangle \tag{3.24}$$

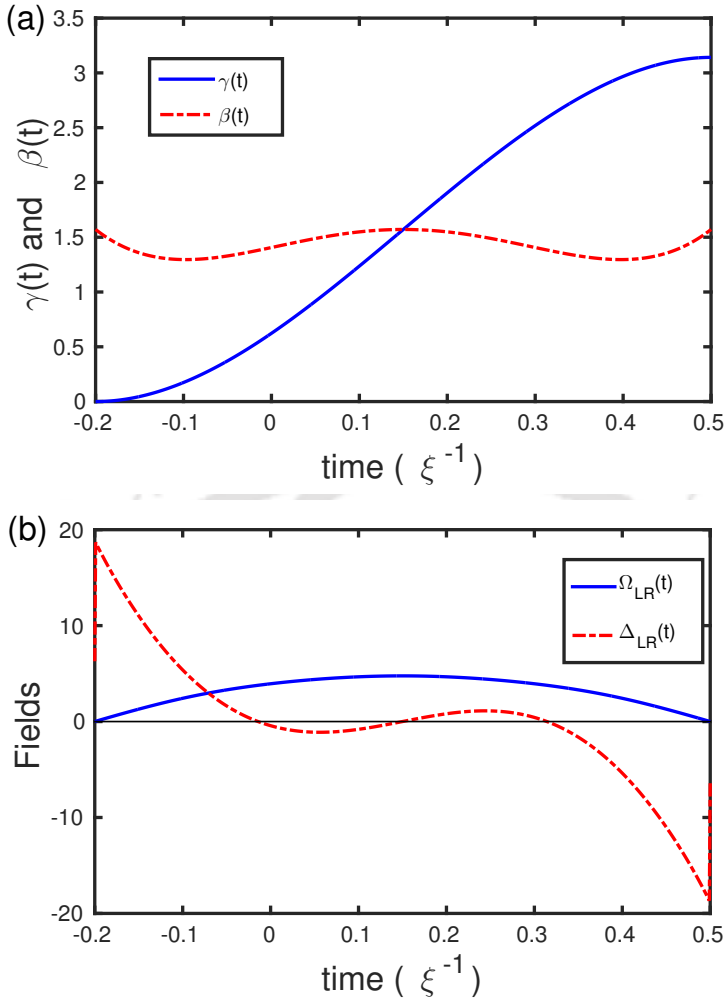

Figure 3.4: (a) Polynomials $\beta(t)$ (dashed red) and $\gamma(t)$ (solid blue) derived from the boundary conditions by using polynomial approach with $\gamma(t) = \sum_{j=0}^{4} g_j t^j$ and $\beta(t) = \sum_{j=0}^{5} b_j t^j$, (b) Forms of the designed external field $\Omega_{LR}(t)$ (solid blue) and $\Delta_{LR}(t)$ (dashed red).

Thus these two sets of eigenstates do not coincide or in other words $H_I(t)$ does not commute with $I(t)$. To inverse engineer this system we design $I(t)$ through the parameters $\gamma(t)$ and $\beta(t)$ with specific boundary conditions so that it commutes with $H_I(t)$ at least at the start and at the end of the evolution i.e.,

$$[H_I(t_i), I(t_i)] = [H_I(t_f), I(t_f)] = 0 \tag{3.25}$$

In this way both $H_I(t)$ and $I(t)$ share same eigenstates at the boundaries. To achieve

such a scenario, the following conditions should be satisfied:

$$\Omega_{LR}(t)\sin\gamma(t)\sin\beta(t)\big|_{t=t_i,t_f} = 0 \tag{3.26a}$$

$$\sqrt{2}\Omega_{LR}(t)\cos\gamma(t)\big|_{t=t_i,t_f} - \Delta_{LR}(t)\sin\gamma(t)e^{\pm i\beta(t)}]\big|_{t=t_i,t_f} = 0 \tag{3.26b}$$

We set our boundary conditions by assuming $|n_{\pm}(t)\rangle$ as our instantaneous eigenstate along which the evolution will take place. As we are driving our system from $|\psi_{\uparrow\uparrow}\rangle$ to the target state $|\psi^{+}_{\downarrow\uparrow}\rangle$ (with or without a phase factor), Eq. (3.22a) leads us to the following conditions:

$$\gamma(t_i) = 0, \;\; \gamma(t_f) = \pi$$

To satisfy Eq. (3.26) following conditions are also needed:

$$\Omega_{LR}(t_i) = 0, \;\; \Omega_{LR}(t_f) = 0$$

These choices are quite in agreement with our choice of the external field for adiabatic evolution. $\Omega_{LR}(t)$ also depends on $\dot{\gamma}(t)$ and to complete the boundary conditions for $\gamma(t)$,using Eq. (3.23a), we can write

$$\dot{\gamma}(t_i) = 0, \;\; \dot{\gamma}(t_f) = 0$$

On the other hand, the choice of $\beta(t)$ is also important for both $\Omega_{LR}(t)$ and $\Delta_{LR}(t)$. However its choice does not affect the final population of the states, but in order to keep $\Omega_{LR}(t)$ finite and minimum we restrict ourselves to the following choices:

$$\beta(t_i) = \frac{\pi}{2}, \qquad \beta(t_f) = \frac{\pi}{2},$$

$$\dot{\beta}(t_i) = \frac{-\pi}{t_f}, \qquad \dot{\beta}(t_f) = \frac{\pi}{t_f}$$

The form of $\dot{\beta}(t)$ is decisive in case of designing $\Delta_{LR}(t)$. For the adiabatic case we chose it to be linear. Similarly, here we took the initial and the final boundary values of $\dot{\beta}(t)$ in such a way that it tends to show a linear nature near t_{12}. To interpolate $\gamma(t)$ and $\beta(t)$ through the intermediate temporal points, we follow the polynomial ansatz. Two polynomials $\gamma(t) = \sum_{j=0}^{4} g_j t^j$ and $\beta(t) = \Sigma_{j=0}^{5} b_j t^j$ are subjected to the above stated boundary conditions. In order to keep $\Omega_{LR}(t)$ centered at t_{12} we choose the following additional conditions:

$$\beta(t_{12}) = \frac{\pi}{2}, \;\; \ddot{\beta}(t_{12}) = 0, \;\; \ddot{\gamma}(t_{12}) = 0$$

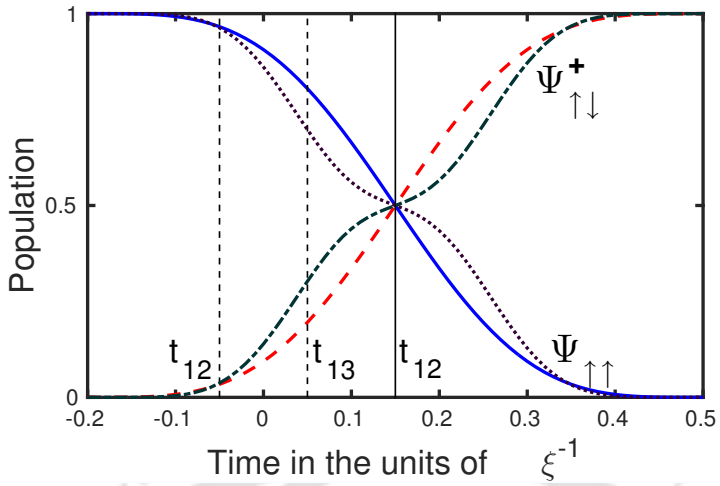

Figure 3.5: Evolution of population for $H(t)$ and $I(t)$ using the functions $\beta(t)$, $\gamma(t)$, $\Omega_{LR}(t)$ and $\Delta_{LR}(t)$. $H(t)$ follows an adiabatic-like path (dashed red and solid blue) while $I(t)$ does not (dotted purple and dot-dashed green).

With such choices $\Delta_{LR}(t)$ could be made cross through the diabatic crossing to replicate the adiabatic system. Fig. (3.4a) shows the nature of time dependent functions $\gamma(t)$ and $\beta(t)$, which are determined by using the boundary conditions. In Fig. (3.4b) we depict the functions $\Delta_{LR}(t)$ and $\Omega_{LR}(t)$ that are derived using Eq. (3.23). To determine the evolution of population, as shown in Fig. (3.5), we put $\Delta_{LR}(t)$ and $\Omega_{LR}(t)$ in the interaction Hamiltonian and also $\gamma(t)$ and $\beta(t)$ into the Invariant to solve the Schrödinger equation numerically. The dynamics of the Hamiltonian follows adiabatic path while the invariant does not, however the end results are same for both the cases.

Both the methods discussed above shows high fidelity in terms of population switching. Here we define fidelity as

$$\mathscr{F} = |\langle \psi^{+}_{\downarrow\uparrow} | \phi_{\pm}(t_f) \rangle|^2 \tag{3.27}$$

In Fig. (3.6) we have shown fidelities with respect to the variation in total transition time. Under the adiabatic regime fidelity shows a slow growth, which imply larger time required for population transfer. However in case of other two methods fidelity is close to unity regardless of the total transition time that is again well beyond the adiabatic condition. The TQD approach shows a value up to $\mathscr{F} = 0.999$, while in case of the LRI based approach fidelity goes even more close to unity.

As far as practical implementation is concerned, one must note that, although here we have presented the shortcut methods in a simple system of two spin $\frac{1}{2}$

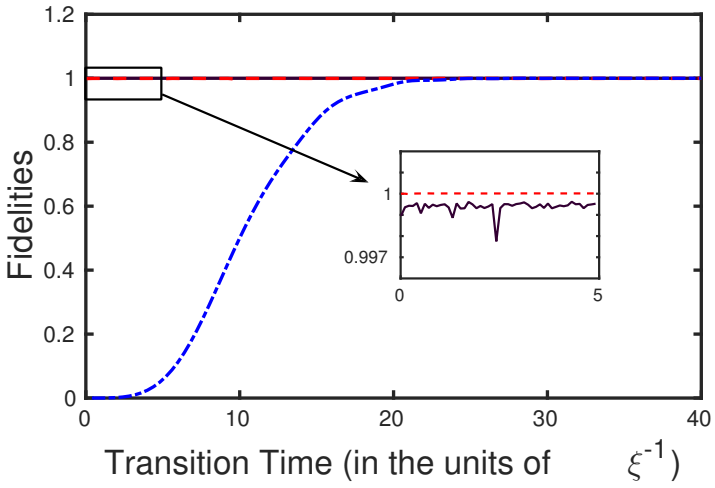

Figure 3.6: Fidelity $\mathscr{F}$ in terms of total transition time for three different approaches, adiabatic (dash-dotted blue), TQD approach (solid purple) and LRI based approach (dashed red).

particles, this study could further be extended to any two qubit systems. It is worthwhile to mention that, it is possible to obtain many special cases of the Hamiltonian [Eq.(3.1)], as pointed out in Ref.[132,133], considered in this work. Hence, the proposed protocols could be realized in a variety of realistic systems, such as: a coherently coupled two-component Bose-Einstein condensate (BEC), two-level ion-trap systems, cavity QED systems, quantum dots and superconducting qubits. As a specific example, one may consider a two-component sodium-BEC system with hyperfine states $|F = 1, M = \pm 1\rangle$ of the sodium as the two internal states while the external coupling field $\overline{B}(t)$ could be provided by a chirped radio-frequency pulse[134]. The advantage of using such a system is that the decoherence induced noise in such systems are insignificant[75,135]. In fact, in a recent experiment, using a two-level quantum system comprising BEC, it is shown that shortcut methods are extremely robust against decoherence[44]. Finally, we note that, in principle, a generalised scheme for entanglement formation with any arbitrary number of spins may also be possible.

3.5 Chapter summary

To summurise, we have applied a set of effective and highly fidel STA methods in a system of two spin $\frac{1}{2}$ particles coupled by an exchange interaction and an external magnetic field. The system is converted to a two level system by choosing the

pulse shape of the transverse magnetic field properly. Adiabatic evolution is used to produce a final entangled state by removing the level crossings between the diabatic states. However it takes a large amount of time and a sufficiently strong external field to achieve perfect population transfer to the entangled state. Introduction of transitionless quantum driving in this system overcomes these issues. Also, this method is robust against strong variation of $\overline{B}_z(t)$. Moreover, the design of the additional pulse entirely depends on the adiabatic parameters itself. On the other hand, in the invariant based approach we have freedom to design $\Omega_{LR}(t)$ and $\Delta_{LR}(t)$ only within a set of relevant boundary conditions for which we chose a polynomial ansatz.

Chapter 4

Efficient and fast optical power transfer in waveguide couplers using shortcut methods

Other than quantum mechanics, there exists a number of branches of physics where quantum methodologies are applicable. Waveguide directional coupler in integrated optics is one very good example. Adiabatic following is applied in such devices to study the eigenmode evolution of optical power through the waveguides. In general, the function of a waveguide coupler is to split coherently an optical field incident on one of the input ports and direct the two parts to the output ports. As the output is directed in two different directions, couplers are also referred to as directional couplers[136]. Adiabatic following is applied in such devices to study the eigenmode evolution of optical power through the waveguides[83]. For a sufficiently long coupler, where adiabaticity is satisfied, the system follows its initial eigenmode, causing power transfer from one waveguide to the other. Mode-evolution-based studies of directional couplers show robust optical power switching between two, three, or even among an array of waveguides[81,82,84]. On the flip side, large device length causes higher transmission loss and makes designing practical devices difficult. However, there are significant opportunities to make couplers more efficient and small in dimension using STA[12,137]. Several new studies in this regard have been reported recently[36,90,93,138,139].

In this chapter[1], we have studied two directional couplers made of two and three evanescently coupled waveguides respectively. We have applied TQD and L-R

[1]Part of the results presented in this chapter have been published in a paper, K. Paul and A. K. Sarma, "*Shortcut to adiabatic passage in a waveguide coupler with a complex-hyperbolic-secant scheme*, " , Phys. Rev. A **91**, 053406 (2015).

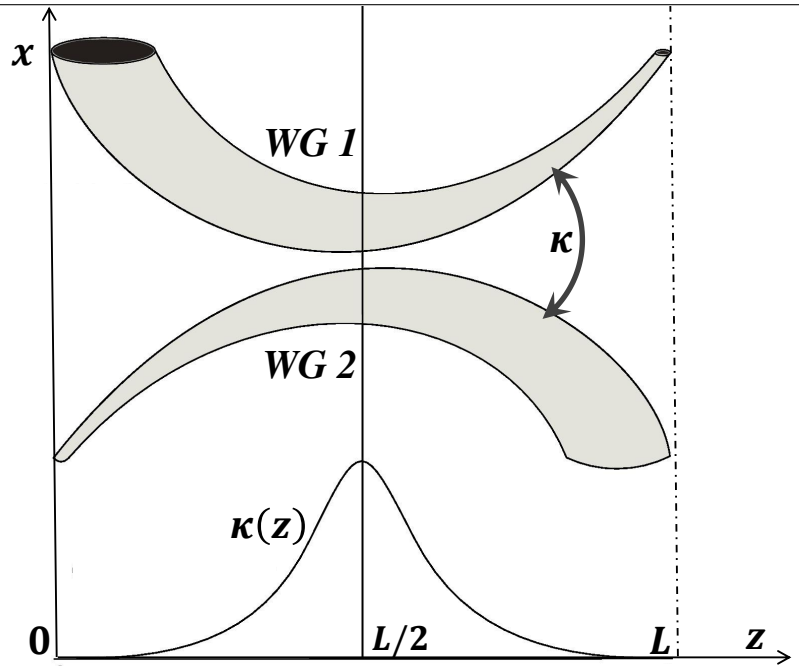

Figure 4.1: Schematic for adiabatic directional coupler with allen-Eberly coupling scheme. β_1 and β_2 are propagation constants for waveguide one and two respectively. Coupler length is L. Maximum of the coupling occurs at $L/2$.

invariant aproach to achieve power switching between the waveguides in relatively small propagation distances.

4.1 Two waveguide coupler

We consider a directional coupler of length L consisting of two lossless waveguides. These waveguides are considered to be single moded and weakly guiding with β_1 and β_2 as propagation constants of the waveguides respectively, which characterizes independent propagation modes inside the waveguides. The schematic of the system is shown in Fig. (4.1). Since we have chosen the waveguides in close proximity, coupled mode theory[140] can be used to estimate the power propagation in the coupler. In fact, it comes out that the prediction of the coupled mode theory very much resembles the Schrödinger equation for two level atomic system[8].

4.1.1 Coupled mode theory

Let us consider $n_1(x, y)$ and $n_2(x, y)$ be the refractive indices in the transverse plane, of waveguide 1 and 2 respectively. If ψ_j is the transverse mode field of the jth

waveguide, then the wave equation for individual waveguides can be written as:

$$\nabla_t^2\psi_j + \left[k_0^2 n_j^2(x,y) - \beta_j^2\right]\psi_j = 0; \qquad j = 1,2 \tag{4.1}$$

where $\nabla_t^2 = \frac{\partial^2}{\partial x^2} + \frac{\partial^2}{\partial y^2}$. β_j is the propagation constant of waveguide j in the absence of the other waveguide. Now, let $\Psi(x,y,z)$ be the total field of the entire directional coupler structure with weak interaction between the waveguides. Then we can write the wave equation as given below:

$$\nabla_t^2\Psi + \frac{\partial^2\Psi}{\partial z^2} + k_0^2 n^2(x,y)\Psi = 0 \tag{4.2}$$

Here $n(x,y)$ represents the refractive index variation of the coupler. Ψ can be mathematically written as the superposition of the fields ψ_1 and ψ_2,

$$\Psi(x,y,z) = B_1(z)\psi_1(x,y)e^{-i\beta_1 z} + B_2(z)\psi_2(x,y)e^{-i\beta_2 z} \tag{4.3}$$

$B_1(z)$ and $B_2(z)$ are the amplitudes of the fields in waveguide 1 and 2 respectively. These amplitudes are z dependent because of the coupling between the waveguides. For a large separation between the waveguides B_1 and B_2 would be z independent. From Eq. (4.2) and Eq. (4.3) we obtain a set of coupled equations, considering $B_1(z)$ and $B_2(z)$ to be slowly varying functions of z, as follows:

$$i\frac{dB_1(z)}{dz} = \kappa_{11}B_1(z) + \kappa_{12}e^{2i\Delta z}B_2(z) \tag{4.4}$$

$$i\frac{dB_2(z)}{dz} = \kappa_{21}e^{2i\Delta z}B_1(z) + \kappa_{22}B_2(z) \tag{4.5}$$

Here $\Delta = (\beta_1 - \beta_2)/2$ is the mismatch parameter and κ_{jk} is given by

$$\kappa_{jk} = \frac{k_0^2}{2\beta_j}\frac{\int\int_{-\infty}^{\infty}\psi_j^*\delta n_k^2\psi_k dxdy}{\int\int_{-\infty}^{\infty}\psi_j^*\psi_j dxdy}, \tag{4.6}$$

where $\delta n_k^2 = n^2(x,y) - n_k^2(x,y)$. κ_{11} and κ_{22} represents the corrections to the propagation constants β_1 and β_2 respectively and are generally neglected. κ_{12} and κ_{21} represents the coupling between the two waveguides. Eq. (4.4) and Eq. (4.5) can be written in a simpler form using the following transformation:

$$a_1(z) = B_1(z)e^{-i\Delta z}, \qquad a_2(z) = B_2(z)e^{i\Delta z} \tag{4.7}$$

Substituting Eq. (4.7) into Eq. (4.4) and Eq. (4.5) we finally obtain:

$$i\frac{da_1(z)}{dz} = \Delta a_1(z) + \kappa a_2(z) \tag{4.8}$$

$$i\frac{da_2(z)}{dz} = \kappa a_1(z) - \Delta a_2(z) \tag{4.9}$$

Here we have asumed $\kappa_{12} \simeq \kappa_{21} = \kappa$. The above equation are the so-called coupled mode equations for a two waveguide coupler.

4.1.2 Adiabaticity in two waveguide coupler

It is easy to recognize from Eq. (4.8 and 4.9) that in the diabatic basis $\{a_j\}$, there exists an operator similar to the Hamiltonian in quantum physics which can be written as

$$H = \begin{pmatrix} \Delta & \kappa \\ \kappa & -\Delta \end{pmatrix} \tag{4.10}$$

To study the adiabatic evolution, first we need to diagonalize Eq. (4.10). This Hamiltonian can be diagonalized using unitary transformation to a new basis $\{A_j\}$ which is basically the adiabatic basis, given by

$$\begin{pmatrix} A_1 \\ A_2 \end{pmatrix} = U_0^{-1} \begin{pmatrix} a_1 \\ a_2 \end{pmatrix} \tag{4.11}$$

where U_0 is two dimensional unitary matrix, and can be taken as

$$U_0 = \begin{pmatrix} cos(\theta/2) & -sin(\theta/2) \\ sin(\theta/2) & cos(\theta/2) \end{pmatrix} \tag{4.12}$$

Here θ is the angle of mixing and is defined as $tan(\theta) = \frac{\kappa(z)}{\Delta(z)}$. The transformed Hamiltonian will be:

$$H'(z) = U_0^{-1} H(z) U_0 - i U_0^{-1} \dot{U}_0 \tag{4.13}$$

where overdot represents derivative with respect to z. The second term is regarded as non adiabatic correction owing to the fact that the first term is diagonal itself and can drive the system adiabatically alone. The adiabatic criterion can be written as:

$$\dot{\theta}/2 \ll \sqrt{\Delta^2 + \kappa^2} \tag{4.14}$$

When Eq. (4.14) is satisfied, non-adiabatic corrections generally goes to zero. For adiabatic evolution we have followed a coupling-mismatch scheme that is very similar to the famous Allen-Eberly scheme[12,141] by choosing:

$$\Delta(z) = \Delta_0 \tanh[2\pi(z - \frac{L}{2})/L], \tag{4.15}$$

$$\kappa(z) = \kappa_0 \operatorname{sech}[2\pi(z - \frac{L}{2})/L], \tag{4.16}$$

The width of the pulse $\kappa(z)$ changes accordingly with the coupler length L and also the mismatch coefficient varies from $-\Delta_0$ to Δ_0. With both Δ and κ being z dependent, the coupler design can not be simple parallel waveguide structure. Rather, the distance between the waveguides will vary along z as depicted in Fig. (4.1). Since $\Delta(z) = (\beta_1 - \beta_2)/2$, the propagation constants become functions of z itself, which results in tapered structure of the waveguides. Moreover, the variation of $\Delta(z)$ should be slow enough to accomplish adiabatic evolution. Also for the choices in Eq. (4.15) and Eq. (4.16), the adiabatic condition itself is reduced to $\kappa_0 L \gg \pi$ and hence it demands the coupler length to be large.

4.1.3 TQD in two waveguide coupler

Under the circumstances when the adiabatic criterion can not be fulfilled, complete power switching does not occur due to the effect of the non-adiabatic terms in the Hamiltonian. To overcome this, we derive a driving Hamiltonian. One Hamiltonian, relevant to our system is simply given by: $H_a = i\sum_j |\partial_z A_j\rangle \langle A_j|$, which when transformed back to the basis $\{a_j\}$, eventually comes out to be

$$H_a = \begin{pmatrix} 0 & -i\dot{\theta}/2 \\ i\dot{\theta}/2 & 0 \end{pmatrix} \tag{4.17}$$

This additional Hamiltonian should be added back to our original Hamiltonian in order to undo the effects of the non-adiabatic terms, which leads to

$$H_{eff} = \begin{pmatrix} \Delta(z) & \kappa(z) - i\kappa_a(z) \\ \kappa(z) + i\kappa_a(z) & -\Delta(z) \end{pmatrix} \tag{4.18}$$

This induces an additional coupling, $\kappa_a = \dot{\theta}/2$ but with some phase difference with the original. Also κ_a should be comparable with κ because the dynamics with H does not need to follow the adiabatic condition. However, we can describe it as a

combination of an effective coupling and a phase term:

$$H_{eff} = \begin{pmatrix} \Delta(z) & \kappa_{eff}(z)e^{-i\phi} \\ \kappa_{eff}(z)e^{i\phi} & -\Delta(z) \end{pmatrix} \tag{4.19}$$

where $\kappa_{eff} = \sqrt{\kappa^2 + \kappa_a^2}$. Using the following transformation one can eliminate the phase dependence,

$$U_1 = \begin{pmatrix} e^{-i\phi/2} & 0 \\ 0 & e^{i\phi/2} \end{pmatrix} \tag{4.20}$$

which again provides a new set of basis $\{A'_j\}$, and the resulting Hamiltonian becomes:

$$H_{eff} = \begin{pmatrix} \Delta_{eff}(z) & \kappa_{eff}(z) \\ \kappa_{eff}(z) & -\Delta_{eff}(z) \end{pmatrix} \tag{4.21}$$

with $\Delta_{eff} = \Delta(z) - \dot{\phi}/2$. It is useful to note that $\{A'_j\}$ is related with the adiabatic basis $\{A_j\}$ by two transformations U_0 and U_1 via parameters θ and ϕ. To keep these bases consistent in terms of the initial and the final states, certain conditions need to be imposed. θ and ϕ has to be adjusted in such a way that $\{A_j\}$ and $\{A'_j\}$ becomes equivalent at the boundary, which leads to the boundary condition $\dot{\theta}(0) = \dot{\theta}(L) = 0$.

4.1.4 Invariant based STA in two waveguide coupler

The Hamiltonian (Eq. (4.10) can be written in the following form:

$$H(z) = \kappa(z)\sigma_x + \Delta(z)\sigma_z \tag{4.22}$$

Here σ_x, σ_y and σ_z are the well-known Pauli matrices for spin 1/2 particles. These operators satisfy Lie algebra: $[\sigma_i, \sigma_j] = 2\epsilon_{ijk}\sigma_k$. The Hamiltonian satisfies SU(2) symmetry and hence there exist an invariant which would satisfy the usual invariant equation: $\mathrm{d}I(z)/\mathrm{d}z = 0$. According to Lewis-Riesenfeld theory [28], this invariant can be written as follows:

$$I(z) = \frac{\Omega}{2} \begin{pmatrix} \cos\gamma(z) & \sin\gamma(z)\mathrm{e}^{-i\beta(z)} \\ \sin\gamma(z)\mathrm{e}^{i\beta(z)}e^{i\phi} & -\cos\gamma(z) \end{pmatrix} \tag{4.23}$$

Here Ω is an arbitrary constant which has the dimension of $\kappa(z)$. $\gamma(z)$ and $\beta(z)$ are the parameters which characterizes $I(z)$ and satisfies the following conditions:

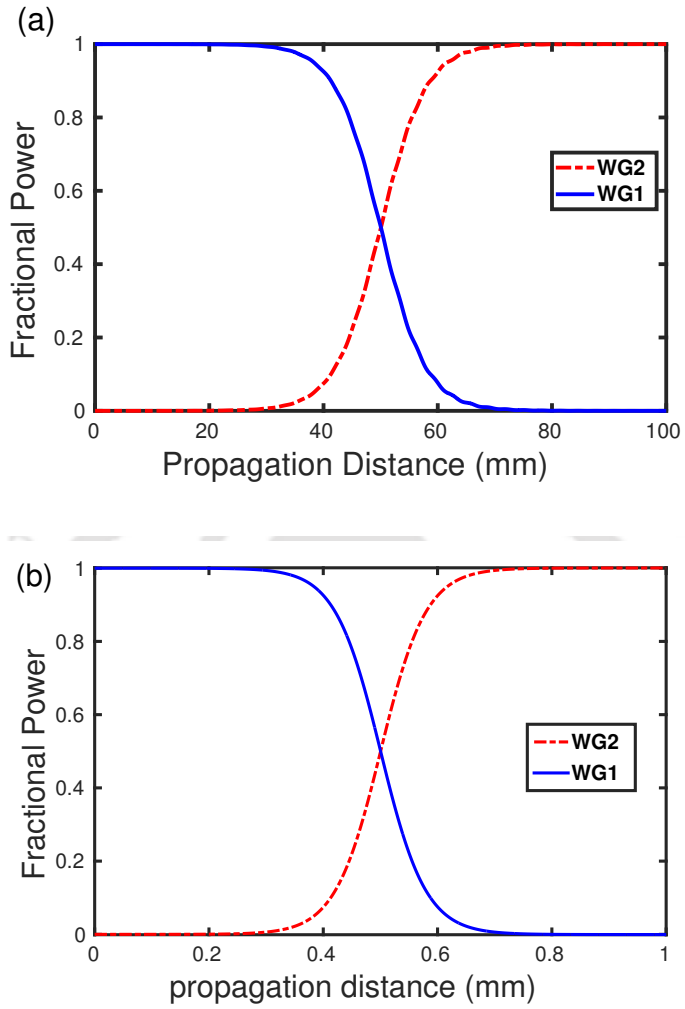

Figure 4.2: Spatial evolution of fractional beam power with respect to z for (a) adiabatic case with $L = 100mm$, (b) STA using TQD where $L = 1mm$,

$$\dot{\gamma}(z) = 2\kappa(z)\sin\beta(z) \tag{4.24a}$$

$$\left[2\Delta(z) + \dot{\beta}(z)\right]\sin\gamma(z) = 2\kappa(z)\cos\gamma(z)\cos\beta(z) \tag{4.24b}$$

It is important to note that $I(z)$ and $H(z)$ does not commute normally. To make $I(z)$ and $H(z)$ commute at the boundaries so that the eigenstates exactly match at the ends of the coupler, we impose $[H(0), I(0)] = 0$ and $[H(L), I(L)] = 0$. With straightforward calculations we obtain the following constraints:

$$\kappa(z)\sin\gamma(z)\sin\beta(z)\big|_{z=0,L} = 0 \tag{4.25a}$$

$$\left[\kappa(z)\cos\gamma(z) - \Delta(z)\sin\gamma(z)e^{\pm i\beta(z)}\right]\big|_{z=0,L} = 0 \tag{4.25b}$$

These constraints help us to determine the required boundary conditions for $\beta(z)$, $\gamma(z)$ and $\kappa(z)$. We find that, the boundary conditions can be satisfied only if $\kappa(0) = \kappa(L) = 0$ and $\sin\gamma(0) = \sin\gamma(L) = 0$. $\beta(z)$ helps us to configure $\kappa(z)$ and $\Delta(z)$. It is to be noted that β cannot be chosen to be zero as $\kappa(z)$ is finite. We chose $\beta(z)$ such that $\kappa(z)$ keeps its amplitude minimal. With the above considerations, we set the boundary conditions as follows:

$$\gamma(0) = \pi; \qquad \gamma(L) = 0 \tag{4.26a}$$

$$\dot{\gamma}(0) = 0; \qquad \dot{\gamma}(L) = 0 \tag{4.26b}$$

$$\beta(0) = -\frac{\pi}{2}; \qquad \beta(L) = -\frac{\pi}{2} \tag{4.26c}$$

$$\dot{\beta}(0) = \frac{3\pi}{2L}; \qquad \dot{\beta}(L) = -\frac{3\pi}{2L} \tag{4.26d}$$

Using the above boundary conditions, one can easily construct the parameters γ and β, and thereby all the other necessary parameters to study the evolution of optical power within the waveguides.

4.1.5 Results and discussion

In order to study the power evolution in the coupler via the TQD method we numerically solved the master equation for the density matrix

$$\dot{\rho} = -i[H, \rho] \tag{4.27}$$

for the Hamiltonians in Eq. (4.10) and Eq. (4.21). On the other hand, for the invariant method we solved the same equation using an inverse engineered Hamiltonian. ρ is the density matrix with matrix elements $\rho_{ij} = a_i a_j^*$. Diagonal elements $\rho_{ii} = |a_i(z)|^2$ represent the power in the i^{th} waveguide, while the off-diagonal elements refer to the coherence between the waveguides.

For the adiabatic coupler, forms of κ and Δ are taken as defined in Eq. (4.16) and Eq. (4.15). The TQD approach has been achieved by taking $\kappa_a = \dot{\theta}(z)$ into account. In Fig. (4.2). we showed the spatial evolution of power, defined by $P_i(z)/P_1(0)$. In our simulation, the input power in the first waveguide is taken to be unity, i.e., $P_1(0) = 1$, while the input power in the second waveguide is kept empty. Other parameters are chosen as $\Delta_0 = \kappa_0 = 1mm^{-1}$. Fig. (4.2a) depicts the power evolution of the adiabatic coupler where we have chosen large coupler length $L = 100mm$

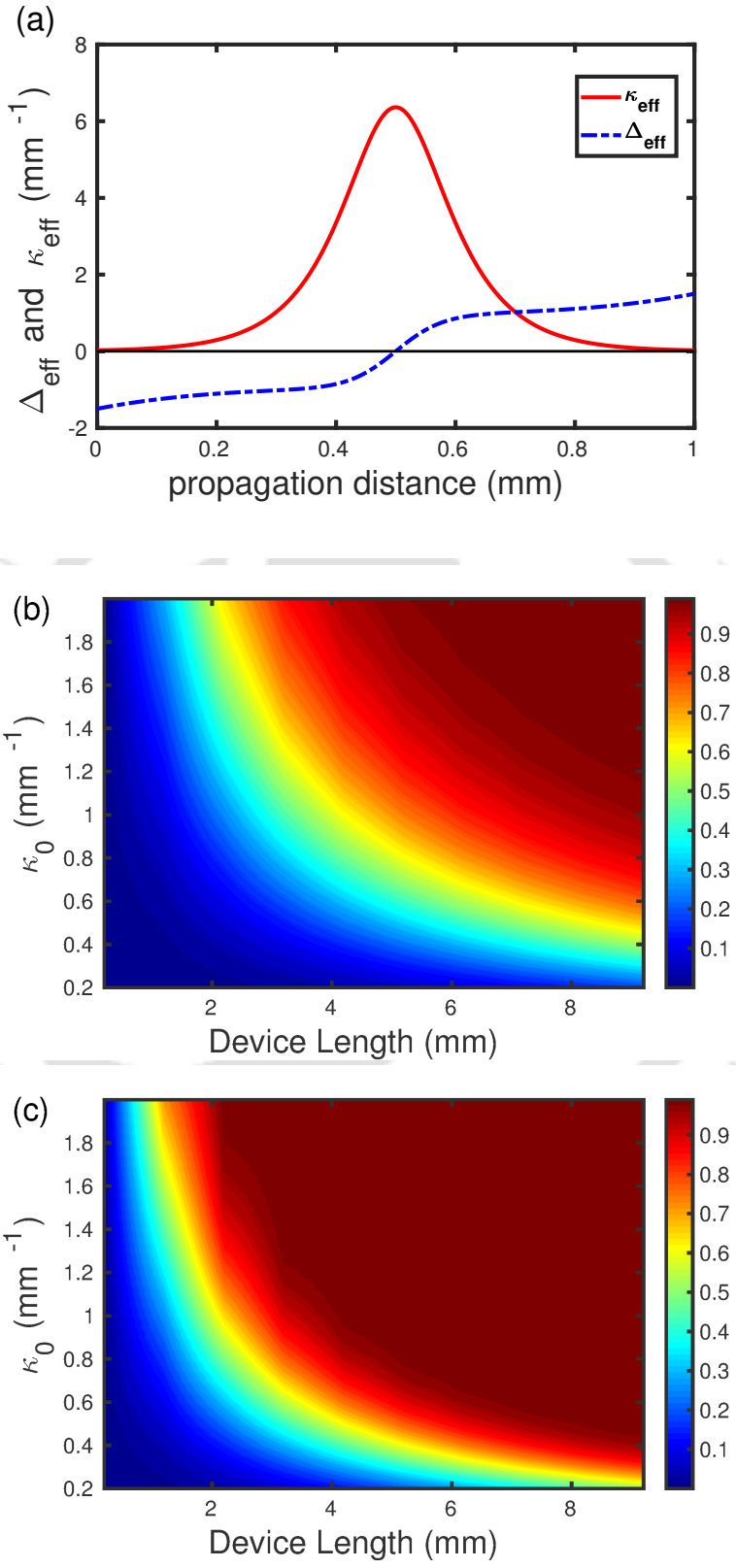

Figure 4.3: Spatial profile of coupling and mismatch. (a) $\Delta_{eff}(z)$ (dashed) and $\kappa_eff(z)$ (z) (solid) determined from transitionless driving method. Contour plots for output power with varying κ_0 and device length L. (b) for adiabatic coupler and (c) for STA coupler. STA coupler shows high fidelity over adiabatic coupler.

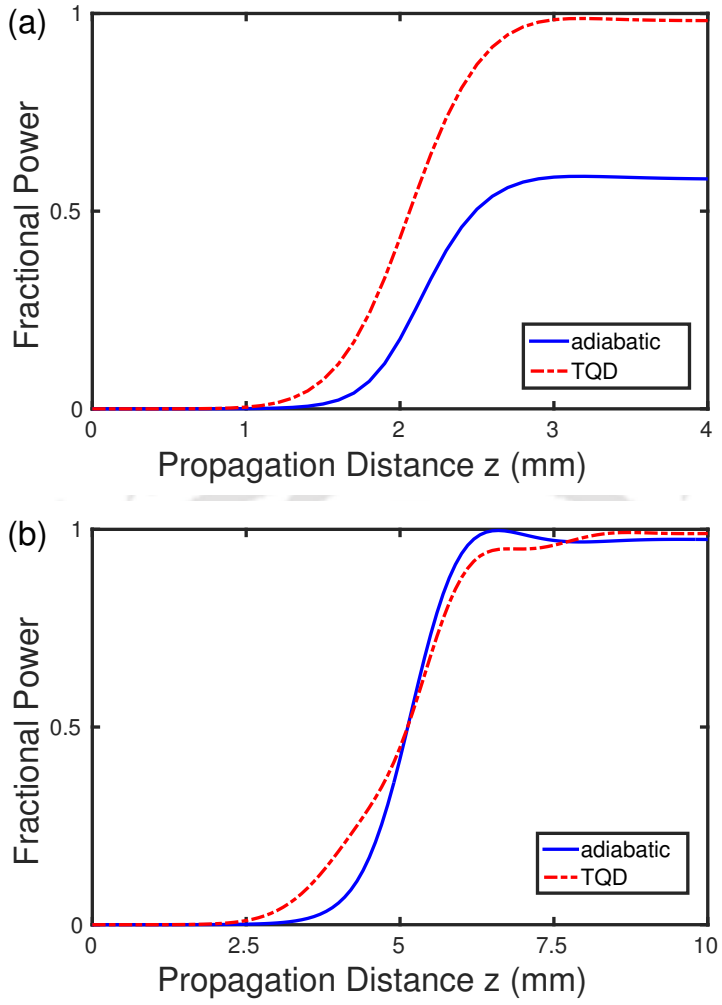

Figure 4.4: Fractional power output ρ_{22} vs propagation distance for $\Delta_0 = \kappa_0 = 1$ (a) for $L = 4mm$, (b) for $L = 10mm$.

which, indeed, satisfies the adiabatic condition. In passing, it is worthwhile to mention that the lengths chosen are not universal numbers and must depend on the waveguide parameters. Our choice of the lengths arose form practical consideration. However, the results and conclusion drawn are equally valid for other choice of lengths as well. It clearly shows complete power transfer. On the other hand, Fig. (4.2b) shows that for TQD, with κ_a taken into account, the power transfer can be achieved for infinitely short coupler length. However in real situations, it is difficult to design κ_a appropriately. Thus for TQD we confined our study with a particular choice of κ_a, given by:

$$\kappa_a = \kappa_0 exp(-(z - \frac{L}{2})^2/z_0^2) \tag{4.28}$$

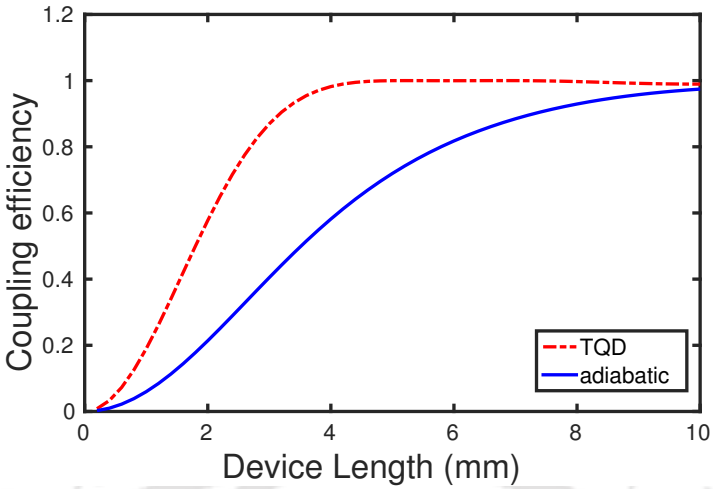

Figure 4.5: Coupling efficiency for adiabatic and STA coupler with varying device length. parameters are same as in Fig. (4.4)

where z_0 is the width of the Gaussian. z_0 is well adjusted with the varying coupler length so that the boundary conditions for θ has been satisfied, that is $\kappa_a \to 0$ at the boundary. Fig. (4.3a) depicts the spatial variation of mismatches and the coupling for TQD based STA coupler. The geometry of the coupler depends on the mutual coupling between the waveguides and the mismatch coefficient. Thus enhancement in those parameters indeed leads to the reshaping of the coupler. Stronger coupling refers to larger separation distances between the waveguides towards the ends the coupler, which indicates significant decrements in device length. On the other hand, the taper of the waveguides is controlled by the mismatch coefficient. As Δ goes higher, β_1 and β_2 tends to change more rapidly throughout the length L. As far as adiabaticity is concerned, larger $\kappa(z)$ is preferable for power transfer as it requires to satisfy the condition $\kappa_0 L \gg \pi$. However that does not contribute in shortening of the coupler length. Whereas in STA couplers, significant amount of coupling length can be reduced with little enhanced coupling.These facts can readily be seen in Fig. (4.3b) and Fig. (4.3c), where we have plotted the final power output as a function of the device length and the coupling amplitude. With a particular choice of $\Delta_0 = 1mm^{-1}$, contours reveal that for large variation of κ_0, the TQD approach shows much superiority in terms of robustness and fidelity in power switching. For any given value of κ_0, the minimum distance required to transfer power between waveguides with adiabatic coupler is at least greater than twice that of the STA couplers. In Fig. (4.4) we have shown the power evolution of the coupler. Parameters taken for this evolution are $\Delta_0 = \kappa_0 = 1mm^{-1}$. For smaller propagation

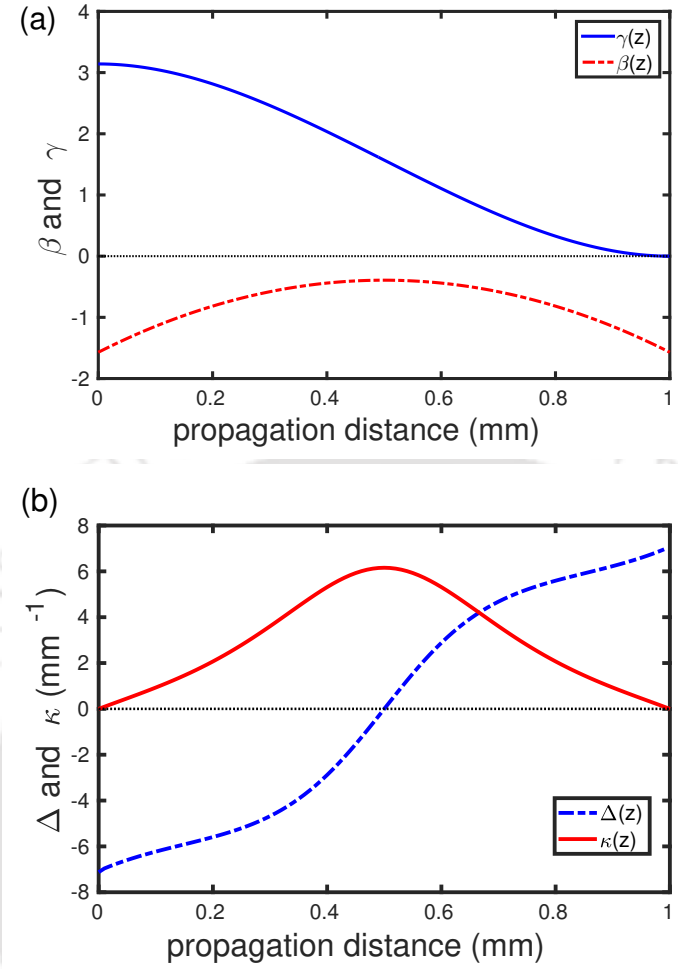

Figure 4.6: (a) Profile of $\beta(z)$ (dashed) and $\gamma(z)$ (solid), determined through polynomial ansatz with the coefficients determined using the boundary conditions, (b) Spatial profile of coupling and mismatch, $\Delta(z)$ (dashed) and $\kappa(z)$ (solid) determined through L-R Invariant based method.

distance, say $z < 4mm$ or so, the fractional power output at the second waveguide, using adiabatic dynamics, never reaches unity. It only shows high transfer probability for larger propagation distances, say $z > 10mm$ or so. However one can achieve nearly 100% power transfer to the second waveguide using the TQD approach. The coupling efficiency calculation also supports our previous results. Fig. (4.5) illustrates the efficiency of both the adiabatic and the TQD based STA coupler with respect to device length. It is quite clear from the plot that the STA coupler achieves 100% efficiency with much shorter distance compared to that of the adiabatic coupler.

For invariant based STA coupler, we followed the polynomial ansatz to interpo-

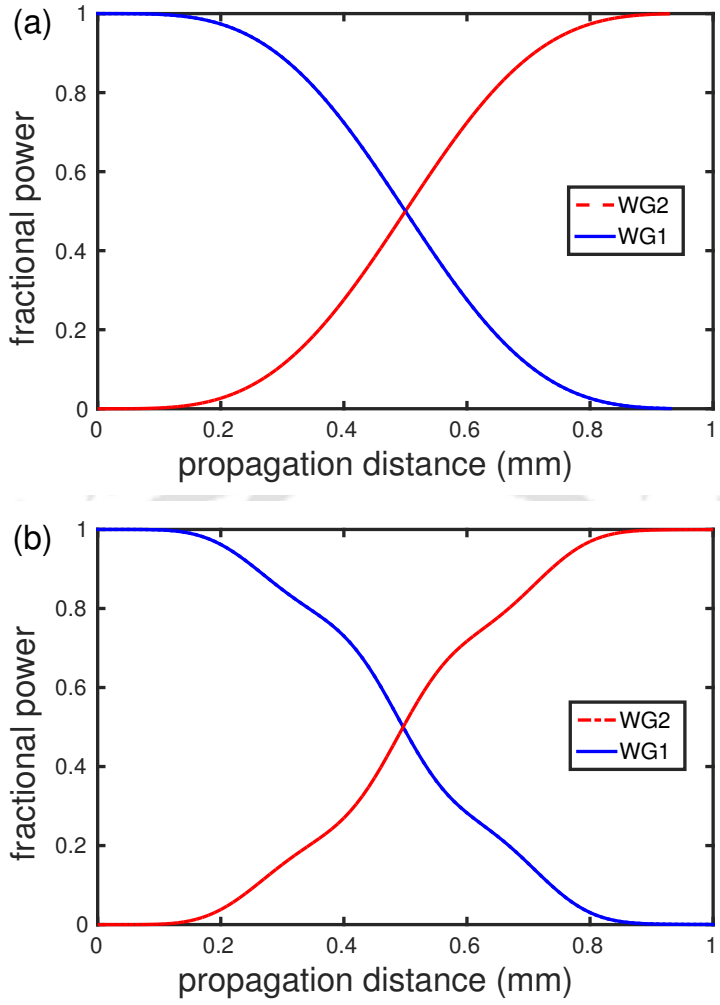

Figure 4.7: Spatial evolution of fractional beam power with respect to z for L-R invariant based approach, (a) using the designed Hamiltonian and (b) using the invariant.

late $\beta(z)$ and $\gamma(z)$ at the intermediate points. We choose them as: $\gamma(z) = \sum_{i=0}^{3} g_j z^j$ and $\beta(z) = \sum_{i=0}^{3} b_j z^j$, where g_js and b_js are determined using the boundary conditions in Eq. (4.26) which are have the following values:

$$g_0 = \pi; \qquad g_1 = 0 \tag{4.29a}$$

$$g_2 = -\frac{3\pi}{L^2}; \qquad g_3 = \frac{2\pi}{L^3} \tag{4.29b}$$

$$b_0 = -\frac{\pi}{2}; \qquad b_1 = \frac{3\pi}{2L} \tag{4.29c}$$

$$b_2 = -\frac{3\pi}{2L^2}; \qquad b_3 = 0 \tag{4.29d}$$

Fig. (4.6a) shows the spatial profile of $\gamma(z)$ and $\beta(z)$. The mismatch parameter $\Delta(z)$ and the coupling coefficient $\kappa(z)$ can be determined through the invariant method using following equations,

$$\kappa(z) = \frac{\dot{\gamma}(z)}{2\sin\beta(z)} \tag{4.30a}$$

$$\Delta(z) = \frac{1}{2}\dot{\gamma}(z)\cot\gamma(z)\cot\beta(z) - \frac{1}{2}\dot{\beta}(z) \tag{4.30b}$$

$\Delta(z)$ and $\kappa(z)$ are shown in Fig. (4.6b). Fig. (4.6) shows that the strength of the couplings determined from the L-R invariant method is almost the same as we have determined using the TQD (Fig. (4.3a)) technique. However, the mismatch is much larger in the case of the invariant method compared to the TQD technique. In Fig. (4.7a), for the spatial power evolution using L-R invariant, $\kappa(z)$ and $\Delta(z)$ are taken according to Eq. (4.24) and used in the original adiabatic Hamiltonian. It exactly shows the adiabatic nature of the evolution but requires very small coupler length for complete the power transfer. In Fig. (4.7b), we have used the L-R invariant instead of the actual Hamiltonian, which precisely matches with Fig. (4.7a) at the boundaries but does not follow the same adiabatic path.

With regard to the practical implementation of the scheme, one may design or fabricate a Silica (SiO_2)-based fiber coupler[136] using the proposed scheme. The effective coupling coefficient (κ_{eff} or the designed κ, for the invariant approach) is the most critical parameter in realizing the proposed waveguide. It could be manipulated with judicious choice of the core radius, the center-to-center separation between the waveguides, and the refractive index difference between the two waveguides. One may choose the parameter z_0 to obtain the effective κ_{eff} theoretically. And then, applying the appropriate mathematical relation between κ_{eff} and the coupler parameters, derivable using the coupled mode theory, one can decide upon the other coupler parameters[142].

4.2 Three waveguide coupler

The phenomenon of Stimulated Raman Adiabatic Passage (STIRAP) is also a well established method for population transfer among the atomic states. When two long lived energy states are connected via pump and Stokes pulses to a metastable state counter intuitively, population gets transferred between those log lived states leaving the metastable state empty. This idea of STIRAP has been studied rigorously

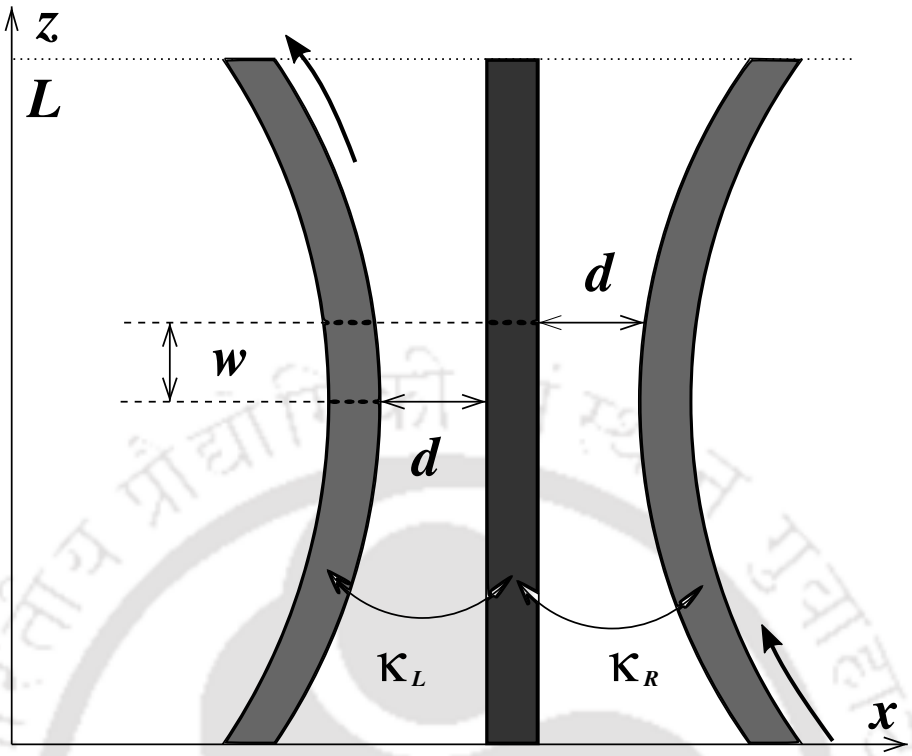

Figure 4.8: Schematic for three waveguide directional coupler with counter intuitive coupling scheme.

in the context of waveguide structures in recent past theoretically, and experiments are also performed to support it [81,84]. To realize such systems one can take three waveguides as shown schematically in Fig. (4.8). The central waveguide is straight and the waveguides on the left and the right are curved so that the separation among them varies along z. This makes the coupling strengths κ_L and κ_R, z dependent. The minimum distance d between the curved and the straight waveguide are displaced by a distance w to make the counter-intuitive coupling plausible, as shown in Fig. (4.8). To mimic the two photon resonance condition in case of STIRAP, the curved waveguides are chosen identical in nature with same propagation constant β_c whereas the straight one is different with slightly different propagation constant β_s. The Hamiltonian for this system, as calculated from the coupled mode theory, can be written as:

$$H = \begin{pmatrix} 0 & \kappa_L(z) & 0 \\ \kappa_L(z) & \Delta & \kappa_R(z) \\ 0 & \kappa_R(z) & 0 \end{pmatrix} \tag{4.31}$$

where Δ is the mismatch between the straight and the curved waveguides which

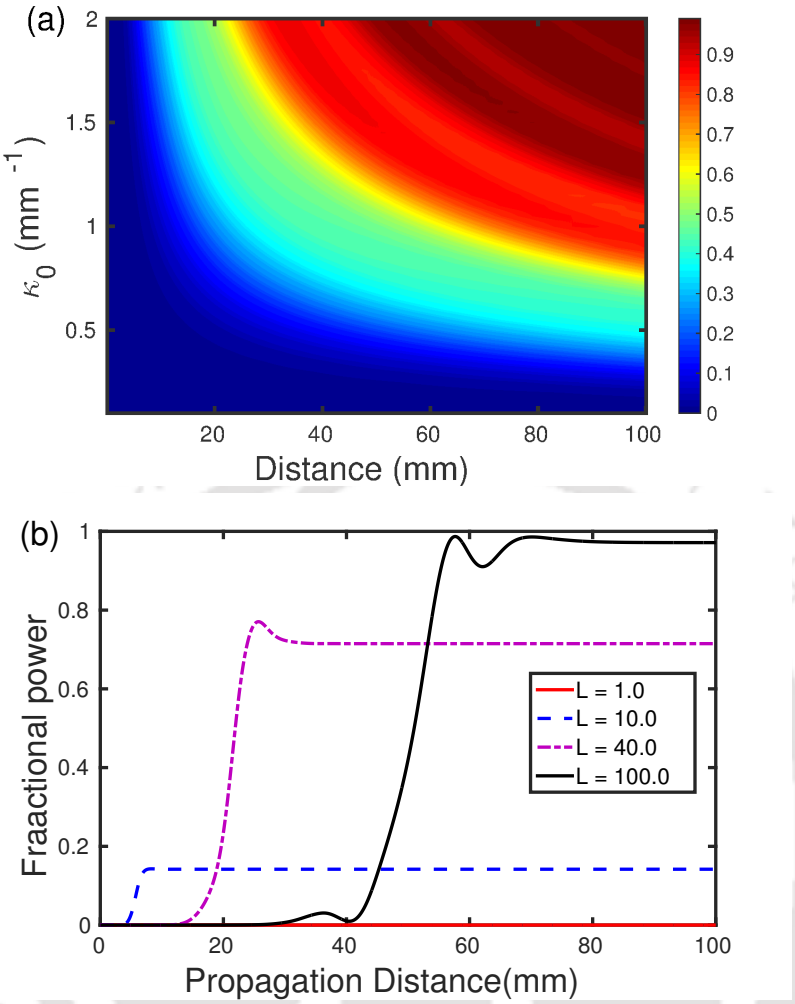

Figure 4.9: (a) Contour plots for output power with varying κ_0 and device length $L = 100mm$ for adiabatic coupler, (b) fractional beam power output vs. propagation distance for $\Delta_0 = \kappa_0 = 1$, adiabatic coupler takes long propagation distance to complete power switch.

is given by $\Delta = \beta_s - \beta_c$. The couplings $\kappa_R(z)$ and $\kappa_L(z)$ are chosen in the following way:

$$\kappa_L(z) = \kappa_0 \,\mathrm{sech}[2\pi(z - z_1)/L], \tag{4.32}$$

$$\kappa_R(z) = \kappa_0 \,\mathrm{sech}[2\pi(z - (z_1 + w))/L], \tag{4.33}$$

When power is launched through one of the curved waveguides, say the one on the left, the power switches to the other waveguide on the right, while power inside the central waveguide remains zero. In Fig. (4.9a) we have plotted the final power

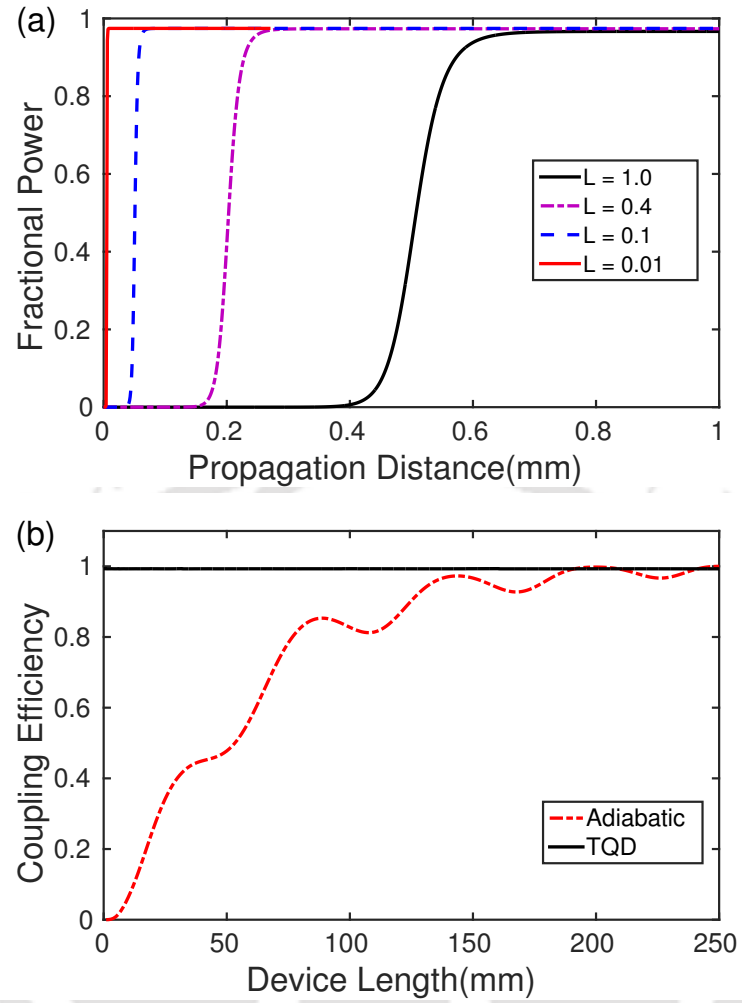

Figure 4.10: (a) fractional beam power output vs. propagation distance for $\Delta_0 = \kappa_0 = 1$, three waveguide STA coupler shows complete power switching regardless of the propagation distance. (b) Coupling efficiency for adiabatic and STA coupler with varying device length.

output (as defined in the previous section) of the right waveguide as a function of the device length and the coupling amplitude. It clearly shows that for adiabatic counter-intuitive approach, one requires large coupling strength and large device length. It is also evident from Fig. (4.9b), where complete power transfer occurs only when the propagation distance is large (close to $100mm$). For smaller distances it barely reaches to unity.

To achieve shortcut, we followed the TQD approach which leads us to the short-

cut Hamiltonian[12]

$$H_1 = \begin{pmatrix} 0 & 0 & i\kappa_a(z) \\ 0 & 0 & 0 \\ -i\kappa_a(z) & 0 & 0 \end{pmatrix} \tag{4.34}$$

Here κ_a is the additional coupling required to overcome the adiabatic criterion and can be written as

$$\kappa_a(z) = \frac{\dot{\kappa}_L(z)\kappa_R(z) - \dot{\kappa}_L(z)\kappa_R(z)}{\kappa_L^2 + \kappa_R^2} \tag{4.35}$$

One noticeable point is that H_1 exhibits coupling between the left and the right waveguides, which is not possible in a planer structure. Hence it requires a three dimensional structure where the central waveguide can be taken in a different plane from the curved waveguides. The power evolution in Fig. (4.10a) shows that, for such configuration power switching can be achieved with very short propagation distances, which eventually leads to the minimization of coupler length. Fig. (4.10b) shows the coupling efficiency with varying device lengths and the output power remains close to unity regardless of the length of the coupler, whereas for the adiabatic approach the efficiency reaches to unity only for large lengths.

4.3 Chapter summary

We have proposed a novel method for highly efficient power transfer in a directional coupler based on STA techniques. The variation in the propagation constants $\beta_1(z)$ and $\beta_2(z)$ (and thereby $\Delta(z)$) for the two waveguide coupler could be achieved by varying the cross-sectional area of the waveguides along the direction of propagation. On the other hand, the coupling parameter $\kappa(z)$ can be adjusted by controlling the adjacent distance between the waveguides. The coupler is studied in the adiabatic regime followed by the application of the TQD and the L-R invariant techniques. It turns out that by using shortcuts, one can reduce the length of the coupler significantly, keeping the power transfer efficiency nearly 100%. This study may open new possibilities of exploiting the STA methods and Allen-Eberly schemes for various applications in integrated optics, specifically within the context of photonic circuits.

Chapter 5

Nonlinear compression of temporal solitons in an optical waveguide via inverse engineering

Solitary waves are localized waves that propagate without any temporal evolution in shape or size when viewed in the reference frame, moving with the group velocity of the wave[143]. The envelope of a solitary wave has one global peak and decays far away from the peak. On the other hand soliton is a nonlinear solitary wave with the additional property that the wave retains it's permanent structure, even after interacting with another soliton. In physics the terms soliton and solitary waves are generally used in the same spirit. In this work, we also take solitary wave and soliton to have the same meaning. Solitons are universal in nature and observed in various platforms ranging from plasmas and fluids to chemical, biological, solid-state, optical and magnetic systems[95–97,144,145]. In this chapter we focus on temporal bright solitons. Temporal bright solitons are formed due to precise balance of the linear group velocity dispersion (GVD) and the positive self-phase modulation (SPM). Here we consider a passive nonlinear Schrödinger system with constant GVD parameter and distributed nonlinear parameter. The system consists of a passive waveguide with varying nonlinearity and we study the compression of temporal bright solitons in it.[1]

We propose a novel method based on the STA techniques to achieve fast compression of solitary waves. Although, in the context of soliton compression, adiabatic methods have been explored earlier in various contexts[107,109,146], very few attempts

[1]Part of the results presented in this chapter have been published in a paper, K. Paul and A. K. Sarma, "*Nonlinear compression of temporal solitons in an optical waveguide via inverse engineering*" , Europhys. Lett **121**, 64001 (2018).

have been made to achieve soliton compression using STA methods. In this regard, one particular study worth mentioning is that of Jing Li *et al.*, where they proposed a method to achieve controlled compression of soliton matter waves in harmonic traps by tunable interaction using STA[110]. In the context of fiber optics, various studies, both theoretically and experimentally, demonstrated the adiabatic soliton compression in optical fibers. The primary disadvantage of such schemes is that one needs a very long fiber. In this work, for the first time to the best our knowledge, we propose a scheme to obtain temporal soliton compression in a nonlinear waveguide at an arbitrarily small length using the shortcut to adiabatic passage technique. The scheme proposed in this work is a combination of the Lagrangian variational approach with STA, first introduced by Jing Li *et al.*[110] in the context of soliton matter waves. It is worthwhile to note that the soliton compression was first elaborated theoretically, using the variational approximation, by Anderson *et al.*[147]. In this work, authors suggested a scheme to compress soliton by engineering the dispersion but keeping the nonlinear coefficient constant. Incidentally, this theoretical prediction was realized experimentally by K. Bertilsson *et al.*[148].

5.1 The model and theory

The general nonlinear wave equation governing pulse propagation in an inhomogeneous passive nonlinear waveguide can be written as[149]:

$$i\frac{\partial\psi}{\partial z}+\frac{\beta_2(z)}{2}\frac{\partial^2\psi}{\partial t^2}+\tilde{\gamma}(z)|\psi|^2\psi=0, \tag{5.1}$$

where, ψ is the beam envelope, β_2 the group velocity dispersion (GVD) parameter. $\tilde{\gamma}$ is the distance dependent nonlinear parameter, with $\tilde{\gamma}(z)=\tilde{\gamma}(0)f(z)$, where $f(z)$ is dimensionless, whereas $\tilde{\gamma}(0)$ has the dimension of $m^{-1}W^{-1}$. Eq. (5.1) could be written in dimensionless form as follows:

$$i\frac{\partial u}{\partial\xi}+\frac{1}{2}\frac{\partial^2 u}{\partial\eta^2}+\gamma|u|^2u=0, \tag{5.2}$$

where $u(\xi,\eta)$ is the normalized amplitude and

$$u=\sqrt{P_0}N\psi, \qquad \eta=t/T_0, \qquad \xi=z/L_D \tag{5.3}$$

in which ξ and η are the normalized propagation distance and time respectively, P_0 is the peak power of the incident pulse and T_0 is the initial pulse width. Also $L_D=$

$T_0^2/|\beta_2|$ is the dispersion length and $N = \sqrt{\tilde{\gamma}(0)P_0L_D}$ is the so called soliton order. In this work, we assume that β_2 is a constant and independent of the propagation distance, while we term $\gamma[= f(\xi)]$ as the dimensionless distance dependent nonlinear parameter. It is worth mentioning that, Eq.(5.1) is valid for input pulse as short as $T_0 = 5ps$. For $T_0 < 5ps$, it is necessary to include higher order nonlinear and dispersive effects such as third-order dispersion, self-steepening and intrapulse Raman scattering effects[145]. Eq. (5.2) has the following well-known (scaling) bright solitary wave solution, given by[150]:

$$u(\xi,\eta) = A(\xi)\,\mathrm{sech}\left[\frac{\eta'}{\alpha(\xi)}\right]\exp\left[i\beta(\xi)\eta'^2 + i\epsilon(\xi)\eta' + i\phi(\xi)\right] \tag{5.4}$$

where $\eta' = \eta - \zeta(\xi)$. Here $A(\xi)$, $\alpha(\xi)$, $\beta(\xi)$, $\epsilon(\xi)$, $\zeta(\xi)$ and $\phi(\xi)$ represent the amplitude, width, chirp, velocity, center position and phase respectively. These are all real functions. It is easy to get that, $\int_{-\infty}^{\infty}|u|^2\,d\eta = 2\alpha A^2 = 2N$,where N is the normalization parameters, such that, $A = \sqrt{N/\alpha}$.

5.1.1 Variational analysis

In this section we apply the variational method, to study the dynamics of soliton width[151–153]. The Lagrangian density[154] corresponding to Eq. (5.2) is:

$$\mathscr{L} = \frac{1}{2}\left(\frac{\partial u}{\partial\xi}u^* - \frac{\partial u^*}{\partial\xi}u\right) - \frac{1}{2}\left|\frac{\partial u}{\partial\eta}\right|^2 + \frac{1}{2}\gamma(\xi)|u|^4 \tag{5.5}$$

Now, inserting Eq. (5.4) into Eq. (5.5), we can find the Lagrangian, $L = \int_{-\infty}^{\infty}\mathscr{L}\,d\eta$. Using the Euler-Lagrange formulas, $\frac{\delta L}{\delta q} = 0$, where q represents one of the parameters $\alpha(\xi)$, $\beta(\xi)$, $\epsilon(\xi)$ and $\zeta(\xi)$, we obtain the following set of coupled differential equations:

$$\frac{d\alpha}{d\xi} = 2\alpha\beta \tag{5.6a}$$

$$\frac{d\beta}{d\xi} = \frac{4}{\pi^2\alpha^4} - 2\beta^2 - \frac{2\gamma N}{\pi^2\alpha^3} + f_0 \tag{5.6b}$$

$$\frac{d\epsilon}{d\xi} = 0 \tag{5.6c}$$

$$\frac{d\zeta}{d\xi} = \epsilon \tag{5.6d}$$

It should be noted that $\frac{\delta L}{\delta \phi} = 0$, implying that ϕ does not play any role in the variational dynamics and hence we put $\phi = 0$ in the rest of the work. Above set of equations could be simplified to the following equations involving only the two main parameters, α and ζ:

$$\ddot{\alpha} = \frac{8}{\pi^2\alpha^3} - \frac{4\gamma N}{\pi^2\alpha^2} \tag{5.7}$$

$$\ddot{\zeta} = 0 \tag{5.8}$$

where dot refers to derivative with respect to ξ. It is obvious from the above equation that the width of the solitary wave, α, is dependent of the Kerr parameter γ. The realistic solution of Eq. (5.8) is simply $\zeta(\xi) = 0$. Thus, we will focus on Eq. (5.7) only for inverse engineering.

5.2 Compression via adiabatic process

Our objective is to achieve fast and perfect solitary wave compression, by judicious designing of the nonlinear Kerr parameter γ, from initial state $u(0,\eta)$ to the final state $u(\xi_f,\eta)$. The expression for $u(0,\eta)$ and $u(\xi_f,\eta)$ are given as follows:

$$u(0,\eta) = \sqrt{\frac{N}{\alpha(0)}}\,\mathrm{sech}\left[\frac{\eta}{\alpha(0)}\right]\exp\left(i\frac{\dot{\alpha}(0)}{2\alpha(0)}\eta^2\right) \tag{5.9a}$$

$$u(\xi_f,\eta) = \sqrt{\frac{N}{\alpha(\xi_f)}}\,\mathrm{sech}\left[\frac{\eta}{\alpha(\xi_f)}\right]\exp\left(i\frac{\dot{\alpha}(\xi_f)}{2\alpha(\xi_f)}\eta^2\right) \tag{5.9b}$$

It may be useful to note that Eq. (5.7) is analogous to a classical particle moving with kinetic energy $\frac{1}{2}\dot{\alpha}^2$, and potential energy of the following form:

$$V(\xi) = \frac{4}{\pi^2\alpha^2} - \frac{4\gamma N}{\pi^2\alpha} \tag{5.10}$$

This enables us to get the adiabatic reference for soliton compression. $\partial V/\partial\alpha = 0$ gives the minimum point of potential, *i.e.*,

$$\alpha_m(\xi) = \frac{2}{\gamma(\xi)N} \tag{5.11}$$

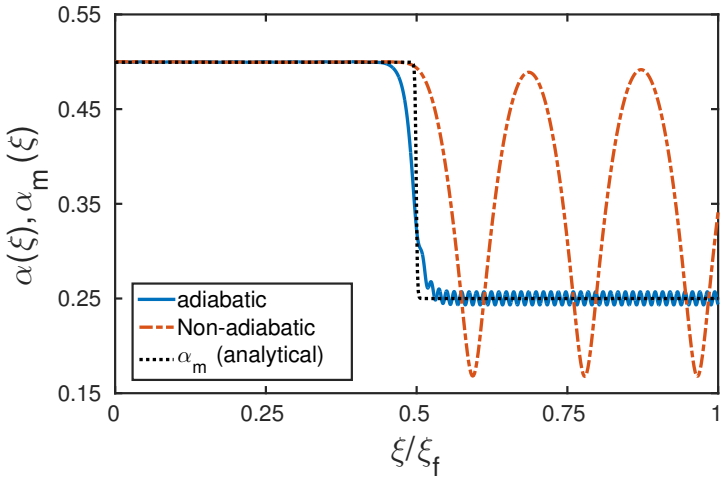

Figure 5.1: Comparison of the compression of Soliton width $\alpha(\xi)$ as a function of ξ with $\gamma_0 = 2$. Adiabatic compression (solid blue) is achieved for $\lambda = 1$, $\delta = 1$, $\xi_f = 50$. Non adiabatic compression (dash-dotted brown) is shown for $\lambda = 1$, $\delta = 10$, $\xi_f = 5$. $\alpha_m(\xi)$ using Eq. (5.11) (dotted black) follows adiabatic path exactly.

Eq. (5.11) yields the minimum perturbed potential of an effective particle, also giving us the adiabatic reference when Kerr nonlinearity $\gamma(\xi)$ is given. The soliton width will be minimum at the minima of this potential. The minimum attainable soliton width, $\alpha_m(\xi)$, explicitly depends on the non-linearity function $\gamma(\xi)$, and it gives us the estimation of compression that can be achieved by adiabatic compression. Hence $\alpha_m(\xi)$ provides the *adiabatic reference* for soliton compression. In this work, we choose the following switching function $\gamma(\xi)$ as given below:

$$\gamma(\xi) = \gamma_0 + \lambda\big[1 + \tanh\big\{\delta(\xi - \frac{\xi_f}{2})\big\}\big] \tag{5.12}$$

Here λ and δ are the control parameters and ξ_f is the final distance. γ_0 is the nonlinear parameter without the control. To understand the adiabatic reference one needs to solve Eq. (5.7) numerically and compare it with $\alpha_m(\xi)$. It is found that $\alpha(\xi)$, the solution of Eq. (5.7) coincides with the minimum value of $\alpha_m(\xi)$ adiabatically.

Fig. (5.1) demonstrates the evolution of temporal soliton width as a function of distance for both adiabatic and non-adiabatic cases. Here we compare the exact result obtained by solving Eq. (5.7) with the adiabatic reference, given by Eq. (5.11). We observe that the exact result nearly matches the adiabatic result; the pulse gets compressed from its initial value $\alpha = 0.5$ to $\alpha = 0.25$ after propagating a distance, $\xi = 50$, for the chosen parameters. On the other hand, while propagating a distance

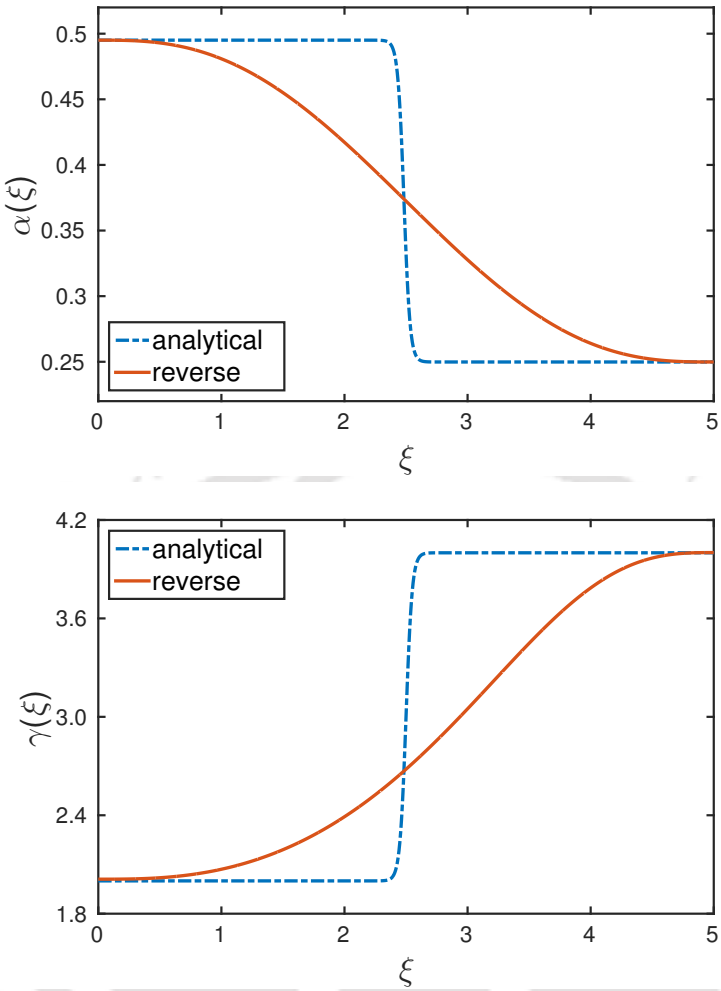

Figure 5.2: Controlling Soliton width using reverse engineering, (a) $\alpha(\xi)$ analytical (dash-dotted blue) and reverse engineered (solid brown) and (b) Non-linearity parameter $\gamma(\xi)$ as chosen in Eq. (5.12) (dash-dotted blue) and reverse engineered (solid brown) with the parameters $\lambda = 1$, $\delta = 10$, $\xi_f = 5$ and $\gamma_0 = 2$.

on the order of $\xi = 5$, the adiabatic reference is no longer followed and one cannot obtain effective pulse compression at such shorter distance. The compression of soliton width requires large propagation distance and low switching rate (small δ). It is quite difficult to achieve the same amount of compression in smaller propagation distances in such set up. However one can use inverse engineering approach in order to create desired compression within small ξ_f value. It should be noted that the amount of compression could be controlled by controlling λ. Higher compression ($\alpha(\xi_f) < 0.25$) can be achieved for larger λ values.

5.3 Compression via inverse engineering

To inverse engineer this system, we choose a set of predefined initial and final state of $\alpha(\xi)$ which coincides with $\alpha_m(\xi)$ and design it using polynomial ansatz[155–157] given by

$$\alpha(\xi) = \sum_{j=0}^{5} a_j \xi^j \tag{5.13}$$

However this needs the application of appropriate boundary conditions. To fix the initial and the final value of the width we set:

$$\alpha(0) = \alpha_m(0), \qquad \alpha(\xi_f) = \alpha_m(\xi_f) \tag{5.14}$$

Another set of boundary conditions is required to satisfy the continuity of $\alpha(\xi)$, which are given by:

$$\dot{\alpha}(0) = \dot{\alpha}_m(0), \qquad \dot{\alpha}(\xi_f) = \dot{\alpha}_m(\xi_f) \tag{5.15}$$

$$\ddot{\alpha}(0) = \ddot{\alpha}_m(0), \qquad \ddot{\alpha}(\xi_f) = \ddot{\alpha}_m(\xi_f) \tag{5.16}$$

a_j's can be found using the boundary conditions stated in Eq. (5.14), (5.15) and (5.16). These boundary conditions preserves the widths at the beginning and at the end of the waveguide, and enables us to perform adiabatic like fast compression. The nonlinearity parameter $\gamma(\xi)$ can also be reverse engineered via Eq. (5.7) and thereby reverse engineered $\alpha(\xi)$. Note that this should also match with the initial and the final value of $\gamma(\xi)$ regardless of the propagation distance.

Fig. (5.2) depicts the reverse engineered soliton pulse width and the corresponding nonlinear profile as a function of distance. It could be observed From Fig. (5.2a) that the soliton pulse width does not follow the adiabatic reference, however, the initial and the final width do coincide. This clearly implies that we can obtain soliton pulse compression by using reverse engineering. Fig. (5.2b) show how to engineer, with respect to the original nonlinearity given by Eq. (5.12), the nonlinear profile of the waveguide with distance in order to achieve efficient soliton compression at a very short distance. In fact one can obtain soliton compression by this technique at an arbitrarily small distance, in principle. It is worthwhile to note that once the desired profile for $\alpha(\xi)$ is chosen, then $\gamma(\xi)$ could be determined (or rather inverse engineered) using Eq. (5.7). However to choose the desired profile for $\alpha(\xi)$, we need the non-linear switching function. To estimate the amount of compression using Eq. (5.12), one requires to define $\gamma(\xi)$ using the parameter λ, δ and γ_0. These

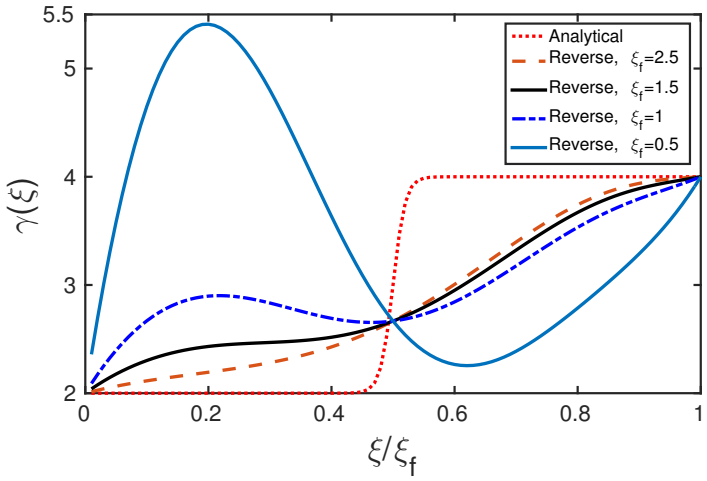

Figure 5.3: Comparison of reverse engineered nonlinear profile $\gamma(\xi)$ with different ξ_f with $\lambda = 1$ and $\xi_f \times \delta = 50$.

parameters determine how much compression can be achieved for a particular set up. Moreover, for the designing of $\alpha(\xi)$, appropriate boundary conditions are required which are given by Eq. (5.14)-(5.16) and the switching function is needed to determine those conditions. It can also be seen from Fig. (5.2b) that the inverse engineered profile of nonlinearity is smoother compared to that given in Eq. (5.12). It shows less switching rate which may be easier to design for practical purposes.

It should be noted that, theoretically and in principle, one could compress a soliton pulse at an arbitrarily small length. However, it may not be realistic as elucidated in Fig. (5.3), which depicts the nonlinear profiles for various lengths of the fiber. It is easy to observe that as one decreases the length of the fiber, the corresponding reverse-engineered nonlinear profile may no longer remains smooth enough for practical implementation. Also, it may be noted that in order to compress a soliton over a very small distance one needs to increase the optical power of the input pulse. This is because, the dispersion length is inversely proportional to the input peak power of the fundamental soliton; for a fundamental soliton N=1. In passing,this issue is reminiscent of the STA protocol proposed in Ref.[158] where having adiabatic transformation between two equilibrium states in an arbitrarily short time span implies a growth of the transient energies and thus limiting the attainment of arbitrarily small final time duration. As an estimate, we may take $\xi_f = 1$ or $z_f = L_D$ as the limiting value. If one takes the fiber length $z_f < L_D$, the peak value of $\gamma(\xi)$ becomes arbitrarily large and the profile shows oscillatory behaviour. In order to illustrate the STA compression in Fig. (5.4a) we plot the

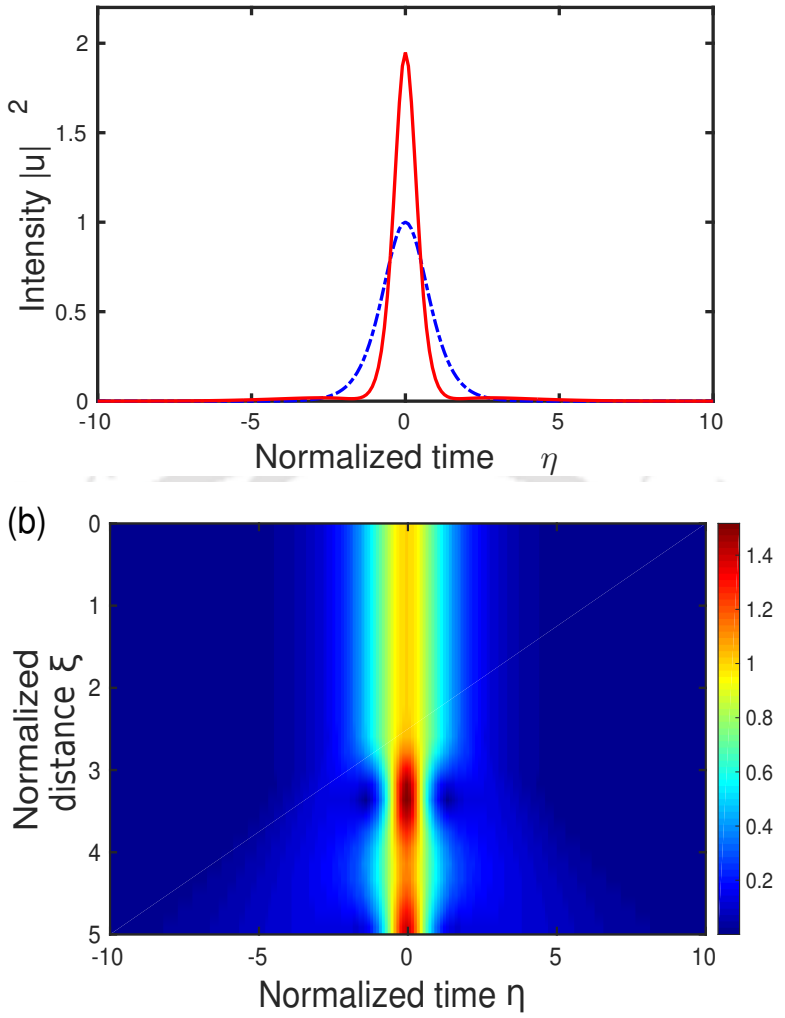

Figure 5.4: (a) Soliton intensity at the input (dotted blue) and the output (solid red) end. (b) Contour plot for spatio-temporal evolution of soliton intensity.

initial and the final soliton pulse profile. On the other hand, Fig. (5.4b) depicts the contour plot for spatio-temporal evolution of soliton intensity. It can be seen that soliton propagation through the STA engineered waveguide is fairly stable. Finally, to have an idea about the utility of the proposed scheme, let us consider a silica optical fiber with $\beta_2 = -20ps^2/km$[145]. Some quick calculations based on the results as illustrated above, we find that the temporal soliton pulse could be compressed from its initial pulse width say, 10 ps to a final pulse width 5 ps, within a length of just 5 km only. This may be considered as a significant improvement over the scheme proposed by Anderson *et al.*[147] and, experimentally verified by by K. Bertilsson *et al.*[148], where adiabatic soliton compression was achieved by

engineering the dispersion but keeping nonlinear coefficient constant. K. Bertilsson *et al.* used a 40 km long fiber to compress a soliton with initial pulse width of 11 ps by a factor of 2.4. One can achieve much higher compression if the nonlinearity profile is designed with a larger λ value. Again, if the scheme is applied to some other waveguides, made of materials other than pure silica, where the GVD parameter, β_2, is quite high, the scheme may be quite successful. For example, one may think of using SOI-based channel waveguides where $\beta_2 = -370ps^2/km$[159] which is near 18 times in magnitude than that of the so-called silica fiber. We anticipate that the proposed scheme could be used for generation of ultrashort soliton pulses apart from numerous possible pulse-compression related applications.

5.4 Chapter summary

Using inverse engineering, we proposed a novel method for temporal soliton compression in a nonlinear waveguide. Starting with a bright solitary wave solution for nonlinear Schrödinger equation, we performed variational analysis in order to find the dynamics of soliton width. We find that the minimum possible soliton width can be achieved only adiabatically for large fiber length. However by inverse engineering of the nonlinearity, based on STA, we demonstrate that soliton compression could be achieved, in principle, at an arbitrarily small distance. This could possibly be exploited for various short-distance communication related applications of temporal soliton and may be even in nonlinear guided wave-optics devices.

Chapter 6

Fast and efficient wireless power transfer via transitionless quantum driving

In modern age, various wireless technologies play crucial role in our day-to-day life. Since the early days of electromagnetics, significant progress has been made in transferring information via wireless communication. In contrast, wireless power transfer[1] (WPT) gained little progress in the last century. However, recent tide in the use of electronic appliances and requirement for short and mid-range wireless energy exchange has helped WPT getting tremendous attention, and studies on WPT systems has gained momentum in the past few years[160,161]. In a recent landmark paper[113], Soljačić's group experimentally demonstrated non-radiative power transfer over a reasonable distance, using self-resonant coils in the strong coupling regime. Since then, studies on WPT experienced a huge leap in number of studies. Various arrangements and different techniques such as, magnetically coupled resonators[116], planar resonators[162], spiral rasonators[163], capacitor loaded loop structures[164,165] and even for bio-medical implants[166–168], are studied in this regard. In all these studies it is extremely important to maintain the resonance in between the coils that are used for WPT. Otherwise it may result in decrease in the efficiency[119]. Few studies has been put forward to solve this issue[120–122]. WPT is also dependent on the coupling distance between the coils and it has been shown in few articles that, in the strong coupling regime, it is possible to enhance efficiency for larger distances[113,117,169].

[1]The results presented in this chapter have been published in a paper, K. Paul and A. K. Sarma, " *Fast and efficient wireless power transfer via transitionless quantum driving* " , Sci. Rep. **8**, 4135 (2018).

In this chapter, we study WPT in a system of two inductively coupled coils, having different resonant frequencies, by exploiting the adiabatic and the TQD techniques. It turns out that, while the TQD based method is much more efficient than the adiabatic one, it requires faster frequency sweep between the two coils. Using coupled mode theory[170], we find out the governing equations (which are similar to the Schrödinger equation for two level system) and devise power transfer mechanism which is impervious to the coupling strength and distance between the coils and intrinsic losses present in the system.

6.1 Coupled mode theory

Let us consider a loss-less LC circuit, with current $I(t)$ flowing in it and voltage, $v(t)$, across L and C. The equations describing the voltage and the current can be written in terms of the following coupled differential equations:

$$v(t) = L\frac{dI(t)}{dt}, \tag{6.1a}$$

$$I(t) = -C\frac{dv(t)}{dt} \tag{6.1b}$$

Above equations could be rewritten, as a second order differential equation for voltage, as follows:

$$\frac{d^2v(t)}{dt^2} + \omega_0^2 v(t) = 0, \tag{6.2}$$

where $\omega_0^2 = 1/LC$. The coupled equations in Eq. (6.1) can be expressed by two uncoupled equations for mode amplitudes $a_+(t)$ and $a_-(t)$:

$$\frac{da_\pm(t)}{dt} = \pm i\omega_0 a_\pm(t), \tag{6.3}$$

where

$$a_\pm(t) = \sqrt{\frac{C}{2}}(v(t) \pm i\sqrt{\frac{L}{C}}I(t)) \tag{6.4}$$

The solutions for the current and the voltage from Eq. (6.1) and Eq. (6.2), when subjected to proper boundary conditions, are given by:

$$v(t) = |V|\cos(\omega_0 t), \tag{6.5}$$

and

$$I(t) = \sqrt{\frac{C}{L}}|V|\sin(\omega_0 t) \tag{6.6}$$

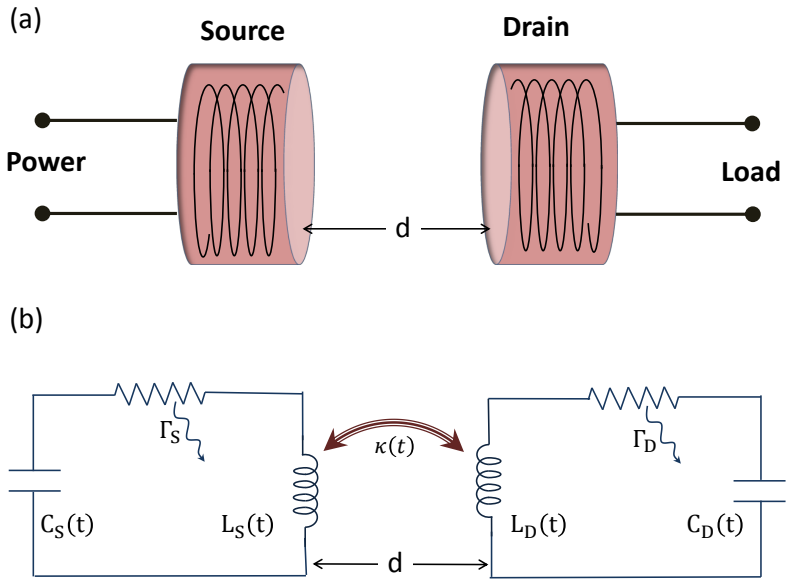

Figure 6.1: (a) Typical wireless power transfer system consists of two coils separated by a distance d, (b) Schematic of the coils. Two lossy LC circuits, *Source* and *Drain* with losses Γ_s and Γ_d respectively, coupled to each other by inductive coupling. The resonant frequencies are ω_s and ω_d and also $\omega_s \neq \omega_d$.

Here $|V|$ is the peak voltage. Using above solutions, the total energy of the system could be obtained as: $|a_\pm|^2 = \frac{C}{2}|V|^2 = W$, where a_+ being the positive frequency component of the mode amplitudes, while a_- is its negative counterpart. In the rest of the analysis,we will consider the positive frequency component only and will drop the '+' subscript for simplicity. Taking loss in the system into account, the equation is written in the following modified form:

$$\frac{da(t)}{dt} = i\omega_0 a(t) - \Gamma a(t), \tag{6.7}$$

where Γ is the decay rate due to the dissipation from the coils. In our study we consider two such coils, namely the *Source* and the *Drain* (Fig. (6.1)), which are coupled by mutual inductance between them. These two coils are off-resonant to each other having different resonant frequencies ω_S and ω_D. The coupling between the coils is given by $\kappa(t) = M(t)\sqrt{\omega_s\omega_d/L_sL_d}$, where $M(t)$ is the mutual inductance between these two coils. The mode amplitudes are $a_s(t)$ and $a_d(t)$ respectively and are coupled to each other. Total energy of the system is $|a_s(t)|^2 + |a_d(t)|^2$. This system can be expressed using the following set of coupled equations:

$$\frac{da_s(t)}{dt} = (i\omega_s - \Gamma_s)a_s(t) + i\kappa a_d(t) \tag{6.8a}$$

$$\frac{da_d(t)}{dt} = (i\omega_d - \Gamma_d - \Gamma_w)a_d(t) + i\kappa a_s(t) \tag{6.8b}$$

Here Γ_s and Γ_d are the intrinsic loss rates of the *source* and the *drain* respectively. Γ_w is the work extracted from the *drain* coil.

6.2 Energy transfer protocols

In order to design the energy transfer protocols, we discuss two methods here: the adiabatic passage and the transitionless quantum driving. From the coupled mode theory, discussed above, we can characterise the system by defining the Hamiltonian in $[a_s(t) \quad a_d(t)]^T$ basis, as follows:

$$H(t) = \begin{pmatrix} -\omega_s - i\Gamma_s & -\kappa(t) \\ -\kappa(t) & -\omega_d - i\Gamma_d - i\Gamma_w \end{pmatrix} \tag{6.9}$$

As the circuits,chosen here, are not resonant to each other, we consider the system in a rotating frame of reference, where the interaction Hamiltonian in the diabatic basis is as follows:

$$H(t) = \begin{pmatrix} \frac{\Delta(t)}{2} - i\Gamma_s & -\kappa(t) \\ -\kappa(t) & -\frac{\Delta(t)}{2} - i\Gamma_d - i\Gamma_w \end{pmatrix} \tag{6.10}$$

The diabatic basis are given by, $b_{s,d}(t) = a_{s,d}\exp[-i(\omega_s + \omega_d)t/2]$.In this new basis, one has to consider only the frequency difference between the coils, given by, $\Delta(t) = \omega_d(t) - \omega_s(t)$.

6.2.1 Adiabatic following

To study the adiabatic following, first let us consider that the intrinsic losses are zero. Therefore, the instantaneous eigenvectors of Eq. (6.10) can be written as,

$$B_+(t) = \cos(\frac{\Theta(t)}{2})b_s(t) - \sin(\frac{\Theta(t)}{2})b_d(t) \tag{6.11a}$$

$$B_-(t) = \sin(\frac{\Theta(t)}{2})b_s(t) + \cos(\frac{\Theta(t)}{2})b_d(t) \tag{6.11b}$$

Here $\Theta(t)$ is the angle of mixing, given by $\Theta(t) = \frac{1}{2}\tan^{-1}(2\kappa/\Delta)$. $B_{\pm}(t)$ are also known as adiabatic states. For adiabatic evolution, one needs to vary the Hamiltonian infinitely slowly or adiabatically so that the system always follows a particular state B_+ or B_- during a complete cycle of the time evolution. To achieve this, the evolution ought to follow the adiabatic condition, which is obtained by comparing the non-adiabatic correction terms to the instantaneous eigen-energies. It is expressed as follows:

$$|\langle \partial_t B_{\pm}(t)|B_{\mp}(t)\rangle| \ll \sqrt{(4\kappa(t)^2 + \Delta(t)^2)} \tag{6.12}$$

The fulfilment of this condition makes the transition probability between $B_+(t)$ and $B_-(t)$ zero. Moreover, if we assume that the system is initially in the state $B_+(t)$ and the power is in the *source* coil at $t = 0$, which refers to $\Theta(0) = 0$, then, by rotating Θ clockwise to π , one could arrive at the final state, $b_d(t)$. Thus the power ends up in the *drain* coil. This rotation could be achieved by sweeping $\Delta(t)$ from a large negative value to a large positive value. For our system, we chose $\kappa(t)$ and $\Delta(t)$ according to the well known Landau-Zener (LZ) scheme[130,171], given by:

$$\kappa(t) = \kappa_0; \qquad \Delta(t) = \delta + \beta(t - t_0) \tag{6.13}$$

where δ is some arbitrary offset between the frequencies of the two coils and β determines the slope in $\Delta(t)$, which eventually controls the speed of the process. Under such choices, large t_0 is needed to satisfy the adiabatic condition and it, effectively, determines the width of the evolution cycle. In passing, we note that, in general, the LZ model shows less adiabaticity. However,in adiabaticity based techniques,usually, one should have good control on the temporal dependence of the Hamiltonian. This amounts to controlling the complex time dependent profiles of Δ and κ. LZ-model, as could be seen in Eq. (6.13), provides simpler profiles for both Δ and κ compared to other models, e.g. the so-called Allen-Eberly scheme[141].

When the loss rates are non-zero in both the *source* and the *drain* coil, the system could be considered as dissipative. These dissipations can be modelled mathematically via the dissipation matrix:

$$\Gamma = \begin{pmatrix} \Gamma_s & 0 \\ 0 & \Gamma_d + \Gamma_w \end{pmatrix} \tag{6.14}$$

It should be noted that, for adiabatic evolution, the intrinsic loss rates Γ_s and Γ_d

should be less than the coupling strength κ_0, otherwise the evolution would not be possible and the power would be lost from the coil itself.

6.2.2 Shortcut to adiabaticity

For shortcut, we first transform our Hamiltonian in Eq. (6.10), in the adiabatic basis, using Eq. (6.11), where the basis states are related as:

$$[B_+(t), B_-(t)]^T = U(\Theta(t))^\dagger [b_s(t), b_d(t)]^T \tag{6.15}$$

The non-adiabatic correction terms are generally negligible under adiabatic approximation. The Landau-Zener formula for the total transition probability between adiabatic states in our case is, $p = \exp[-2\pi\kappa_0^2/\beta]$. One can obtain $p \simeq 0$ when Eq. (6.12) is satisfied, which can be written simply as $\beta \ll 8\kappa_0^2$. However if one wants to drive the evolution faster, non-adiabatic corrections becomes stronger and p no longer remains zero. To avoid such a scenario, the adiabatic Hamiltonian needs to be diagonalized exactly. To serve this cause, we add the additional interaction to the adiabatic Hamiltonian as proposed by Berry.[11] To find the additional interaction, we use the following equation:

$$H_1(t) = i \sum_{n=\pm} \left[|\partial_t B_n(t)\rangle \langle B_n(t)| - \langle B_n(t)| \partial_t B_n(t)\rangle |B_n(t)\rangle \langle B_n(t)| \right] \tag{6.16}$$

The second term in Eq. (6.16) vanishes owing to the orthogonality of $B_\pm(t)$. The first term can be written in the adiabatic basis as follows:

$$H_1(t) = i \begin{pmatrix} 0 & \kappa_a(t) \\ -\kappa_a(t) & 0 \end{pmatrix} \tag{6.17}$$

The total Hamiltonian, required for the transitionless driving, is given by

$$H_{6.eff}(t) = \begin{pmatrix} (\Delta - \dot{\phi})/2 & \sqrt{\kappa^2(t) + \kappa_a^2(t)} \\ \sqrt{\kappa^2(t) + \kappa_a^2(t)} & -(\Delta - \dot{\phi}/2) \end{pmatrix}, \tag{6.18}$$

where

$$\kappa_a(t) = \frac{|\dot{\Delta}(t)\kappa(t) - \dot{\kappa}(t)\Delta(t)|}{\Delta^2(t) + 4\kappa^2(t)} \tag{6.19}$$

and

$$\dot{\phi}(t) = \frac{2\Delta(t)\dot{\Delta}^2(t)}{\Delta^2(t) + 4\kappa^2(t) + \dot{\Delta}^2(t)} \tag{6.20}$$

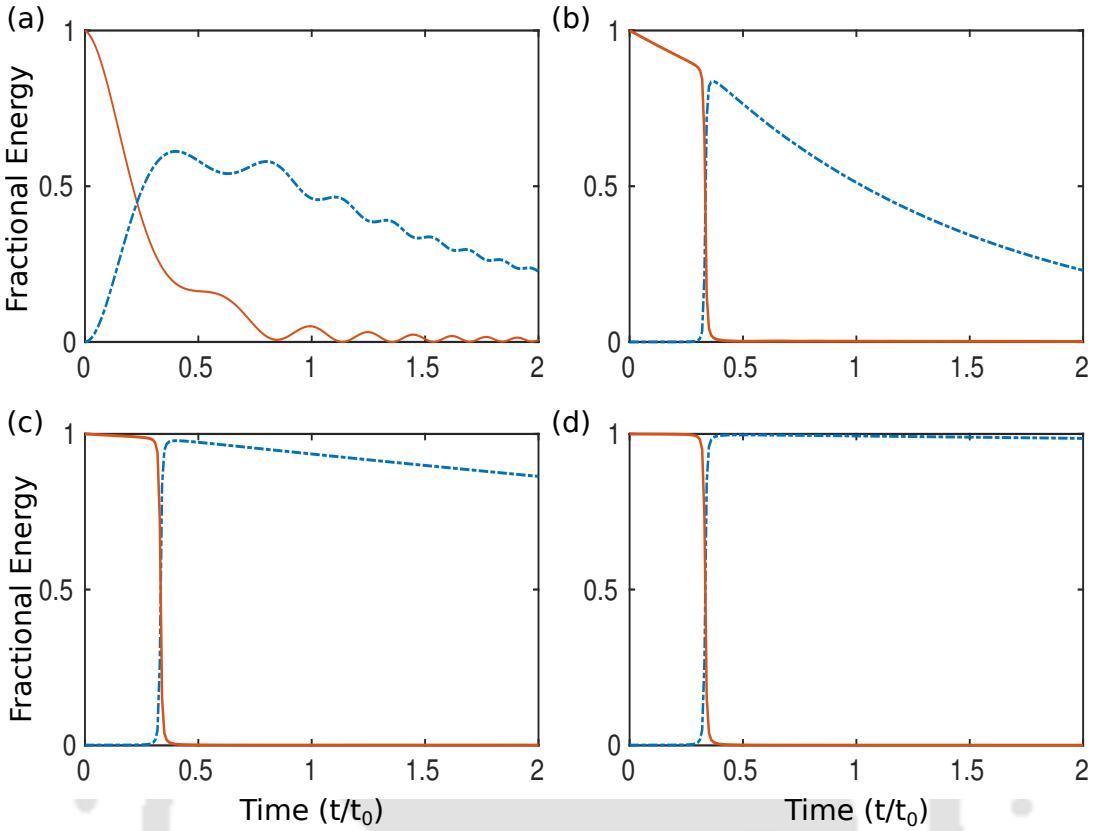

Figure 6.2: Evolution of energy from the *Source* coil (solid red) to the *Drain* coil (dash-dotted blue) with $\Gamma_s = \Gamma_d = 4 \times 10^3 s^{-1}$, $\delta = 2 \times 10^5 s^{-1}$. (a) Adiabatic evolution for the time window $2t_0$ where $\kappa_0 = 4 \times 10^4 s^{-1}$, $\beta = 3 \times 10^9 s^{-2}$ and $t_0 = 10^{-4} s$, followed by energy evolution using TQD with weaker coupling strenght $\kappa_0 = 4 \times 10^2 s^{-1}$ and decreasing time windows (b) $\beta = 3 \times 10^9 s^{-2}$ and $t_0 = 10^{-4} s$, (c) $\beta = 3 \times 10^{10} s^{-2}$ and $t_0 = 10^{-5} s$, (d) $\beta = 3 \times 10^{11} s^{-2}$ and $t_0 = 10^{-6} s$,

Here $(\Delta - \dot{\phi})/2$ is the effective frequency offset and $\sqrt{\kappa^2(t) + \kappa_a^2(t)} = \kappa_{eff}$ is the modified coupling between the two coils. ϕ characterizes another unitary rotation given by

$$\begin{pmatrix} b'_s \\ b'_d \end{pmatrix} = \begin{pmatrix} e^{-i\phi/2} & 0 \\ 0 & e^{i\phi/2} \end{pmatrix} \begin{pmatrix} b_s \\ b_d \end{pmatrix} \tag{6.21}$$

With all these unitary transformations, one needs to keep track of all the bases used in the process and keep them consistent. The mixing angle Θ should be adjusted properly via the boundary conditions, given by $\Theta(0) = 0$, $\Theta(T) = \pi$ and $\kappa_a(0) = \kappa_a(T) = 0$.

6.3 Results and discussion

To envisage the transfer of energy from the *source* to the *drain* ,with the effects of intrinsic losses taken into account, we followed the standard density matrix approach and therefore solved the master equation, given by

$$\frac{d\rho}{dt} = -i[H, \rho] - \frac{1}{2}\{\Gamma, \rho\} \tag{6.22}$$

Here $\rho(t)$ is the density matrix and Γ represents the dissipation matrix as described in Eq. (6.14). The diagonal elements of $\rho(t)$ are $\rho_{ss} = |b_s|^2$ and $\rho_{dd} = |b_d|^2$ which represents the energy of the *source* and the *drain* coil respectively. For adiabatic evolution we chose the interaction Hamiltonian in Eq. (6.10) and for TQD, $H(t)$ is taken from Eq. (6.18).

In Fig. (6.2), we present the results showing the evolution of fractional energies, $|b_{s,d}(t)|^2/|b_s(0)|^2$, in presence of intrinsic losses, using both the adiabatic and the TQD algorithm. Even when the adiabatic condition is being satisfied, as shown in Fig. (6.2a) , as a result of adiabatic evolution, the fractional energy attains the value, on the order of 0.25 or so, at the end of the given time window. The requirement of large time, i.e. $t_0 = 10^{-4}s$, so that the adiabaticity condition is maintained, results in energy dissipation due to the intrinsic losses. However, when TQD is applied, fractional energy of the *drain* coil almost attains nearly the same value for the same period of time (Fig. (6.2b)). But when the adiabatic condition is violated i.e. $\beta \geq 8\kappa_0^2$, enhancement of energy in the drain coil could be observed in Fig. (6.2c). The affects of intrinsic losses are almost eliminated as the time period becomes shorter and shorter(Fig. (6.2d)). It is worthwhile to note the effect of β on the power transfer mechanism. Physically, β determines the slope of Δ and thereby it controls the time period required to complete a single power transfer cycle. In the adiabatic regime, β is relatively small and hence the required period $T_{adiabatic}$ is larger and because of that, power is dissipated from the source coil during the process. When β is large, the frequency sweep becomes faster and $\omega_s(t)$ becomes steeper (here ω_d is taken as constant) as shown in Fig. (6.3) which results in squeezing of the period. Thus the power is transferred to the *drain* in short time with minimum loss from the *source*. Also it is obvious that one needs to repeat the cycle over and over again to transfer power for practical purposes. It may be noted that wireless power transfer is generally studied in the steady-state limit of continuous-wave excitation[172]. In our study, we have analysed power transfer in the setting where the source coil is prepared in a state with all the energy and the drain coil with none. In a way, it

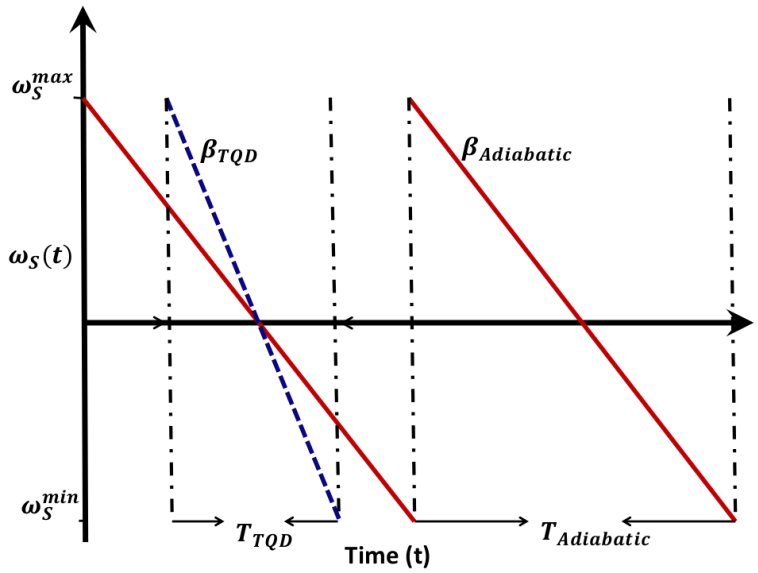

Figure 6.3: Schematic representation of Frequency sweep of $\omega_s(t)$ (or $\Delta(t)$ when ω_d = constant). The sweep is linear with slope β according to L-Z model. For adiabatic evolution $|\beta| = \beta_{adiabatic}$ is small (solid red) and $|\beta| = \beta_{TQD}$ is high for the TQD method. Time period required for adiabatic case is large accordingly i.e. $T_{TQD} < T_{Adiabatic}$.

is a kind of pulsed excitation. However, it could be extended to the case of near continuous excitation by fast repetition of the cycle.

The work efficiency of our system is defined as the ratio between the useful extracted power from the drain, $P_{work} = \Gamma_w \int_0^T |b_d(t)|^2 dt$ to the total time averaged power P_{total} in the system over a particular time period T, given by

$$\eta = \frac{\Gamma_w \int_0^T |b_d(t)|^2 dt}{\Gamma_s \int_0^T |b_s(t)|^2 dt + (\Gamma_d + \Gamma_w) \int_0^T |b_d(t)|^2 dt} \tag{6.23}$$

We studied efficiency of the system against the variation of the initial frequency difference between the coils for different values of $\kappa_0/\Gamma_{s,d}$. The efficiency strongly depends on the coupling strength κ_0 for both the adiabatic and the TQD approach and it increases with increasing κ_0 as depicted in Fig. (6.4a) . Although this is not that surprising, but in the beyond adiabatic regime (for shorter periods), efficiency for adiabatic method decreases rapidly. However efficiency remains intact for TQD algorithm which can be seen from Fig. 6.4b.

The coupling between the coils for WPT systems are generally very sensitive to the distance, d , between the coils and it decays very rapidly with larger coupling distances[113,119]. In Fig. 6.5(a) and 6.5(b) we depict the dependence of coupling strength $\kappa(d)$ and efficiency $\eta(d)$ respectively on the distance d between the coils.

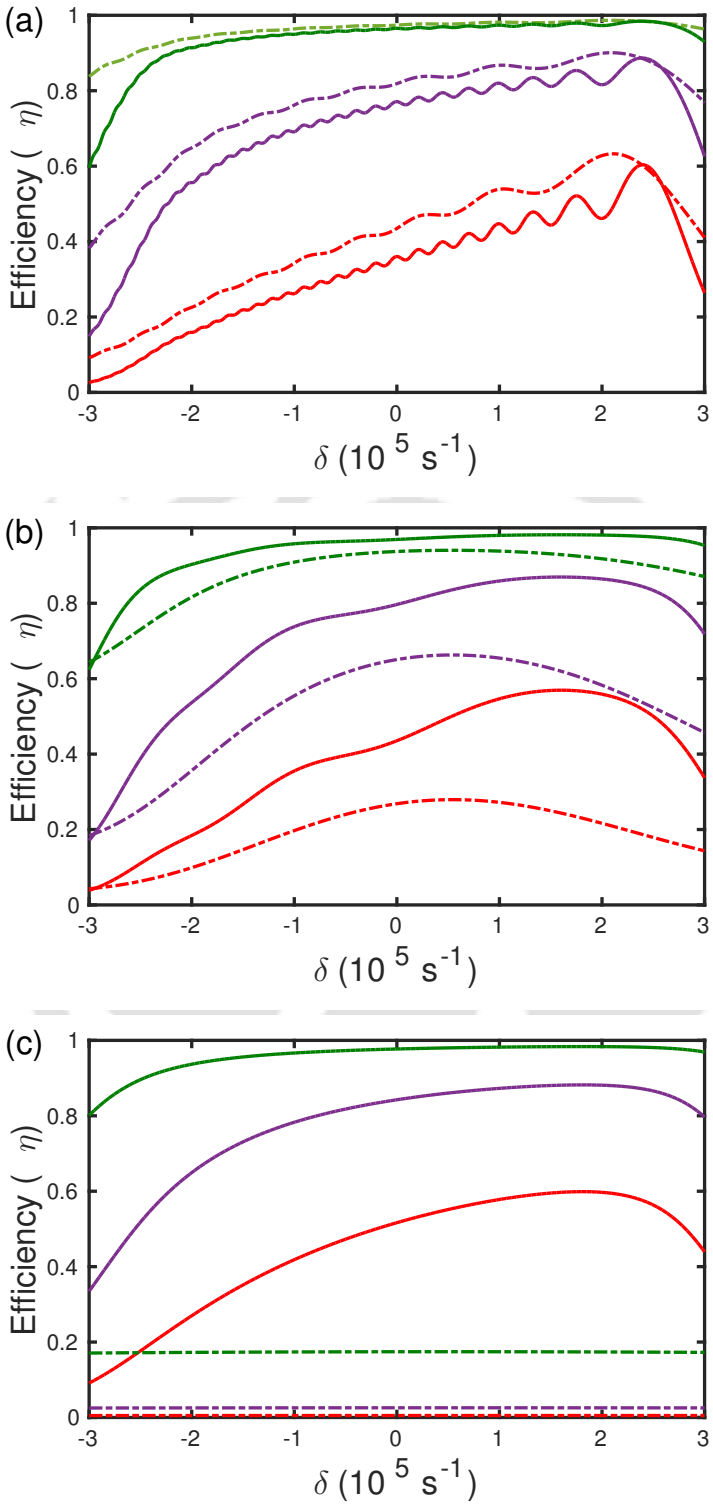

Figure 6.4: Comparison of efficiency (η) as a function of δ between adiabatic (dashed-dotted) and tqd based methods (solid) for different $\kappa_0/\Gamma_{s,d}$ values: $\kappa_0/\Gamma_{s,d} = 10$ (red), $\kappa_0/\Gamma_{s,d} = 50$ (purple), $\kappa_0/\Gamma_{s,d}$=100 (green) where $\Gamma_w = 10^4 s^{-1}$. Time windows (T) for the evolution are as follows: (a) $T = 200\mu s$, (b)$T = 20\mu s$ (c) $T = 2\mu s$.

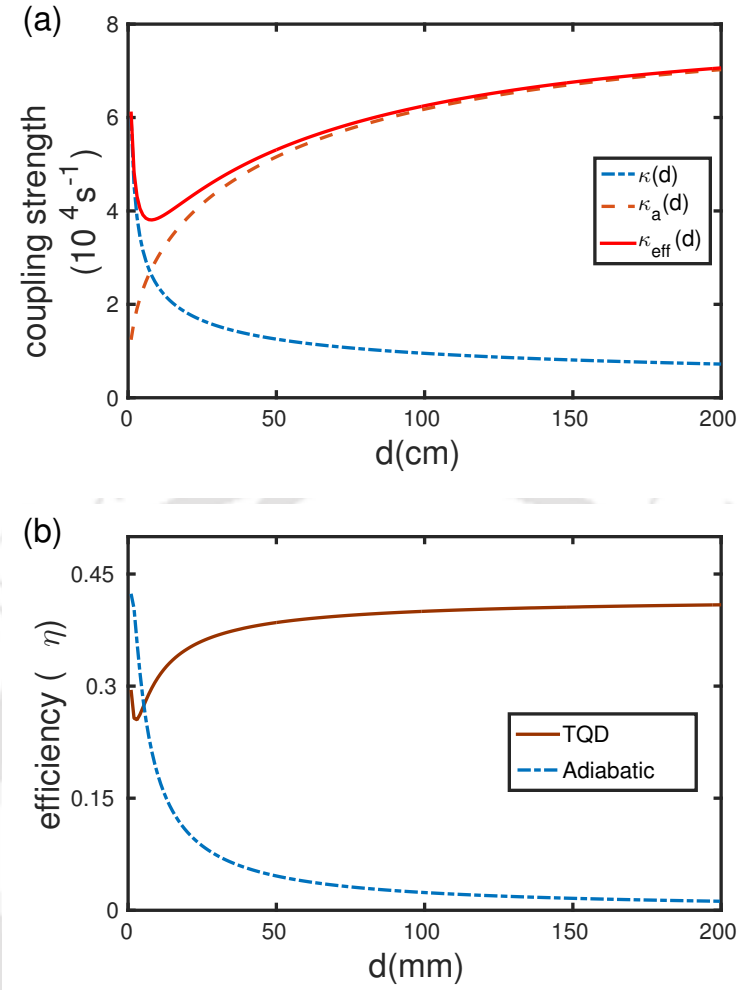

Figure 6.5: Dependence on the distance d of the (a) coupling $\kappa(d)$ between the *source* and the *drain* coil (dash-dotted blue), additional coupling $\kappa_a(d)$ (dotted brown) and effective coupling $\kappa_{eff}(d)$ for TQD (solid red), (b) efficiency $\eta(d)$ for adiabatic method (dash-dotted blue) and for TQD (solid brown) .

From Fig. (6.5b) it is clear that, even in the adiabatic regime, the efficiency for the adiabatic case decreases with increasing d. η tends to zero for $d = 2m$ or so as the strength of κ goes down. But in the case of TQD, η maintains a steady value for large d and that certainly gets enhanced with larger β values. The reason behind such behavior could be understood from the formalism of inverse engineering. We can observe from Fig. (6.5a) that as κ decreases with distance, we require an additional coupling κ_a which increases with distance so that the effective coupling κ_{eff} constitutes a reasonable strength for sustained power transfer over a certain range of distance. We have also studied the efficiency of our scheme against the variations in κ_0 and the intrinsic losses ($\Gamma_s = \Gamma_d$). From the contour plots in

Fig. (6.6), we observe that η is nearly unity for lower losses and higher κ_0 in the adiabatic regime. As we move from Fig. (6.6a) to Fig. (6.6c), adiabaticity gradually breaks down and efficiency also decreases gradually. Finally it goes to zero when $t_0 = 10^{-6}$s for any reasonable amount of losses. On the other hand, using TQD, we find that the achievable efficiency is highly robust against variations in κ_0 and $\Gamma_{s,d}$ unlike its adiabatic counterpart. Also the efficiency is found to get enhanced with decreasing time window. However, it may be appropriate and relevant to discuss briefly about the energy cost involved in the implementation of the proposed scheme. The energy of the coupling required for adiabatic power transfer will be on the order of the difference of the resonance frequencies of the source and the drain coils, i.e., $\Delta = \omega_d - \omega_s$. In order to estimate the required energy to implement TQD, we need to calculate the *Energy cost* of the process defined as[173–176]:

$$\Sigma(\tau) = \frac{1}{\tau}\int_0^\tau ||H||^2 \mathrm{d}t \tag{6.24}$$

Here $||H||$ is the Hilbert-Schmidt norm, given by $Tr\sqrt{H^\dagger H}$. It is important to note that the quantification of the time-energy cost in Eq. (6.24) is first pioneered by Demirplak and Rice[176]. This was further used by A. del Campo and his co-workers[24,177] and others[178,179]. We calculated the ratio of the energy cost for adiabatic and additional interaction, Σ_{TQD}/Σ_{Ad} for the coupling strength parameter used in this work. As shown in Fig. (6.7), it is clear that the energy cost for implementing TQD is less compared to the adiabatic case up to the region of a few microseconds and it increases exponentially as the time window is reduced further. Although in principle, we can transfer the power in infinitely short time, but it is the energy cost that restrict the process up to a time limit for its feasibility. In this case, there is a clear trade-off between the energy cost and the transfer time[180]. Therefore, with the coupling parameter values chosen in Fig. (6.2), it is possible, using the proposed TQD-based scheme,to achieve fast power transfer up to a few microseconds for a reasonable energy cost. We find that, with the chosen parameter regime, one could negate the effect of losses and thereby preserving the robustness and the efficiency of the scheme.

Finally, we would like to make a few comments on the practical implementation of the proposed scheme. The scheme rely on the frequency sweeping of both the source and the drain coils. As the resonance frequency of each coil is given by: $\omega_{s,d}^2 = 1/L_{s,d}C_{s,d}$, clearly, one needs to have time dependence either in the inductance or in the capacitance or both. Variable capacitor is one possibility in this

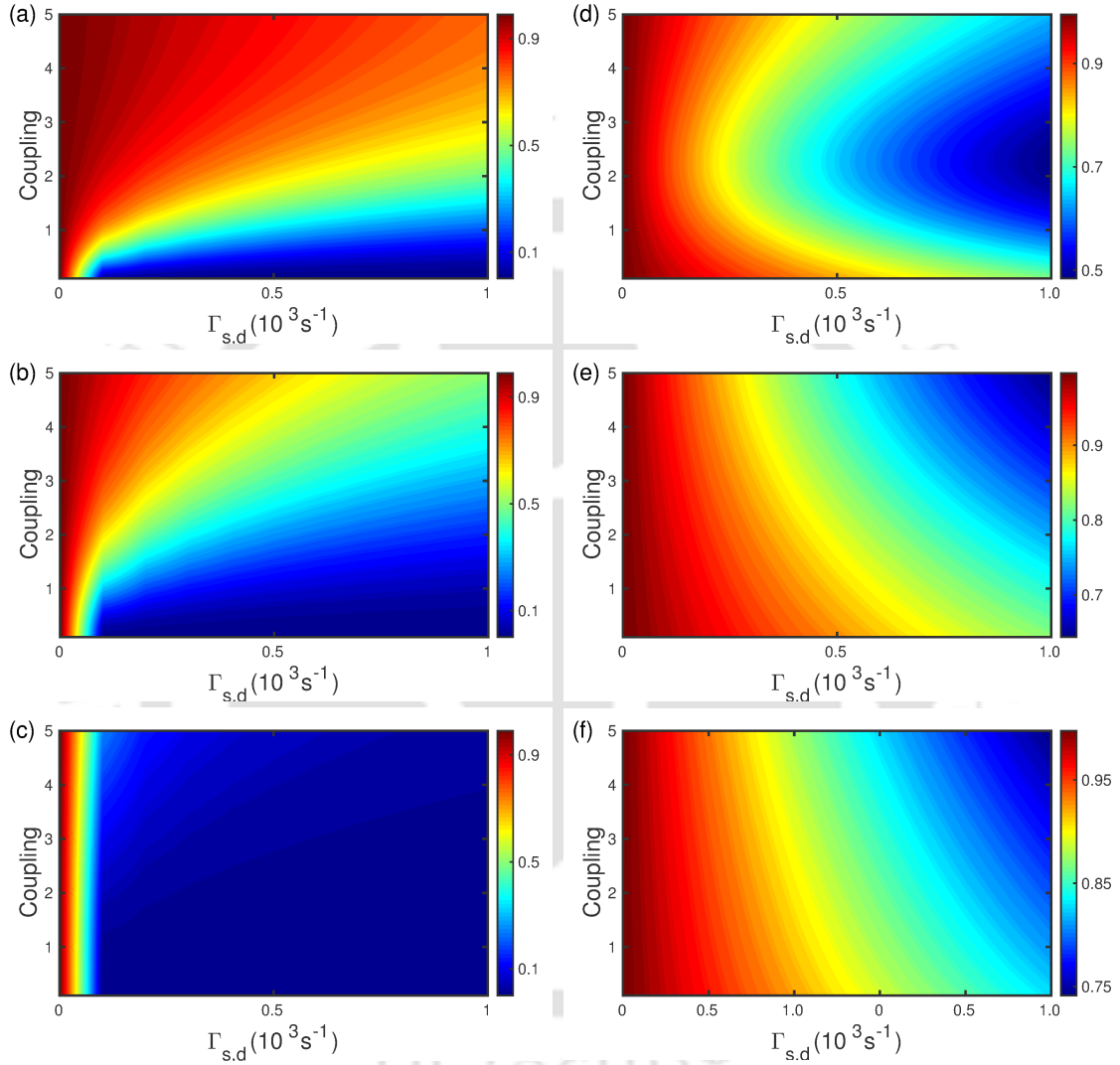

Figure 6.6: Contour plots for efficiency with respect to the variations in κ ($\times 10^4 s^{-1}$) and intrinsic losses $\Gamma_s = \Gamma_d$ ($\times 10^3 s^{-1}$) and $\Gamma_w = 10^4 s^{-1}$. (a), (b), (c) for adiabatic case and (d), (e), (f) for TQD method with $t_0 = 10^{-4} s$ in (a) and (d), $t_0 = 10^{-5} s$ in (b) and (e) and $t_0 = 10^{-6} s$ in (c) and (f).

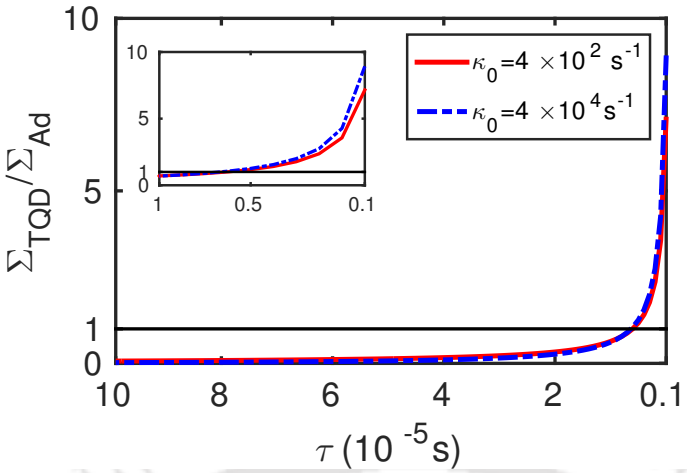

Figure 6.7: Ratio of energy cost for TQD and adiabatic power transfer with respect to decreasing time window, $\kappa_0 = 4 \times 10^2 s^{-1}$ (solid red) and $\kappa_0 = 4 \times 10^4 s^{-1}$ (dash-dotted blue).

regard. In a few recent studies, such capacitors have been used for tuning the coils to the exact resonance[165,181]. One important study is[182], where authors have used 'digital capacitance tuning' in order to optimize the wireless power transfer. These tunable capacitors could certainly be used to achieve frequency sweeping. On the other hand, inductance depends mainly on the orientation and the geometry of the coils. So to obtain a time varying inductance one needs to change the orientation periodically by rotating or oscillating one of the coils. However in that case, the coupling will also be time dependent, for which a similar study could be carried out easily. Apart from frequency sweeping, we need to use a third agency as well in order to facilitate efficient WPT between the coils, which is akin to engineer the additional Hamiltonian in mathematical sense, as proposed in our scheme. In fact there already exists a couple of such methods to tune the operating frequency for different coil separations[172] . One method of immense significance is to use magnetic field to couple the resonators[113]. The additional Hamiltonian in our scheme could be engineered to take into the effect of such magnetic field coupling. Another recent findings show that it is possible to exploit a parity-time-symmetric circuit, incorporating a nonlinear gain saturation element, to induce robust wireless power transfer between the coils[183]. In a yet another method, a third coil is utilised to mediate efficient wireless power transfer between the coils[184]. Hence, we anticipate that the proposed TQD based scheme could be implemented practically.

6.4 Chapter summary

We have explored a wireless power transfer (WPT) system in the light of adiabatic method and transitionless quantum driving method. Our findings could be summarized as follows. The adiabatic evolution of power is a useful way to transfer power between two coils. Unlike resonant WPT systems, it uses two off-resonant coils and frequency sweeping is used for power transfer. However, it has to fulfil the adiabatic condition which makes the time required to transfer power in each cycle longer, resulting in dissipation of power from the source coil and hence efficiency decreases. On the other hand, the TQD algorithm enables us to enhance the efficiency of power transfer. The algorithm suggest that, it is possible to decrease the transfer time and increase the efficiency by invoking an additional interaction between the coils.The amount of power dissipated from the *source* also gets decreased. The WPT method using TQD shows more robustness compared to the adiabatic one against the variations in the parameters like the coupling strength, intrinsic losses and the coupling distance.

Chapter 7

Conclusion

Shortcut to adiabaticity methods, which were proposed as alternative processes to the so-called quantum adiabatic processes (QAP) in order to circumvent the shortcomings associated with it, are now well-eastablished methods in quantum physics. Interestingly, application of STA methods are no longer limited to quantum physics only. Drawing inspiration from the isomorphism between the quantum physics systems and various classical physics systems, STA methods are now widely applied in various branches of physics and engineering. This thesis shows that the STA techniques are applicable not only in the quantum systems but also in systems that are not quantum mechanical in nature, such as the waveguides and LC circuits. We find that numerous useful insights could be gained via the implementation of STA techniques in such systems.

After providing a brief introduction to the STA techniques with appropriate literature survey, in chapter 2, we give a detailed account of the two STA methods, namely the transitionless quantum driving and the Lewis-Riesenfeld invariant based methods used in this thesis. In Chapter 3, a quantum mechanical system is studied. We proposed a novel method to prepare the Bell state from an unentangled state, in a system of a coupled pair of spin 1/2 particles, using STA methods. Our study shows that adiabatic evolution ccould be useful to produce a final entangled state starting from a pure diabatic state. However, introduction of STA methods in this system reduces the requirement for long transition time and the high strength of the field amplitude considerably. The robustness and the fidelity have also been enhanced with the application of STA.

Next two chapters are dedicated for the study of application of STA techniques in waveguide based systems. In chapter 4, we have described power transfer in waveguide couplers using STA methods and the coupled mode theory for waveg-

uides. We have shown that with judicious choice of the coupling coefficient and the mismatch profile, it is possible to construct a coupler, which is considerably small in size compared to the so-called adiabatic couplers. With recent development of fabrication techniques, separation between the waveguides and profile of taper could be controlled accurately and hence designing κ and Δ, as predicted by these theories, should be achievable. Chapter 5 shows the application of the inverse engineering to achieve soliton compression in optical fibers with distributed nonlinearity and constant GVD parameter. Using variational analysis, we showed that maximum soliton compression can be achieved only for large fiber length. However, if the nonlinearity is designed using inverse engineering with proper boundary conditions, it is possible to compress the soliton in considerably small fiber lengths.

In the last chapter, we studied TQD in a completely different system. This chapter presents a study of wireless power transfer in a pair of off-resonant coupled LC circuits. Our study shows, with decreasing time window, using TQD, one can eliminate the effect of intrinsic losses and thereby enhance the efficiency significantly. We also present the distance dependent study where it is shown that with the application of the additional field, it is possible to transfer power over comparatively large distances.

Future aspects

As a topic of research, the STA techniques are thriving in recent years. There are significant opportunities for exploring STA techniques in various branches of physics. Various topics in the context of quantum information theory such as quantum gates, entanglement, ion and atom traps, atom-cavity interaction, various topics in modern quantum optics like optomechanics, optoelectronics, superconducting circuits are few examples where significant improvement can be done using STA methods. State engineering using STA, till now, are studied only for atomic systems. Engineering of molecular states would be a bright prospect in this regard. STA methods could certainly be used to study ultra-cold atomic and moleculer systems. It may even find application in the so-called ultracold chemistry and in biology.

In this thesis, for the first time, STA methods are applied for soliton compression in optical fiber and in wireless power transfer. There are possibilities for several advancement in these systems. For example, one can apply the TQD technique in coupled LC circuits, using a mediator coil, to study EIT or STIRAP like phenomena, in the context of WPT. For soliton compression, the group velocity dispersion can

also be inverse engineered using STA protocols in order to achieve better control over compression.

Bibliography

[1] A. Einstein, *Zur quantentheorie der strahlung*, Phys. Z. **18**, 121 (1917).

[2] B. W. Shore, *Manipulating Quantum Structures Using Laser Pulses*, Cambridge University Press, 2011.

[3] N. V. Vitanov, T. Halfmann, B. W. Shore, and K. Bergmann, *Laser-induced population transfer by adiabatic passage techniques*, Annual Review of Physical Chemistry **52**, 763 (2001), PMID: 11326080.

[4] K. Bergmann, H. Theuer, and B. W. Shore, *Coherent population transfer among quantum states of atoms and molecules*, Rev. Mod. Phys. **70**, 1003 (1998).

[5] P. Král, I. Thanopulos, and M. Shapiro, *Colloquium: Coherently controlled adiabatic passage*, Rev. Mod. Phys. **79**, 53 (2007).

[6] N. V. Vitanov, A. A. Rangelov, B. W. Shore, and K. Bergmann, *Stimulated Raman adiabatic passage in physics, chemistry, and beyond*, Rev. Mod. Phys. **89**, 015006 (2017).

[7] J. Siewert and T. Brandes, *Applications of Adiabatic Passage in Solid-State Devices*, pages 181–189, Springer Berlin Heidelberg, Berlin, Heidelberg, 2004.

[8] S. Longhi, *Quantum-optical analogies using photonic structures*, Laser & Photonics Reviews **3**, 243 (2009).

[9] M. Demirplak and S. A. Rice, *Adiabatic Population Transfer with Control Fields*, The Journal of Physical Chemistry A **107**, 9937 (2003).

[10] M. Demirplak and S. A. Rice, *Assisted Adiabatic Passage Revisited*, The Journal of Physical Chemistry B **109**, 6838 (2005), PMID: 16851769.

[11] M. V. Berry, *Transitionless quantum driving*, Journal of Physics A: Mathematical and Theoretical **42**, 365303 (2009).

[12] X. Chen, I. Lizuain, A. Ruschhaupt, D. Guéry-Odelin, and J. G. Muga, *Shortcut to Adiabatic Passage in Two- and Three-Level Atoms*, Phys. Rev. Lett. **105**, 123003 (2010).

[13] A. Ruschhaupt, X. Chen, D. Alonso, and J. G. Muga, *Optimally robust shortcuts to population inversion in two-level quantum systems*, New Journal of Physics **14**, 093040 (2012).

[14] K. Takahashi, *Fast-forward scaling in a finite-dimensional Hilbert space*, Phys. Rev. A **89**, 042113 (2014).

[15] J. Chen and L. F. Wei, *Implementation speed of deterministic population passages*

compared to that of Rabi pulses, Phys. Rev. A **91**, 023405 (2015).

[16] J.-F. Schaff, X.-L. Song, P. Capuzzi, P. Vignolo, and G. Labeyrie, *Shortcut to adiabaticity for an interacting Bose-Einstein condensate*, EPL (Europhysics Letters) **93**, 23001 (2011).

[17] J.-F. Schaff, P. Capuzzi, G. Labeyrie, and P. Vignolo, *Shortcuts to adiabaticity for trapped ultracold gases*, New Journal of Physics **13**, 113017 (2011).

[18] S. Ibáñez and J. G. Muga, *Adiabaticity condition for non-Hermitian Hamiltonians*, Phys. Rev. A **89**, 033403 (2014).

[19] S. Ibáñez, S. Martínez-Garaot, X. Chen, E. Torrontegui, and J. G. Muga, *Shortcuts to adiabaticity for non-Hermitian systems*, Phys. Rev. A **84**, 023415 (2011).

[20] B. T. Torosov, G. Della Valle, and S. Longhi, *Non-Hermitian shortcut to stimulated Raman adiabatic passage*, Phys. Rev. A **89**, 063412 (2014).

[21] M. Palmero, E. Torrontegui, D. Guéry-Odelin, and J. G. Muga, *Fast transport of two ions in an anharmonic trap*, Phys. Rev. A **88**, 053423 (2013).

[22] M. Palmero, S. Martínez-Garaot, U. G. Poschinger, A. Ruschhaupt, and J. G. Muga, *Fast separation of two trapped ions*, New Journal of Physics **17**, 093031 (2015).

[23] A. del Campo, *Shortcuts to Adiabaticity by Counterdiabatic Driving*, Phys. Rev. Lett. **111**, 100502 (2013).

[24] A. del Campo, M. M. Rams, and W. H. Zurek, *Assisted Finite-Rate Adiabatic Passage Across a Quantum Critical Point: Exact Solution for the Quantum Ising Model*, Phys. Rev. Lett. **109**, 115703 (2012).

[25] S. Ibáñez, X. Chen, E. Torrontegui, J. G. Muga, and A. Ruschhaupt, *Multiple Schrödinger Pictures and Dynamics in Shortcuts to Adiabaticity*, Phys. Rev. Lett. **109**, 100403 (2012).

[26] S. Ibáñez, X. Chen, and J. G. Muga, *Improving shortcuts to adiabaticity by iterative interaction pictures*, Phys. Rev. A **87**, 043402 (2013).

[27] L. Giannelli and E. Arimondo, *Three-level superadiabatic quantum driving*, Phys. Rev. A **89**, 033419 (2014).

[28] H. R. L. Jr and W. B. Riesenfeld, *An Exact Quantum Theory of the TimeDependent Harmonic Oscillator and of a Charged Particle in a TimeDependent Electromagnetic Field*, Journal of Mathematical Physics **10**, 1458 (1969).

[29] X. Chen, E. Torrontegui, and J. G. Muga, *Lewis-Riesenfeld invariants and transitionless quantum driving*, Phys. Rev. A **83**, 062116 (2011).

[30] X.-B. Huang, Y.-H. Chen, and Z. Wang, *Fast generation of three-qubit Greenberger-Horne-Zeilinger state based on the Lewis-Riesenfeld invariants in coupled cavities*, Sci. Rep. **6**, 25707 (2016).

[31] K.-H. Song and M.-F. Chen, *Shortcuts to adiabatic passage for generation of W states of distant atoms*, Quantum Information Processing **15**, 3169 (2016).

[32] J.-L. Wu, C. Song, X. Ji, and S. Zhang, *Fast generation of three-dimensional entanglement between two spatially separated atoms via invariant-based shortcut*, J. Opt.

Soc. Am. B **33**, 2026 (2016).

[33] S. Martínez-Garaot, E. Torrontegui, X. Chen, and J. G. Muga, *Shortcuts to adiabaticity in three-level systems using Lie transforms*, Phys. Rev. A **89**, 053408 (2014).

[34] Y.-H. Chen, Y. Xia, Q.-Q. Chen, and J. Song, *Efficient shortcuts to adiabatic passage for fast population transfer in multiparticle systems*, Phys. Rev. A **89**, 033856 (2014).

[35] K. H. Chien, C. S. Yeih, and S. Y. Tseng, *Mode Conversion/Splitting in Multimode Waveguides Based on Invariant Engineering*, Journal of Lightwave Technology **31**, 3387 (2013).

[36] S. Y. Tseng and Y. W. Jhang, *Fast and Robust Beam Coupling in a Three Waveguide Directional Coupler*, IEEE Photonics Technology Letters **25**, 2478 (2013).

[37] S. Deffner, C. Jarzynski, and A. del Campo, *Classical and Quantum Shortcuts to Adiabaticity for Scale-Invariant Driving*, Phys. Rev. X **4**, 021013 (2014).

[38] A. del Campo and M. G. Boshier, *Shortcuts to adiabaticity in a time-dependent box*, Scientific reports **2**, 648 (2012).

[39] A. del Campo, *Fast frictionless dynamics as a toolbox for low-dimensional Bose-Einstein condensates*, EPL (Europhysics Letters) **96**, 60005 (2011).

[40] A. del Campo, *Frictionless quantum quenches in ultracold gases: A quantum-dynamical microscope*, Phys. Rev. A **84**, 031606 (2011).

[41] A. Del Campo, J. Goold, and M. Paternostro, *More bang for your buck: Super-adiabatic quantum engines*, Scientific Reports **4**, 6208 (2014).

[42] J. Zhang et al., *Experimental Implementation of Assisted Quantum Adiabatic Passage in a Single Spin*, Phys. Rev. Lett. **110**, 240501 (2013).

[43] N. Malossi, M. G. Bason, M. Viteau, E. Arimondo, D. Ciampini, R. Mannella, and O. Morsch, *Quantum driving of a two level system: quantum speed limit and superadiabatic protocols an experimental investigation*, Journal of Physics: Conference Series **442**, 012062 (2013).

[44] M. G. Bason et al., *High-fidelity quantum driving*, Nat. Phys. **8**, 147 (2012).

[45] B. B. Zhou et al., *Accelerated quantum control using superadiabatic dynamics in a solid-state lambda system*, Nature Physics **13**, 330 (2017).

[46] S. An, D. Lv, A. Del Campo, and K. Kim, *Shortcuts to adiabaticity by counterdiabatic driving for trapped-ion displacement in phase space*, Nature communications **7**, 12999 (2016).

[47] S. Deng, P. Diao, Q. Yu, A. del Campo, and H. Wu, *Shortcuts to adiabaticity in the strongly coupled regime: Nonadiabatic control of a unitary Fermi gas*, Phys. Rev. A **97**, 013628 (2018).

[48] S. Deng et al., *Superadiabatic quantum friction suppression in finite-time thermodynamics*, Preprint, Arxiv:1711.00650 [cond-nat.quant-gas] (2017).

[49] S. Masuda and K. Nakamura, *Fast-forward problem in quantum mechanics*, Phys. Rev. A **78**, 062108 (2008).

[50] S. Masuda and K. Nakamura, *Fast-forward of adiabatic dynamics in quantum mechanics*, Proceedings of the Royal Society of London A: Mathematical, Physical and

Engineering Sciences **466**, 1135 (2010).

[51] S. Masuda and K. Nakamura, *Acceleration of adiabatic quantum dynamics in electromagnetic fields*, Phys. Rev. A **84**, 043434 (2011).

[52] S. Masuda and S. A. Rice, *Fast-Forward Assisted STIRAP*, The Journal of Physical Chemistry A **119**, 3479 (2015), PMID: 25775133.

[53] I. Setiawan, B. Eka Gunara, S. Masuda, and K. Nakamura, *Fast forward of the adiabatic spin dynamics of entangled states*, Phys. Rev. A **96**, 052106 (2017).

[54] D. M. Greenberger, M. A. Horne, A. Shimony, and A. Zeilinger, *Bells theorem without inequalities*, American Journal of Physics **58**, 1131 (1990).

[55] W. Dür, G. Vidal, and J. I. Cirac, *Three qubits can be entangled in two inequivalent ways*, Phys. Rev. A **62**, 062314 (2000).

[56] B. L. Higgins, D. W. Berry, S. D. Bartlett, H. M. Wiseman, and G. J. Pryde, *Entanglement-free Heisenberg-limited phase estimation*, Nat. **450**, 393 (2015).

[57] M. Kitagawa and M. Ueda, *Squeezed spin states*, Phys. Rev. A **47**, 5138 (1993).

[58] M. L. Fanto, R. K. Erdmann, P. M. Alsing, C. J. Peters, and E. J. Galvez, *Multipli-entangled photon spontaneous parametric down-conversion source*, Proc. SPIE **8057**, 8057 (2011).

[59] T.-C. Wei and P. M. Goldbart, *Geometric measure of entanglement and applications to bipartite and multipartite quantum states*, Phys. Rev. A **68**, 042307 (2003).

[60] M. Yang and Z.-L. Cao, *Generation of pure ionic entangled states via linear optics*, Phys. Rev. A **72**, 042307 (2005).

[61] J.-H. Zou and X.-M. Hu, *Entangled atomic state generation via adiabatic evolution of dark eigenstates in cavity QED*, Optics Communications **281**, 5067 (2008).

[62] M. Barbieri, F. De Martini, G. Di Nepi, and P. Mataloni, *Generation and Characterization of Werner States and Maximally Entangled Mixed States by a Universal Source of Entanglement*, Phys. Rev. Lett. **92**, 177901 (2004).

[63] A. Ling, P. Y. Han, A. Lamas-Linares, and C. Kurtsiefer, *Preparation of bell states with controlled white noise*, Laser Physics **16**, 1140 (2006).

[64] B. Kraus, H. P. Büchler, S. Diehl, A. Kantian, A. Micheli, and P. Zoller, *Preparation of entangled states by quantum Markov processes*, Phys. Rev. A **78**, 042307 (2008).

[65] Y. Lin et al., *Preparation of Entangled States through Hilbert Space Engineering*, Phys. Rev. Lett. **117**, 140502 (2016).

[66] K. Stannigel, P. Rabl, and P. Zoller, *Driven-dissipative preparation of entangled states in cascaded quantum-optical networks*, New Journal of Physics **14**, 063014 (2012).

[67] J. Chen, H. Zhou, C. Duan, and X. Peng, *Preparing Greenberger-Horne-Zeilinger and W states on a long-range Ising spin model by global controls*, Phys. Rev. A **95**, 032340 (2017).

[68] R. G. Unanyan, N. V. Vitanov, and K. Bergmann, *Preparation of Entangled States by Adiabatic Passage*, Phys. Rev. Lett. **87**, 137902 (2001).

[69] L.-B. Chen, M.-Y. Ye, G.-W. Lin, Q.-H. Du, and X.-M. Lin, *Generation of entan-*

glement via adiabatic passage, Phys. Rev. A **76**, 062304 (2007).

[70] J. Song, Y. Xia, and H.-S. Song, *Entangled state generation via adiabatic passage in two distant cavities*, Journal of Physics B: Atomic, Molecular and Optical Physics **40**, 4503 (2007).

[71] Y. Liang, S.-L. Su, Q.-C. Wu, X. Ji, and S. Zhang, *Adiabatic passage for three-dimensional entanglement generation through quantum Zeno dynamics*, Opt. Express **23**, 5064 (2015).

[72] C. Marr, A. Beige, and G. Rempe, *Entangled-state preparation via dissipation-assisted adiabatic passages*, Phys. Rev. A **68**, 033817 (2003).

[73] Y.-H. Chen, Y. Xia, J. Song, and Q.-Q. Chen, *Shortcuts to adiabatic passage for fast generation of Greenberger-Horne-Zeilinger states by transitionless quantum driving*, Sci. Rep. **5**, 15616 (2015).

[74] J. Chen and L. F. Wei, *Deterministic generations of photonic NOON states in cavities via shortcuts to adiabaticity*, Phys. Rev. A **95**, 033838 (2017).

[75] Z. Chen, Y.-H. Chen, Y. Xia, J. Song, and B.-H. Huang, *Fast generation of three-atom singlet state by transitionless quantum driving*, Sci. Rep. **6**, 22202 (2016).

[76] S. He et al., *Efficient shortcuts to adiabatic passage for three-dimensional entanglement generation via transitionless quantum driving*, Sci. Rep. **6**, 30929 (2016).

[77] X.-Q. Yang, D.-Y. Huang, P. Xue, Y.-Y. Gong, J.-L. Wu, and X. Ji, *Feasible superadiabatic-based shortcuts for the fast generation of 3D entanglement between two atoms*, Laser Physics Letters **14**, 055209 (2017).

[78] M. Lu, Y. Xia, L.-T. Shen, J. Song, and N. B. An, *Shortcuts to adiabatic passage for population transfer and maximum entanglement creation between two atoms in a cavity*, Phys. Rev. A **89**, 012326 (2014).

[79] K. G. Makris, D. N. Christodoulides, O. Peleg, M. Segev, and D. Kip, *Optical transitions and Rabi oscillations in waveguide arrays*, Opt. Express **16**, 10309 (2008).

[80] M. Ornigotti, G. D. Valle, T. T. Fernandez, A. Coppa, V. Foglietti, P. Laporta, and S. Longhi, *Visualization of two-photon Rabi oscillations in evanescently coupled optical waveguides*, Journal of Physics B: Atomic, Molecular and Optical Physics **41**, 085402 (2008).

[81] G. D. Valle, M. Ornigotti, T. T. Fernandez, P. Laporta, S. Longhi, A. Coppa, and V. Foglietti, *Adiabatic light transfer via dressed states in optical waveguide arrays*, Applied Physics Letters **92**, 011106 (2008).

[82] S. Longhi, G. Della Valle, M. Ornigotti, and P. Laporta, *Coherent tunneling by adiabatic passage in an optical waveguide system*, Phys. Rev. B **76**, 201101 (2007).

[83] S. Longhi, *Adiabatic passage of light in coupled optical waveguides*, Phys. Rev. E **73**, 026607 (2006).

[84] A. Salandrino, K. Makris, D. N. Christodoulides, Y. Lahini, Y. Silberberg, and R. Morandotti, *Analysis of a three-core adiabatic directional coupler*, Optics Communications **282**, 4524 (2009).

[85] S. Kazazis and E. Paspalakis, *Effects of nonlinearity in asymmetric adiabatic three-waveguide directional couplers*, Journal of Modern Optics **57**, 2123 (2010).

[86] A. M. Kenis, I. Vorobeichik, M. Orenstein, and N. Moiseyev, *Non-evanescent adiabatic directional coupler*, IEEE Journal of Quantum Electronics **37**, 1321 (2001).

[87] T. A. Ramadan, R. Scarmozzino, and R. M. Osgood, *Adiabatic couplers: design rules and optimization*, Journal of Lightwave Technology **16**, 277 (1998).

[88] X. Sun, H.-C. Liu, and A. Yariv, *Adiabaticity criterion and the shortest adiabatic mode transformer in a coupled-waveguide system*, Opt. Lett. **34**, 280 (2009).

[89] F. Dreisow, A. Szameit, M. Heinrich, R. Keil, S. Nolte, A. Tünnermann, and S. Longhi, *Adiabatic transfer of light via a continuum in optical waveguides*, Opt. Lett. **34**, 2405 (2009).

[90] S.-Y. Tseng, *Counterdiabatic mode-evolution based coupled-waveguide devices*, Opt. Express **21**, 21224 (2013).

[91] T.-H. Pan and S.-Y. Tseng, *Short and robust silicon mode (de)multiplexers using shortcuts to adiabaticity*, Opt. Express **23**, 10405 (2015).

[92] X. Chen, H.-W. Wang, Y. Ban, and S.-Y. Tseng, *Short-length and robust polarization rotators in periodically poled lithium niobate via shortcuts to adiabaticity*, Opt. Express **22**, 24169 (2014).

[93] S.-Y. Tseng, R.-D. Wen, Y.-F. Chiu, and X. Chen, *Short and robust directional couplers designed by shortcuts to adiabaticity*, Opt. Express **22**, 18849 (2014).

[94] G. D. Valle, G. Perozziello, and S. Longhi, *Shortcut to adiabaticity in full-wave optics for ultra-compact waveguide junctions*, Journal of Optics **18**, 09LT03 (2016).

[95] M. Remoissenet, *Waves Called Solitons: Concepts and Experiments*, Advanced Texts in Physics, Springer, 1999.

[96] M. S. Ruderman, *Freak waves in laboratory and space plasmas*, The European Physical Journal Special Topics **185**, 57 (2010).

[97] N. J. Zabusky and M. D. Kruskal, *Interaction of "Solitons" in a Collisionless Plasma and the Recurrence of Initial States*, Phys. Rev. Lett. **15**, 240 (1965).

[98] D. R. Solli, C. Ropers, P. Koonath, and B. Jalali, *Optical rogue waves*, Nature **450**, 1054 (2007).

[99] F. Gérôme, K. Cook, A. K. George, W. J. Wadsworth, and J. C. Knight, *Delivery of sub-100fs pulses through 8m of hollow-core fiber using soliton compression*, Opt. Express **15**, 7126 (2007).

[100] D. G. Ouzounov, C. J. Hensley, A. L. Gaeta, N. Venkateraman, M. T. Gallagher, and K. W. Koch, *Soliton pulse compression in photonic band-gap fibers.*, Opt. Express **13**, 6153 (2005).

[101] P. Colman, C. Husko, S. Combrié, I. Sagnes, C. W. Wong, and A. De Rossi, *Temporal solitons and pulse compression in photonic crystal waveguides*, Nature Photonics **4**, 862 (2010).

[102] A. Blanco-Redondo, C. Husko, D. Eades, Y. Zhang, J. Li, T. Krauss, and B. Eggle-

ton, *Observation of soliton compression in silicon photonic crystals*, Nature communications **5**, 3160 (2014).

[103] P. K. A. Wai and W. hua Cao, *Ultrashort soliton generation through higher-order soliton compression in a nonlinear optical loop mirror constructed from dispersion-decreasing fiber*, J. Opt. Soc. Am. B **20**, 1346 (2003).

[104] S. Ashihara, J. Nishina, T. Shimura, and K. Kuroda, *Soliton compression of femtosecond pulses in quadratic media*, J. Opt. Soc. Am. B **19**, 2505 (2002).

[105] M. D. Pelusi and H.-F. Liu, *Higher order soliton pulse compression in dispersion-decreasing optical fibers*, IEEE Journal of Quantum Electronics **33**, 1430 (1997).

[106] J. Moses and F. W. Wise, *Soliton compression in quadratic media: high-energy few-cycle pulses with a frequency-doubling crystal*, Opt. Lett. **31**, 1881 (2006).

[107] M. L. Quiroga-Teixeiro, D. Anderson, A. Berntson, and M. Lisak, *Compression of optical solitons by conversion of nonlinear modes*, J. Opt. Soc. Am. B **12**, 1110 (1995).

[108] S. V. Chernikov, E. M. Dianov, D. J. Richardson, and D. N. Payne, *Soliton pulse compression in dispersion-decreasing fiber*, Opt. Lett. **18**, 476 (1993).

[109] F. K. Abdullaev and M. Salerno, *Adiabatic compression of soliton matter waves*, Journal of Physics B: Atomic, Molecular and Optical Physics **36**, 2851 (2003).

[110] J. Li, K. Sun, and X. Chen, *Shortcut to adiabatic control of soliton matter waves by tunable interaction*, Sci. Rep. **6**, 38258 (2016).

[111] J. Agbinya, *Wireless Power Transfer*, River Publishers Series in Communications, River Publishers, 2015.

[112] S. Y. R. Hui, W. Zhong, and C. K. Lee, *A Critical Review of Recent Progress in Mid-Range Wireless Power Transfer*, IEEE Transactions on Power Electronics **29**, 4500 (2014).

[113] A. Kurs, A. Karalis, R. Moffatt, J. D. Joannopoulos, P. Fisher, and M. Soljačić, *Wireless Power Transfer via Strongly Coupled Magnetic Resonances*, Science **317**, 83 (2007).

[114] B. L. Cannon, J. F. Hoburg, D. D. Stancil, and S. C. Goldstein, *Magnetic Resonant Coupling As a Potential Means for Wireless Power Transfer to Multiple Small Receivers*, IEEE Transactions on Power Electronics **24**, 1819 (2009).

[115] T. Imura, H. Okabe, and Y. Hori, Basic experimental study on helical antennas of wireless power transfer for electric vehicles by using magnetic resonant couplings, in *2009 IEEE Vehicle Power and Propulsion Conference*, pages 936–940, 2009.

[116] A. P. Sample, D. T. Meyer, and J. R. Smith, *Analysis, Experimental Results, and Range Adaptation of Magnetically Coupled Resonators for Wireless Power Transfer*, IEEE Transactions on Industrial Electronics **58**, 544 (2011).

[117] T. Imura and Y. Hori, *Maximizing Air Gap and Efficiency of Magnetic Resonant Coupling for Wireless Power Transfer Using Equivalent Circuit and Neumann Formula*, IEEE Transactions on Industrial Electronics **58**, 4746 (2011).

[118] Z. N. Low, R. A. Chinga, R. Tseng, and J. Lin, *Design and Test of a High-Power High-Efficiency Loosely Coupled Planar Wireless Power Transfer System*, IEEE Transactions on Industrial Electronics **56**, 1801 (2009).

[119] A. Karalis, J. Joannopoulos, and M. Soljačić, *Efficient wireless non-radiative mid-range energy transfer*, Annals of Physics **323**, 34 (2008), January Special Issue 2008.

[120] A. Rangelov, H. Suchowski, Y. Silberberg, and N. Vitanov, *Wireless adiabatic power transfer*, Annals of Physics **326**, 626 (2011).

[121] A. Rangelov and N. Vitanov, *Mid-range adiabatic wireless energy transfer via a mediator coil*, Annals of Physics **327**, 2245 (2012).

[122] R. E. Hamam, A. Karalis, J. Joannopoulos, and M. Soljačić, *Efficient weakly-radiative wireless energy transfer: An EIT-like approach*, Annals of Physics **324**, 1783 (2009).

[123] E. Torrontegui et al., Chapter 2 - shortcuts to adiabaticity, in *Advances in Atomic, Molecular, and Optical Physics*, edited by E. Arimondo, P. R. Berman, and C. C. Lin, volume 62 of *Advances In Atomic, Molecular, and Optical Physics*, pages 117 – 169, Academic Press, 2013.

[124] L. D. Faddeev, L. A. Khalfin, and I. V. Komarov, *V.A. Fock - Selected Works: Quantum Mechanics and Quantum Field Theory*, CRC Press, 2004.

[125] D. J. Griffiths, *Introduction to Quantum Mechanics*, Cambridge University Press, 2016.

[126] A. Messiah, *Quantum Mechanics*, Number v. 2 in Quantum Mechanics, North-Holland, 1981.

[127] D. J. Tannor, *Introduction to Quantum Mechanics*, University Science Books, 2007.

[128] D. T. Haar, *Collected Papers of L.D. Landau*, Elsevier Science, 2013.

[129] C. Zener, *Non-adiabatic crossing of energy levels*, Proceedings of the Royal Society of London A: Mathematical, Physical and Engineering Sciences **137**, 696 (1932).

[130] N. V. Vitanov and B. M. Garraway, *Landau-Zener model: Effects of finite coupling duration*, Phys. Rev. A **53**, 4288 (1996).

[131] A. Abragam, *The Principles of Nuclear Magnetism*, International series of monographs on physics, Clarendon Press, 1961.

[132] R. G. Unanyan, M. Fleischhauer, N. V. Vitanov, and K. Bergmann, *Entanglement generation by adiabatic navigation in the space of symmetric multiparticle states*, Phys. Rev. A **66**, 042101 (2002).

[133] R. T. Brierley, C. Creatore, P. B. Littlewood, and P. R. Eastham, *Adiabatic State Preparation of Interacting Two-Level Systems*, Phys. Rev. Lett. **109**, 043002 (2012).

[134] J. Stenger, S. Inouye, D. M. Stamper-Kurn, H.-J. Miesner, A. P. Chikkatur, and W. Ketterle, *Spin domains in ground-state BoseEinstein condensates*, Nature **396**, 345 (1998).

[135] C. Anastopoulos and B. L. Hu, *Two-level atom-field interaction: Exact master equa-*

tions for non-Markovian dynamics, decoherence, and relaxation, Phys. Rev. A **62**, 033821 (2000).

[136] G. P. Agrawal, *Applications of Nonlinear Fiber Optics*, Number v. 10 in Applications of nonlinear fiber optics, Elsevier, 2008.

[137] S. Martínez-Garaot, S.-Y. Tseng, and J. G. Muga, *Compact and high conversion efficiency mode-sorting asymmetric Y junction using shortcuts to adiabaticity*, Opt. Lett. **39**, 2306 (2014).

[138] C. S. Yeih, H. X. Cao, and S. Y. Tseng, *Shortcut to Mode Conversion via Level Crossing in Engineered Multimode Waveguides*, IEEE Photonics Technology Letters **26**, 123 (2014).

[139] S.-Y. Tseng, *Robust coupled-waveguide devices using shortcuts to adiabaticity*, Opt. Lett. **39**, 6600 (2014).

[140] A. Ghatak and K. Thyagarajan, *An Introduction to Fiber Optics*, Cambridge University Press, 1998.

[141] L. Allen and J. H. Eberly, *Optical Resonance and Two-level Atoms*, Dover books on physics and chemistry, Dover, 1975.

[142] A. W. Snyder and J. Love, *Optical Waveguide Theory*, Science paperbacks, Springer US, 1983.

[143] T. Dauxois and M. Peyrard, *Physics of Solitons*, Cambridge University Press, 2006.

[144] L. Lam, *Introduction to Nonlinear Physics*, Undergraduate Texts in Mathematics, Springer, 1997.

[145] G. P. Agrawal, *Nonlinear Fiber Optics*, Optics and Photonics Series, Academic Press, 2013.

[146] P. V. Mamyshev, P. G. J. Wigley, J. Wilson, G. I. Stegeman, V. A. Semeonov, E. M. Dianov, and S. I. Miroshnichenko, *Adiabatic compression of Schrödinger solitons due to the combined perturbations of higher-order dispersion and delayed nonlinear response*, Phys. Rev. Lett. **71**, 73 (1993).

[147] D. Anderson, M. Lisak, B. Malomed, and M. Quiroga-Teixeiro, *Tunneling of an optical soliton through a fiber junction*, J. Opt. Soc. Am. B **11**, 2380 (1994).

[148] K. Bertilsson, T. Aakjer, M. L. Quiroga-Teixeiro, P. A. Andrekson, and P.-O. Hedekvist, *Investigation of Soliton Compression by Propagation through Fiber Junctions*, Optical Fiber Technology **1**, 117 (1995).

[149] V. I. Kruglov, A. C. Peacock, and J. D. Harvey, *Exact Self-Similar Solutions of the Generalized Nonlinear Schrödinger Equation with Distributed Coefficients*, Phys. Rev. Lett. **90**, 113902 (2003).

[150] J. Yang, *Nonlinear Waves in Integrable and Nonintegrable Systems*, Mathematical Modeling and Computation, Society for Industrial and Applied Mathematics (SIAM, 3600 Market Street, Floor 6, Philadelphia, PA 19104), 2010.

[151] V. M. Pérez-García, H. Michinel, J. I. Cirac, M. Lewenstein, and P. Zoller, *Dynamics of Bose-Einstein condensates: Variational solutions of the Gross-Pitaevskii*

equations, Phys. Rev. A **56**, 1424 (1997).

[152] H. Saito and M. Ueda, *Dynamically Stabilized Bright Solitons in a Two-Dimensional Bose-Einstein Condensate*, Phys. Rev. Lett. **90**, 040403 (2003).

[153] V. M. Pérez-García, V. V. Konotop, and V. A. Brazhnyi, *Feshbach Resonance Induced Shock Waves in Bose-Einstein Condensates*, Phys. Rev. Lett. **92**, 220403 (2004).

[154] G. B. Whitham, *Linear and Nonlinear Waves*, Pure and Applied Mathematics: A Wiley Series of Texts, Monographs and Tracts, Wiley, 1999.

[155] X. Chen, A. Ruschhaupt, S. Schmidt, A. del Campo, D. Guéry-Odelin, and J. G. Muga, *Fast Optimal Frictionless Atom Cooling in Harmonic Traps: Shortcut to Adiabaticity*, Phys. Rev. Lett. **104**, 063002 (2010).

[156] Y.-Y. Cui, X. Chen, and J. G. Muga, *Transient Particle Energies in Shortcuts to Adiabatic Expansions of Harmonic Traps*, The Journal of Physical Chemistry A **120**, 2962 (2016), PMID: 26237328.

[157] J. G. Muga, X. Chen, A. Ruschhaupt, and D. Gury-Odelin, *Frictionless dynamics of BoseEinstein condensates under fast trap variations*, Journal of Physics B: Atomic, Molecular and Optical Physics **42**, 241001 (2009).

[158] D. Guéry-Odelin, J. G. Muga, M. J. Ruiz-Montero, and E. Trizac, *Nonequilibrium Solutions of the Boltzmann Equation under the Action of an External Force*, Phys. Rev. Lett. **112**, 180602 (2014).

[159] R. Marchetti et al., *Group-velocity dispersion in SOI-based channel waveguides with reduced-height*, Opt. Express **25**, 9761 (2017).

[160] X. Yu, S. Sandhu, S. Beiker, R. Sassoon, and S. Fan, *Wireless energy transfer with the presence of metallic planes*, Applied Physics Letters **99**, 214102 (2011).

[161] S. Kim, J. S. Ho, and A. S. Y. Poon, *Midfield Wireless Powering of Subwavelength Autonomous Devices*, Phys. Rev. Lett. **110**, 203905 (2013).

[162] A. Klein and N. Katz, *Strong coupling optimization with planar spiral resonators*, Current Applied Physics **11**, 1188 (2011).

[163] O. Jonah, A. Merwaday, S. V. Georgakopoulos, and M. M. Tentzeris, *Spiral resonators for optimally efficient strongly coupled magnetic resonant systems*, Wireless Power Transfer **1**, 21 (2014).

[164] C. Li and H. Ling, A planarized, capacitor-loaded loop structure for wireless power transfer, in *2013 IEEE Antennas and Propagation Society International Symposium (APSURSI)*, pages 840–841, 2013.

[165] C. J. Li and H. Ling, *Investigation of wireless power transfer using planarized, capacitor-loaded coupled loops*, Progress In Electromagnetics Research **148**, 223 (2014).

[166] X. Zhang et al., *Design of high-efficiency inductive power transfer coils for biomedical implants*, page 1 (2013).

[167] R. F. Xue, K. W. Cheng, and M. Je, *High-Efficiency Wireless Power Transfer for*

Biomedical Implants by Optimal Resonant Load Transformation, IEEE Transactions on Circuits and Systems I: Regular Papers **60**, 867 (2013).

[168] S. Kim, J. S. Ho, L. Y. Chen, and A. S. Y. Poon, *Wireless power transfer to a cardiac implant*, Applied Physics Letters **101**, 073701 (2012).

[169] X. Y. Zhang, C. D. Xue, and J. K. Lin, *Distance-Insensitive Wireless Power Transfer Using Mixed Electric and Magnetic Coupling for Frequency Splitting Suppression*, IEEE Transactions on Microwave Theory and Techniques **65**, 4307 (2017).

[170] H. Haus, *Waves and fields in optoelectronics*, Prentice-Hall Series in Solid State Physical Electronics, Prentice Hall, Incorporated, 1984.

[171] R. Khomeriki and S. Ruffo, *Nonadiabatic Landau-Zener Tunneling in Waveguide Arrays with a Step in the Refractive Index*, Phys. Rev. Lett. **94**, 113904 (2005).

[172] A. P. Sample, B. H. Waters, S. T. Wisdom, and J. R. Smith, *Enabling Seamless Wireless Power Delivery in Dynamic Environments*, Proceedings of the IEEE **101**, 1343 (2013).

[173] L. I. Mandel'shtam and I. E. Tamm, *Energy–time uncertainty relationship in non-relativistic quantum mechanics*, Izv. Akad. Nauk SSSR Ser. Fiz **9**, 122 (1945).

[174] Y. Aharonov and D. Bohm, *Time in the Quantum Theory and the Uncertainty Relation for Time and Energy*, Phys. Rev. **122**, 1649 (1961).

[175] J. Anandan and Y. Aharonov, *Geometry of quantum evolution*, Phys. Rev. Lett. **65**, 1697 (1990).

[176] M. Demirplak and S. A. Rice, *On the consistency, extremal, and global properties of counterdiabatic fields*, The Journal of Chemical Physics **129**, 154111 (2008).

[177] K. Funo, J.-N. Zhang, C. Chatou, K. Kim, M. Ueda, and A. del Campo, *Universal Work Fluctuations During Shortcuts to Adiabaticity by Counterdiabatic Driving*, Phys. Rev. Lett. **118**, 100602 (2017).

[178] A. C. Santos and M. S. Sarandy, *Superadiabatic controlled evolutions and universal quantum computation*, Scientific reports **5**, 15775 (2015).

[179] Y. Zheng, S. Campbell, G. De Chiara, and D. Poletti, *Cost of counterdiabatic driving and work output*, Phys. Rev. A **94**, 042132 (2016).

[180] S. Campbell and S. Deffner, *Trade-Off Between Speed and Cost in Shortcuts to Adiabaticity*, Phys. Rev. Lett. **118**, 100601 (2017).

[181] Y. Luo, Y. Yang, and Z. Chen, *Self-tuning wireless power transmission scheme based on on-line scattering parameters measurement and two-side power matching*, Scientific reports **4**, 4332 (2014).

[182] D. S. Ricketts, M. J. Chabalko, and A. Hillenius, *Optimization of wireless power transfer for mobile receivers using automatic digital capacitance tuning*, page 515 (2013).

[183] S. Assawaworrarit, X. Yu, and S. Fan, *Robust wireless power transfer using a nonlinear parity–time-symmetric circuit*, Nature **546**, 387 (2017).

[184] W. X. Zhong, C. Zhang, X. Liu, and S. Y. R. Hui, *A Methodology for Making a*

Three-Coil Wireless Power Transfer System More Energy Efficient Than a Two-Coil Counterpart for Extended Transfer Distance, IEEE Transactions on Power Electronics **30**, 933 (2015).

Vita

Koushik Paul was born on 3rd of April, 1990 in West Bengal, India. He did his B.Sc. with Physics Honours in 2010 and M.Sc. in physics in 2012 from Visva Bharati, West Bengal, India. He qualified Graduate Aptitude Test in Engineering (GATE) in 2012 and CSIR-UGC National Eeligibility Test (NET) in 2013. He had enrolled into the Ph.D programme at Indian Institute of Technology Guwahati in December, 2012. He was awarded Junior Research Fellowship in 2013 and Senior Research Fellowship in 2015 by Ministry of Human Resource Development, Government of India.